

# Power Measurement of Modes in Few-Mode Fibre

by

**Ross Summerfield**

Submitted in partial fulfillment of the requirements for the degree of

Master of Engineering

Faculty of Engineering and Information Technology,

Australian National University

13/12/2012



For the following special people who have made my education possible:

Daisy Summerfield,  
the late Joyce and Leslie Summerfield  
and  
Gloria and the late Rodolfo Badilles.

*“The way is won! The way is won!  
And straightway from the barren coast  
There came a westward-marching host,  
That aye and ever onward prest  
With eager faces to the West,  
Along the pathway of the sun.”*

A.B Paterson, *The Collected Verse of A. B. Paterson*, 1921

## **STATEMENT OF ORIGINALITY**

This thesis contains no material which has been accepted for the award of any other degree or diploma in any university. To the best of the author's knowledge, it contains no material previously published or written by another person, except where due reference is made in the text.

Signed:

\_\_\_\_\_  
Ross Summerfield

Date:

---

## **ACKNOWLEDGEMENTS**

A number of people have contributed in many ways to my Honours year, without whose help I could not have completed this thesis. First, I would like to thank my supervisors, Prof. John Love, Dr David Moser, and Dr Simon Hewlett whose advice and guidance was critical to success. Prof. John Love's advice and guidance, cajoling (where necessary) and correcting, has been valuable in both steering me on the right path with some of the theory as well as in guiding me in preparing a polished thesis, including guiding me in translation of some of the Strine into English. In addition, the timeless book that Allan Snider and he published so long ago has been a most invaluable guide to understanding the important concepts that have gone into this thesis.

I would also like to thank the good nature of AOFR for the provision of their testing facilities, as well as the most valuable and extremely important time that Dr David Moser and Dr Simon Hewlett have put into helping me get through this. In the end, I hope the output is at least of some value to them.

Additionally, without the provision of leave for study and other support of the management of the Department of Human Services, my study leading up to and including this thesis could not have gone anywhere near as well as it has. Particular support has been provided there by Mr Pat Fegan, Mr Peter Qui and Mr Steve McCauley, with ultimate support from the CEOs and Secretaries of the day (Mr Jeff Whalan AO, Ms Carolyn Hogg, Mr Finn Pratt and Ms Kathryn Campbell). I would also like to thank the Department's former CIO, Mr John Wadeson, who has been particularly supportive. I hope that the technology that this thesis goes towards building does end up helping out the Australian Government through access to higher density data transmission technology.

Finally, I wish to thank my family for enduring my temperament on this journey and for helping me through it. My spouse, Daisy, has been particularly supportive.

---

## **ABSTRACT**

With the information explosion currently occurring in society, which is, for instance, driving an 80 per cent per annum growth in data storage, data transmission bandwidth is currently of primary concern. In the interests of increasing data transmission density, there is currently considerable interest in mode-division multiplexing. In addition, there is currently considerable interest in high power laser amplifier construction using large mode area fibres. Both of these areas require a detailed understanding of the nature of power amplification of the higher order modes, with the former having the aim of evenly spreading power amongst modes and the latter having the aim maximising the power in the fundamental mode.

A key component of analysing power in each of the modes of a few mode (or large mode area) fibre is, as with analysis of anything, being able to measure it. That problem is compounded by the fact that good models of the power in each mode operate at the near-field, but nearly all technology available operates in the far-field. This challenge is accompanied by much hearsay and corporate analysis of the problems associated with mapping the far-field onto the near-field. The concerns are real as the far-field measurements are accompanied by noise and by a spreading, or spraying if you will, of the output from the end of a fibre. Indeed, antenna theorists have spent a great deal of time trying to tackle this mapping problem. While the concept presented herein more-or-less does that, it achieves its goal by looking at the problem from the other angle, namely mapping the near-field onto the far-field. The results are not perfect and currently only deal with the one and two mode case, but are adequate for comparative analysis and do lend themselves to a great deal more improvement through a small amount of gentle refinement.

Initial analysis of the power in one and two modes show that, in fact, a single mode travelling through a cladding-pumped large mode area rare-earth doped fibre amplifier will not amplify as much as two modes. This is understandable when considering that the fields of a few modes (two in this case) extend further out into the cladding than for a single mode, thus providing more opportunity for amplification. Further, in the case of two-mode amplification, if the second mode has in the order of 25 per cent more power than the fundamental mode (for instance), then the degree of amplification is very close to the same for each mode. This is resultant from the effect of the pump power delivering logarithmic fibre gain. Such a consideration offers a feature to exploit in order to even out power amplification of the modes if that is the intention.

# TABLE OF CONTENTS

STATEMENT OF ORIGINALITY . . . . .	ii
ACKNOWLEDGEMENTS . . . . .	iii
ABSTRACT . . . . .	iv
TABLE OF CONTENTS . . . . .	v
LIST OF FIGURES . . . . .	vii
LIST OF TABLES . . . . .	ix
<b>CHAPTER 1: Introduction</b>	<b>1</b>
1.1 What's the Problem? . . . . .	1
1.2 History and Characteristics of Optic Fibre . . . . .	2
1.3 Packing It In With Few-Mode Fibre . . . . .	4
1.4 Optical Fibre In-Line Amplification . . . . .	4
<b>CHAPTER 2: Literature Review</b>	<b>7</b>
2.1 Few-Mode Fibre Transmission . . . . .	7
2.2 Modal Power Theory . . . . .	8
2.3 Amplification Power Theory . . . . .	8
2.4 Power Measurement . . . . .	11
2.5 Far-Field Profiling and Analysis . . . . .	13
<b>CHAPTER 3: Theory</b>	<b>16</b>
3.1 Foundation Mathematics . . . . .	16
3.2 Fraction of Power Curves . . . . .	16
3.3 Power in the Modes . . . . .	20
<b>CHAPTER 4: System Design</b>	<b>24</b>
4.1 Specifications, Metrics and Functional Analysis . . . . .	24
4.2 Concept Generation and Screening . . . . .	24
4.3 System Construction . . . . .	26
4.4 System Testing . . . . .	28
<b>CHAPTER 5: Modal Amplitude</b>	<b>29</b>
5.1 Un-amplified Few-Mode Fibre . . . . .	29
5.2 Short Distance Mode Orientation . . . . .	32
5.3 Amplification of Few-Mode Fibre . . . . .	32
<b>CHAPTER 6: Conclusions and Recommendations</b>	<b>34</b>
6.1 Outcomes . . . . .	34
6.2 Further Work . . . . .	34
<b>REFERENCES</b>	<b>35</b>
<b>APPENDIX A: Detailed Customer Needs and Metrics</b>	<b>41</b>

---

A.1	Customer Needs . . . . .	41
<b>APPENDIX B: Design Details</b>		<b>44</b>
B.1	Concept Selection of Power Detector . . . . .	44
B.2	Concept Generation of 3-Dimensional Intensity Extraction . . . . .	46
B.3	Concept Selection of Power Profile Formula . . . . .	49
<b>APPENDIX C: Design Drawings</b>		<b>52</b>
<b>APPENDIX D: Detailed Equation Development</b>		<b>53</b>
D.1	Eigenvalue Equations Weakly Guiding Fibre . . . . .	53
D.2	Modal Power Distribution . . . . .	57
<b>APPENDIX E: Pseudo and Source Code for Graph Production and Amplification Processing</b>		<b>63</b>
E.1	Goniometric Radiometer Data Extraction . . . . .	63
E.2	Modal Intensity to Amplification Power Conversion . . . . .	71
<b>APPENDIX F: Test Reports</b>		<b>84</b>
F.1	2 Mode Fibre Bending Loss . . . . .	84
F.2	2-Mode Fibre Amplification Measurement . . . . .	91
F.3	Fibre Power Calibration Measurement . . . . .	101

## LIST OF FIGURES

1.1	Numerical solution of the eigenvalue equations for modes against wavelength, Numerical Aperture and core radius. . . . .	5
1.2	Energy level for lasing of rare-earth elements (Love, 2011, sl 2) . . . . .	5
1.3	Cladding-pumped laser (Love, 2011) . . . . .	5
1.4	Ytterbium doped fibre laser set-up for Q-switched operation (Renaud et al., 1999) . . . . .	6
1.5	Gold-embedded silica grating coupler with a normal incident pump applied (Huang et al., 2012) . . . . .	6
2.1	Modal separation and selection (Shaklan, 1991) . . . . .	12
2.2	Interpretation of the description of the configuration used by Andermahr et al. (2008b) . . . . .	12
2.3	Spatially and spectrally resolved imaging set-up (Nicholson et al., 2008) . . . . .	13
2.4	Spherical coordinate system and its relationship to the fibre for far-field calculations (Gambling et al., 1976a) . . . . .	14
2.5	The set-up for measuring the far-field intensity partner (Michtchenko and Nava, 2006) . . . . .	15
3.1	Fibre bound modes . . . . .	18
3.2	U against V Plot of the Eigenvalues for a step profile fibre using the weak guidance approximation for the $HE_{lm}$ , $TE_{lm}$ , $EH_{lm}$ (as appropriate) modes (Snyder and Love, 1983, pp 254,320) . . . . .	19
3.3	Parameter arrangement for the analysis of power in the modes in a length of amplifying fibre . . . . .	20
3.4	Intensity profile for two modes (an elevation view) . . . . .	21
4.1	Function diagram of the fibre mode power measurement device . . . . .	24
4.2	Function Diagram for the Level 2 Data Output Format Management function decomposition . . . . .	25
4.3	Total System Block Diagram, showing how hardware and software within hardware maps on to the functional decomposition. . . . .	27
4.4	As-built test system key components . . . . .	27
4.5	Layout of the system for a bend radius test of 2-mode fibre, showing up to the Goniometric Radiometer interface to the system. . . . .	28
4.6	Layout of the system for a bend radius test of 2-mode fibre undergoing few-mode power amplification, showing up to the Goniometric Radiometer interface to the system. . . . .	28
4.7	Second Mode Creation in the fibre alignment jig . . . . .	28
5.1	Run 7 on 3.7m LMA-YDF-15/123, one of the two mode tests made prior to the power amplification test, showing the effect of the centre of the modes being offset . . . . .	29
5.2	Power level accuracy test . . . . .	30
5.3	Bend radius tests . . . . .	31
5.4	Calculated bend loss for LMA-GSF-15/123 . . . . .	32
5.5	Ytterbium Doped Fibre Amplifier (YDFA) pump power to gain relationship . . . . .	33
5.6	Gain Coefficient . . . . .	33
B.1	Classification tree for the power detector . . . . .	44

B.2	Calculation of $r = f(\phi)$ for a line in polar coordinate system . . . . .	47
B.3	Calculation of the distance, $d$ , between two points . . . . .	49
B.4	Classification tree for the power profile formula . . . . .	49
B.5	Translation of a mode from the origin to an offset (second mode shown shifted here) . . . . .	51
D.1	Fundamental mode field profile . . . . .	57
D.2	Second mode field profile . . . . .	58
E.1	Example 3-dimensional plot of the mapping of theoretical to measured power. Gain=80dB, with axis swap of second mode excitation direction on the Ericsson FSU 995 PM that was used to hold the fibres. . . . .	79
F.1	Test set-up for measuring power under differing bending radii using the Photon Inc. Goniometric Radiometer . . . . .	85
F.2	Injection of source laser into fibre for two modes . . . . .	86
F.3	Two mode injection far-field rectangular view of the LMA-GSF-15-123 fibre for $\phi = 0^\circ$ and $\phi = 90^\circ$ . . . . .	87
F.5	Two mode injection far-field rectangular view of the LMA-GSF-15-123 fibre for $\phi = 0^\circ$ and $\phi = 90^\circ$ with the second mode excited orthogonally to that originally . . . . .	87
F.4	Orthogonal injection of source laser into fibre for two modes . . . . .	88
F.6	Bending response of the 2 mode fibre . . . . .	89
F.7	Power for bend radius above the radius where the second mode is stripped out . . . . .	89
F.8	Few-mode power amplification test set-up . . . . .	92
F.9	Run 7 two mode power measurement recorded for the test set-up validation on the 3.7m fibre, where the blue profile is the theoretical and the red profile is that measured with the goniometric radiometer. . . . .	94
F.10	Re-run recording plot of the bend radius against power in each of the modes for the injection of 2 modes into the 2.4m fibre . . . . .	94
F.11	Run 3 two mode power measurement recorded for the 1+1 combiner joined to the 2.4m fibre test set-up validation, where the blue profile is the theoretical and the red profile is that measured with the Radiometric Goniometer. . . . .	97
F.12	Power diode output response against current . . . . .	98
F.13	Power measurements from the gain fibre with the pump laser switched on . . . . .	99
F.14	Typical amplified signal output for the first round of amplified signal measurements (in both cases, radius=280mm, pump power=0.58W) . . . . .	99
F.15	Ytterbium-doped fibre amplifier amplification comparisons . . . . .	102
F.16	Pump power to Ytterbium-doped amplifier gain relationship . . . . .	102
F.17	Power level accuracy test . . . . .	103

## LIST OF TABLES

4.1	Alternatives for Power Level Detection . . . . .	25
4.2	Alternatives for Power Modelling . . . . .	26
A.1	Customer statements and interpreted needs . . . . .	41
A.2	Interpreted Needs Hierarchy . . . . .	42
A.3	Importance Ratings for Primary Customer Needs . . . . .	43
B.1	Option design for each of the functional blocks . . . . .	44
B.2	Concept screening for the Power Detector . . . . .	45
B.3	Match rating for the power detector against interpreted customer needs (1=much worse, 3=same, 5=much better) . . . . .	46
B.4	Concept screening for the power profile formula . . . . .	50
B.5	Match rating for the power profile formula against interpreted customer needs (1=much worse, 3=same, 5=much better) . . . . .	50
F.1	Specifications for Nufern LMA-GSF-15/123 fibre . . . . .	84
F.2	Details of the recordings for the injection of 1 mode into the fibre . . . . .	86
F.3	Details of the recordings for the injection of 2 modes into the fibre . . . . .	87
F.4	Details of the recordings for the injection of 2 modes into the fibre in the orthogonal direction to that in Table F.3. . . . .	88
F.5	Power measurements for the bend radius testing of few mode fibre . . . . .	88
F.6	Specifications for Nufern LMA-YDF-15/130 fibre . . . . .	92
F.7	Details of the bend radius re-run recordings for the injection of 2 modes into the 3.7m fibre . . . . .	95
F.8	Details of the bend radius re-run recordings for the injection of 2 modes into the 2.4m fibre . . . . .	96
F.9	Power measurements from the gain fibre with the pump laser switched off . . . . .	96
F.10	Optical Spectrum Analyser measurements of the power in the system with and without amplification (bend radius=280mm for all runs except for the first entry, which was a direct connection between the 1060nm source and the OSA). . . . .	97
F.11	Second set of Optical Spectrum Analyser measurements of the power in the system (bend radius ~280mm for all runs). . . . .	100
F.12	Second run for the unamplified signal - baseline test . . . . .	100
F.13	Second run for the amplified signal for one mode . . . . .	101
F.14	Second run for the amplified signal for 2 modes . . . . .	105
F.15	Details of the bend radius recordings for the power calibration test . . . . .	106

# CHAPTER 1: INTRODUCTION

## 1.1 What's the Problem?

There is a fair bit of interest around the world at the moment in few-mode fibre in order to increase data transmission rates. The Australian National University (ANU) is amongst those investigating techniques, with a doctoral research project currently investigating communication using several modes in few-mode fibre (see, for example, Love and Riesen (2012); Riesen et al. (2012); Riesen and Love (2011)). Work to date outside of the ANU on the same problem has been successful using bulk optics and Multiple-Input Multiple-Output (MIMO) technology for separating the modal data at the far end of the transmission system. These few-mode fibres need each mode to have similar (that is, relatively even) power levels as they are amplified periodically along a system.

AOFR Pty Ltd is currently researching and refining the development of cladding-pumped, few-mode fibre amplifiers. Neodymium- or ytterbium-doped double-clad fibre can be used for increasing output power to a few kW (Paschotta, 2012), but erbium is also used (see Section 1.4 for some background on cladding-pumped fibre amplifiers). In AOFR's case, the objective is for as much of the pump power as possible to be applied to the fundamental mode, for mainly industrial applications.

In addition, large modern data centres incorporate extensive internal deployment of fibre. For instance, within the Australian Government, large departments such as the Department of Human Services employ many thousands of kilometres of fibre linking hundreds of servers. At the present point in time, around fifty per cent of the fibre used in the leading edge data centres is single-mode, the rest being multimode, with that ratio increasing in the favour of single-mode, to accommodate the bandwidth and speed required. Moore's law applies to data centres, both in terms of increasing processing density and increasing speed of communications required. Communications distances within these data centres are in the order of a few hundred metres at most and allowable mainframe Sysplex<sup>1</sup> timing delays impose a practical limit on distance between high-speed 'active-active' data centres to less than 20km. As a consequence, and unlike with national and global communications trunks, attenuation in the fibre is not a significant issue.

It is not easy to replace data centre fibre once it is put in place particularly as the cable trays fill up over time. However, it would be a straightforward matter as a part of standard communications equipment upgrades, to replace single-mode switches with few-mode switches that have Small Form-factor Pluggable (SFP) transceivers operating at a shorter wavelength, thus reusing the existing single-mode fibre at a lower wavelength for higher-density, few-mode based communications.

The objective of this work is to develop a power amplification measurement technique to quantify the power in each mode of few-mode fibre using cladding mode pumping for their amplification. This would achieve the business goal of developing a fibre power meter for measuring modal power amplification that can be used for measuring the amplification (or, at least, the relative amplitudes) of power in the fundamental mode and the higher-order modes in a low-power, cladding-pumped data transmission system Erbium-Doped Fibre Amplifier (EDFA) to determine the evenness of power spread across the modes. It would also achieve the business goal of a fibre power meter for a cladding pumped high power laser to determine the degree of bias of power toward the fundamental mode.

---

<sup>1</sup>An IBM mainframe-to-mainframe connection, including communications protocol (XCF), used to synchronise and control the machines such that they and their storage can be used as a single logical machine.

## 1.2 History and Characteristics of Optic Fibre

### 1.2.1 Reinventing Glass as a Pure Substance

In 1955, at the encouragement of Dr Basil Hirschowitz at the University of Michigan, Prof. Wilbur Peters and his student, Lawrence (Larry) E. Curtiss, who was studying as an undergraduate physicist, developed the first cladded optical fibre for use in a gastroscope (Curtiss et al., 1957; Zorn, 2009). The work was based on prior papers published by van Heel, Hopkins, Kapany and, indirectly, O'Brien (Hecht, 2004, pp 46-66). This fibre was assembled from a glass rod of higher refractive index being inserted into a glass tube of lower refractive index, heated to near melting point, then drawn down from one end into a thin fibre. This technique came to be known as the 'rod-in-tube method' for fibre fabrication. It was the first time that a glass core had been clad in a cladding of lower refractive index glass (Zorn, 2009).

In the late 1950s, Dr Charles Kao, an electrical engineer began working at STC in Harlow, UK, and in 1966 he and his colleague George Hockham observed that a very pure glass single-mode (but could be multimode) waveguide could propagate light with losses below  $20\text{dB}/\text{km}$  (Kao and Hockham, 1966; Davis and Murphy, 2011). While Kao and Hockham (1966) did measure the losses in various materials, they did not have the low-loss glass available to them for testing. This low loss was achieved in fibre by Kapron et al. (1970) using  $632.8\text{nm}$  light in  $3 - 4\mu\text{m}$  core diameter single-mode fibre of a few hundred metres in length, and they calculated they should have a scattering loss coefficient in the order of  $5\text{dB}/\text{km}$  at that wavelength ( $7.2\text{dB}/\text{km}$  was measured). After an initial provisional patent registration in 1971, Graeme Ogilvie at the CSIRO reported in *Electronics Letters* on tetrachloroethylene-based liquid-core multimode fibre, which had a loss of  $6.5\text{dB}/\text{km}$  at  $1280\text{nm}$ , in 1972 and subsequently installed a  $1\text{km}$  length at the ANU in 1974 (Ogilvie et al., 1972; Tucker, 2005; Love, 2009a, sl 12). Current lowest loss in single-mode fibre is around  $0.17\text{dB}/\text{km}$  at  $1550\text{nm}$  wavelength (Davis and Murphy, 2011).

In the 1970s and throughout the 1980s, a tremendous amount of development work was done to advance fibre optics to the point where it was commercially deployed, initially mostly for long haul communications, but also for non-communications applications. There was, for instance, work done by Petermann (1979) on fibre splicing and the wavelength dependence on the amount of loss in multimode fibre, and work done by Byron and Pitt (1985) on power transmission limits when using the fibre for laser welding. Originally installed as a back-up video link, fibre optics were first used as the main transmission link for a live television production in the 1980 Winter Olympics due to its superior quality and reliability over the copper-based link (Jachetta, 2008).

### 1.2.2 Fibre Mathematics

A fair bit has been written about fibres, initially in papers written in scientific journals such as *Applied Optics*, *IEEE Transactions on Communications*, *IEEE Transactions on Electron Devices*, *Electronics Letters*, *Journal of Lightwave Technology*, *Journal of the Optical Society of America*, *Optics Express*, *IEEE Photonics Journal* and *IEEE Photonics Technology Letters*. This information has made its way into reference books such as "Optical Waveguide Theory" by Snyder and Love (1983) (which mostly directly cites and references published papers) and "Photonic Devices" by Liu (2005) (which predominantly references other text books to summarise the material). Additionally, a number of these papers refer back to work by James Clerk Maxwell (a clear and concise description of Maxwell's equations can be found in Fleisch (2008)), whose equations form the foundation of optical waveguide theory.

Amongst the immense history of literature describing the mathematics (some mentioned in Section

1.2.1 above) is a paper by Gloge (1971) (itself containing a summary of prior work) that outlines some of the mathematics involved in determining the modes in a weakly guiding fibre. Gloge (1971), using the papers by Snyder (1969a,b), outlines the formulae for  $V$ ,  $U_j$  and  $W_j$  (which are also defined in Snyder and Love (1983, pp 226-228)) and then goes on to describe the criteria for weak guidance, namely that  $\Delta = (n_c - n)/n \ll 1$  (where Gloge defines  $n_c$  as the core index and  $n$  as the cladding index). With weak guidance, the modes have their transverse field polarised in one direction, and are known as Linearly Polarised (LP) modes, with a characteristic equation of  $U [J_{l-1}(U)/J_l(U)] = -W [K_{l-1}(W)/K_l(W)]$  (Gloge, 1971).

### 1.2.3 Multi-Mode Fibre

Although single-mode fibres were developed by Corning in 1970, multimode fibres initially dominated the market due to the lack of coupling of transmitters and receivers into single-mode, consequential to the core diameter of several micrometres (Hecht, N.D.). Even today, experience is that single-mode Small Form-factor Pluggable (SFP) transceivers (which cost around \$600 each (I-Tech, 2012)) are quite a bit more expensive than those for multimode (which cost around \$200 each (Router-Switch, 2012)), due to the typically higher power level (needed for their predominant use in long-distance transmission) and cost of fabrication of the 1550nm laser in the single-mode SFP.

As noted above, after four years of struggle, Keck, Schultz and Maurer at Corning hit upon the formula for the fibre material, which involved vapour deposition inside a fused silica tube, a process invented by Dr Frank Hyde, achieving 17dB/km in August 1970 (Keck, 2000). Keck and Schultz (1973) and Carpenter (1974), from Corning, were granted patents for the chemical vapour deposition (CVD) process. Sommer et al. (1976) subsequently reported on the use of  $P_2O_5 - GeO_2 - SiO_2$  deposited via CVD on the inside of Corning code 7913 glass, which they measured to have 10ppm of  $Fe$  impurity. The resultant  $63\mu m$  core diameter ( $110\mu m$  cladding diameter) multimode fibre had a loss of  $4.0dB/km$  at  $820nm$  and a loss of  $1.8dB/km$  at  $1060nm$ .

In 1972, Dr Don Nicol and colleagues at Amalgamated Wireless Australasia (AWA) Limited in Sydney commenced work on producing low loss optical fibres, initially in conjunction with the CSIRO, culminating in using the chemical vapour deposition (CVD) process for their manufacture. They did a trial of a 2.3 km, 3-fibre link operating at 6MBps at a Department of Defence establishment in St Marys, NSW, in 1977, which reported total end-to-end losses of up to  $7dB/km$  ( $3.6dB/km$  at  $850nm$  before cabling - the difference attributed to micro-bending) (Nicol et al., 1978). It used a phospho-silicate ( $\sim 7SiO_2 : 1P_2O_5$ ) glass core, a small cladding of borosilicate ( $7SiO_2 : 1B_2O_3$ ) glass, an outer cladding of either pure silica or VYCOR (Corning  $24SiO_2 : 1B_2O_3$  glass) and a coating of polyurethane, with the fibres threaded through a small cavity in a steel wire reinforced nylon coated polythene cable (Nicol et al., 1978).

### 1.2.4 Single-Mode Fibre

As briefly discussed in Section 1.2.1, Kao and Hockham (1966) postulated that single-mode fibre could support greater bandwidths (1GBps) than alternative communications methods, even operating at (what is now extremely conservatively) a loss of just under  $20dB/km$ . In 1983, Corning introduced their SMF-21 single-mode fibre, then introduced their famous and still commonly used SMF-28 single-mode fibre in 1986, with SMF-28e being introduced in 2001 (Corning, 2012).

Bassett et al. (2004) noted that single-mode fibre is not truly single-mode because the supported mode is the  $HE_{11}$  mode, which is two-fold degenerate by having two polarisation states. In 2003, Bassett et al.

(2004) submitted a patent application for a single-mode fibre design that guides the optical signal in such a way as to only occupy one non-degenerate  $TE_{01}$  mode. This design contains a hole through the core and the inventors claim the core can be set such that its effective refractive index guides the  $TE_{01}$  mode but is below the refractive index of the cladding region for the  $TM_{01}$  mode and therefore does not guide it.

## 1.2.5 Wavelength Division Multiplexing (WDM)

After Nippon Telegraph and Telephone (NTT) produced low-loss single-mode fibre with attenuation of 0.2dB/km at 1550nm in 1978, Will Hicks set about devising and patenting wavelength division multiplexing (WDM), using seed capital from Corning to fund his start-up, 1984 Inc. (Hecht, 2004, pp 188-189). In 1995, Bell Labs at Crawford Hill built a demonstration system that packed 340 Gb/s down one single-mode fibre with the use of WDM, and by early 1996 had increased the capacity to 1 Tb/s over 55km of fibre through a 50 channel WDM (Hecht, 2004, pp 234-235). That was followed shortly afterwards by 1.1 Tb/s over 150km of fibre through a 55 channel WDM and NTT Laboratories sent 1 Tb/s over 40km of fibre through a 10 channel WDM (Hecht, 2004, pp 235). To be truly successful, WDM needed EDFAs and dispersion compensating fibre, technology that had been completely developed by 1995, just in time for the Internet bubble (Hecht, 2004, pp 246-247).

## 1.3 Packing It In With Few-Mode Fibre

Few-mode fibre work is in its early days with, for instance, work being done by Randel et al. (2011), Koebele et al. (2011b) and Ip et al. (2011). In those cases, disentangling the modes at the receiving end has been a problem that they have left to electronics in the form of a Multiple-Input Multiple-Output (MIMO) algorithm executed by a digital signal processor. Also in 2011, Riesen and Love (2011) claim to have designed the first practical few-mode fibre with virtually zero inter-modal dispersion.

Few-mode fibre needs a larger core diameter when compared to single mode and the size required can be readily determined from plots of the normalised frequency (also known as the fibre parameter),  $V$ , against the modal parameter,  $U$ , as shown in Figure 3.2 and rearranged to show the relationship between modes and core radius in Figure 1.1. The curves are produced in accordance with the formulae outlined in Section 3.2. For instance, at 1550nm, Corning SMF-28 has a core diameter of  $8.2\mu\text{m}$  and a Numerical Aperture (NA) of 0.14 (Corning, 2011), which has  $V = (2\pi \times 4.1 \times 10^{-6}) / (1550 \times 10^{-9}) \times 0.14 = 2.404$ . From the curves, it supports just the  $HE_{11}$  mode at this value, making it single mode.

## 1.4 Optical Fibre In-Line Amplification

### 1.4.1 Erbium Doping

Fibre-based amplification started from Eli Snitzer's work in the 1960s, when he doped fibre cores with the rare earth element neodymium (Hecht, 2004, pp213-214). After experimenting with neodymium and perfecting the process of solution doping rare earths into silica, Simon Poole and Dave Payne from the University of Southampton determined that erbium was the dopant required for the 1550nm single mode band. In 1985 the Erbium Doped Fibre Amplifier (EDFA) was born (Mears et al., 1986; Poole et al., 1985; Mears et al., 1985; Hecht, 2004).

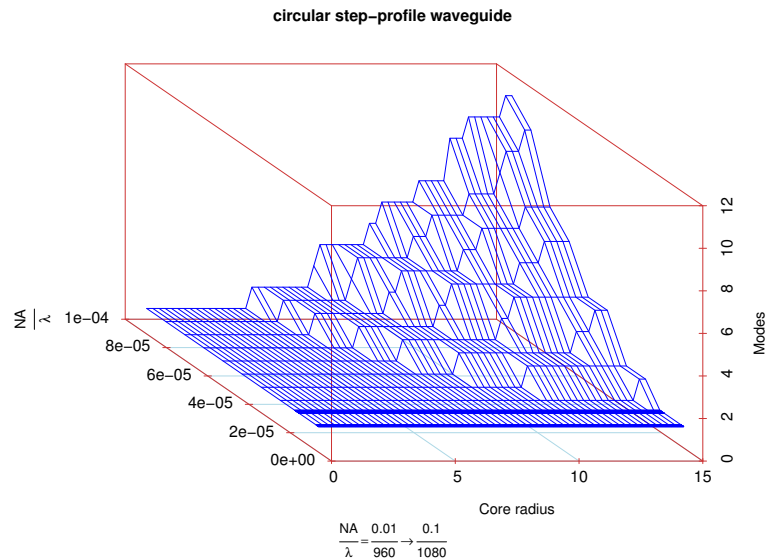


**Figure 1.1:** Numerical solution of the eigenvalue equations for modes against wavelength, Numerical Aperture and core radius.

A rare earth optical amplifier works by exciting the rare earth with light at a specific wavelength, known as the “pump wavelength”, to raise the energy in the electrons from their ground state to the excited state. When the electrons’ energy drops back to the ground state via a meta-stable state, which occurs with a rare-earth element such as erbium or ytterbium, it gives off a photon at a longer wavelength. The wavelength is longer as a consequence of the energy lost being lower between the meta-stable excited state and the ground state. This process is shown in Figure 1.2. A typical single-mode Erbium-Doped Fibre Amplifier has its pump power coupled in at one end using a Wavelength Division Multiplexing single mode coupler and any residual power either similarly coupled out or otherwise filtered (Love, 2011).

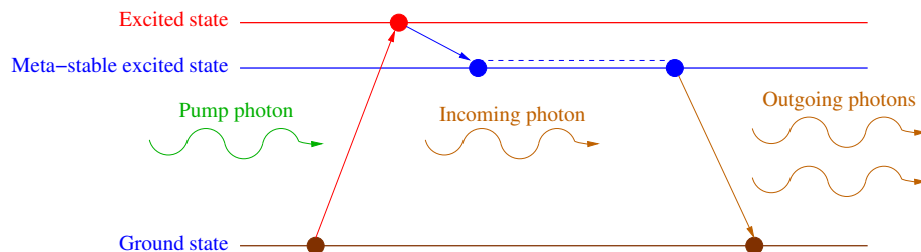


**Figure 1.2:** Energy level for lasing of rare-earth elements (Love, 2011, sl 2)

Cladding pumping is achieved as per Figure 1.3. Here, to couple the large amounts of optical energy in, the cladding modes (that is, those modes whose fields extend across both the core and cladding) are excited. The cladding is built to be highly multimode. Amplification is increased by writing Bragg gratings into the ends of the pump fibre to act as partial reflectors (Love, 2011).

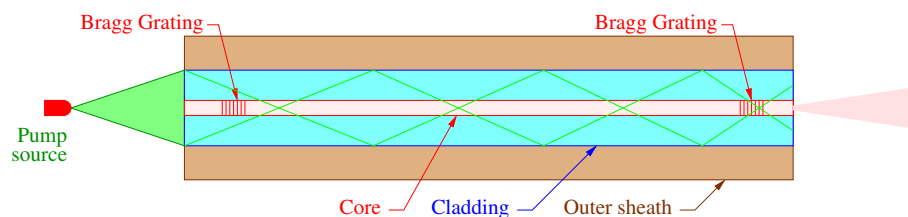


**Figure 1.3:** Cladding-pumped laser (Love, 2011)

While the vast majority of double-clad fibre available is ytterbium-doped, erbium-doped fibre is also available. For instance, CorActive (2011) provide models DCF-ER-35/125 and DCF-ER-70/250.

## 1.4.2 Ytterbium Doping

The attractiveness of ytterbium is its wide range of amplification wavelengths, ranging from about 975 to 1200 nm as well as its high power output and high power conversion efficiency (Paschotta et al., 1997). Early work with ytterbium included its use as a co-dopant with erbium by, for example, Fermann et al. (1988), which built on work done by Eli Snitzer in 1966. The use of ytterbium on its own in a laser was described by, for example, Hanna et al. (1988a,b), which built on Eli Snitzer's work in 1962 that had been shelved due to the neodymium work. Subsequent research (for example, Armitage et al. (1989) at BTRL) improved the quality of the laser beam. Building on research on neodymium by Eli Snitzer in 1988 and his cladding pumping reported in 1989, Paschotta et al. (1997) describe the technique of using double-clad fibres for cladding pumped ytterbium amplifiers. These devices originally contained a typically single-mode doped core, surrounded by a multimode (to take high input power because of the larger spot size) undoped inner cladding (outer core) into which the pump light is launched. Such a ytterbium-based device was demonstrated in 1994, with up to 80 per cent slope efficiency for the pump power (Pask et al., 1994). Subsequently, Paschotta et al. (1997, pp 1055) claimed to have demonstrated an amplifier where the Yb dopant was placed in a ring around the core, resulting in an increase in the pump energy capacity.

Two cladding techniques are typically used, namely the mainstream use of mode-shaping optics to transform the line-shaped laser diode array optical beams into square or circular shaped modes for launch into double-clad fibre, and butt-coupling of the individual laser diode array elements into a fibre array, which are side-launched into the double-clad fibre via a tapered fibre bundle coupler (Huang et al., 2012). The method used by Renaud et al. (1999) couples 2W of power from diode laser into the inner cladding at each end of a length of of a double clad ytterbium fibre through a carefully tapered silicone rubber clad fibre, as shown in Figure 1.4. Huang et al. (2012) proposed a method that side-launches light from a 1cm wide laser diode array into double clad ytterbium fibre through a grating coupler as shown in Figure 1.5. To minimise thermal expansion effects and the backward-diffraction of light internally reflected at the fibre boundary, a gold-embedded silica grating is used (Huang et al., 2012).

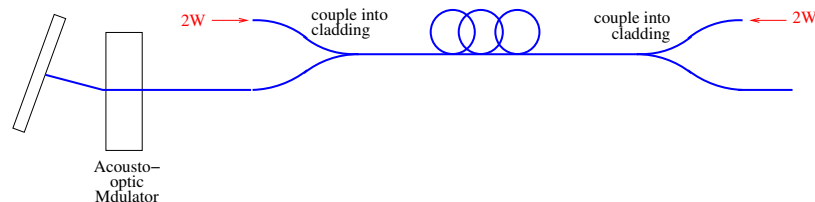


**Figure 1.4:** Ytterbium doped fibre laser set-up for Q-switched operation (Renaud et al., 1999)

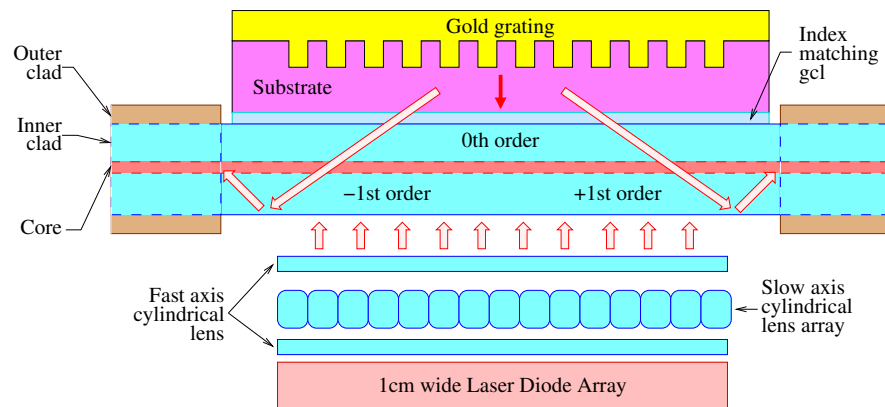


**Figure 1.5:** Gold-embedded silica grating coupler with a normal incident pump applied (Huang et al., 2012)

## CHAPTER 2: LITERATURE REVIEW

### 2.1 Few-Mode Fibre Transmission

Typical single-mode fibre bandwidths are between 10Gbps and 40Gbps, mostly limited by the cost of the Small Form-factor Pluggable transceivers (SFPs) and associated switches. Ip et al. (2011) talk of single-mode fibres operating at 112Gbps and Dense Wavelength Division Multiplexers (DWDMs) operating at 88 channels in their treatise on a 50km three-mode fibre system. As a practical example, the Department of Human Services uses paired configurations of two sets (for redundancy) of three (for data volume) ADVA FSP 3000 128-channel DWDMs to interconnect mainframe processors and mainframe storage between each of its data centres (see ADVA (2011) and Openreach (2012) for details on this device). Koebele et al. (2011b) observed that increasing constellation complexity, for instance by going to a polarisation division multiplexed 16 quadrature amplitude modulation, is the common method of increasing transmission capacity. But it has a detrimental effect of reducing distance. Ip et al. (2011) noted the demonstration by Qian et al of 100Tb/s transmission using the C+L bands for wavelength division multiplexing in single-mode fibre at a spectral frequency of 11b/s/Hz. This was done via a  $370 \times 294$ Gbps polarisation multiplexed 128-state quadrature amplitude modulation orthogonal frequency division multiplexing (PDM-128QAM-OFDM) transmission.

Randel et al. (2011) claim to have demonstrated transmission of  $6 \times 56$ Gb/s over few-mode fibre, using bulk optics to take the input signals and process them into each of the modes and a 6x6 Multiple Input Multiple Output electronic device as a part of the demultiplexer to untangle the 6 streams extracted at the far end. Koebele et al. (2011b) claim to have conducted two mode transmission at 100Gb/s for each mode over a 40km long few-mode fibre. For their mode division multiplexer, they used mode converters that incorporate a liquid crystal-on-silicon spatial light modulator, a digital signal processor using a multiple-input multiple-output algorithm for correct ordering of the demultiplexed signal, and few-mode fibre for transmitting two independent modes via the two degenerate variants of the anti-symmetric  $LP_{11}$  mode. Koebele et al. (2011a) explain that each Linearly Polarised (LP) mode, annotated  $LP_{lm}$ , for the situation where  $l \neq 0$ , has two degenerate variants that are spatially rotated by  $\pi/(2 \cdot l)$  and are considered to have the same propagation constant.

Ip et al. (2011) demonstrated the transmission of mode division multiplexed data from three 88-channel DWDMs which are fed into the  $LP_{01}$  and  $LP_{11}$  (specifically, the  $LP_{11o}$  and  $LP_{11e}$ ) modes of a 50km length of few-mode fibre. Their solution achieved a transmission of 26.4Tb/s. They used phase plates for the few-mode modulation and demodulation, and a  $6 \times 6$  multiple input/multiple output device to sort out the modes at the receiver.

Consideration has been given to the use of polarising fibre to control the mode polarity and thereby allow better separation in few-mode fibres, with research dating back to the 1990s on some aspects (Riesen et al., 2012). Building on this historical work, Riesen et al. (2012) devised a polarisation maintaining elliptical fibre arrangement that can use asymmetric Y-junction splitters to separate out the modes and avoid the use of MIMO technology, thereby keeping costs down on SFP manufacture and compatibility. The approach would allow multiplexing three or possibly four modes. However, this approach would require the replacement of existing fibre installation, so would be best applied to new (or refitted) data centres at the time of product commercialisation.

Love and Riesen (2012) proposed an alternative approach that is applicable to very few (up to four or five) modes that uses asymmetric multi-arm Y-junctions. This approach, while modelled at 1550nm (for convenience), could be applied to existing data centre deployment of single-mode fibre by reducing the

wavelength down from 1550nm to a level to yield two or three modes, notwithstanding limits that may be imposed by material dispersion. This should yield a low cost solution that could be readily and cheaply integrated into a SFP transceiver device for data centres, while also being a practical alternative at the 1550nm wavelength for large distance metropolitan area and long-haul networks.

## 2.2 Modal Power Theory

Gloge (1971) derived expressions for the power in a mode as per Equation 2.1, where the core power  $P_{co}$  is defined as per Equation 2.2 and the cladding power  $P_{cl}$  is defined as per Equation 2.3 and the small difference between the core refractive index  $n_{co}$  and the cladding refractive index  $n_{cl}$  is ignored.

$$P = P_{co} + P_{cl} = \left(\frac{V^2}{U^2}\right) \left(\frac{1}{\kappa}\right) \left(\frac{\pi\rho^2}{2}\right) \left(\frac{Z_0}{n_{cl}}\right) E_l^2 \quad (2.1)$$

$$P_{co} = \left[1 + \left(\frac{W^2}{U^2}\right) \left(\frac{1}{\kappa}\right)\right] \left(\frac{\pi\rho^2}{2}\right) \left(\frac{Z_0}{n_{co}}\right) E_l^2 \quad (2.2)$$

$$P_{cl} = \left[\left(\frac{1}{\kappa}\right) - 1\right] \left(\frac{\pi\rho^2}{2}\right) \left(\frac{Z_0}{n_{cl}}\right) E_l^2 \quad (2.3)$$

In these equations,  $V$ ,  $U$  and  $W$  are the normalised frequency, core scalar mode (Bessel function argument) and cladding scalar mode (modified Hankel function argument) fibre parameters (see Section 3.2.3 for a full definition),  $\rho$  is the core radius,  $\kappa \approx 1 - \left(\frac{1}{V}\right)$  for large  $W$ ,  $Z_0$  is the plane wave impedance in a vacuum and  $E_l$  is the electric field strength at the interface (Gloge, 1971).

## 2.3 Amplification Power Theory

Early during Erbium-doped fibre amplifier development, Saleh et al. (1990) developed a few general equations for the power in an arbitrary number  $N$  of input rays, wavelength  $\lambda_k$  and power  $P_k(z, t)$  (measured at photon division time) travelling through the amplifier of length  $L$  at direction  $u_k$  (where  $z = 0 \Rightarrow u_k = 1$ ;  $z = L \Rightarrow u_k = -1$ , that is, it indicates if the beam's direction is forward or backward through the fibre). They calculate the power in Equation 2.4 where  $P_k^{in}$  is input power,  $P_k^{out}$  is output power of ray number  $k$ ,  $\alpha_k$  is the absorption constant (Equation 2.5) and  $P_k^{IS}$  is the intrinsic saturation power of the  $k^{th}$  ray (Equation 2.6).

$$P_k^{out} = P_k^{in} e^{-\alpha_k L} e^{\frac{(P_k^{in} - P_k^{out})}{P_k^{IS}}} \quad (2.4)$$

$$\alpha_k = \rho \Gamma_k \sigma_k^a \quad (2.5)$$

$$P_k^{IS} = \frac{A}{\Gamma_k (\sigma_k^e + \sigma_k^a) \tau} \quad (2.6)$$

In Equation 2.5 and Equation 2.6,  $\rho$  is the density of active atoms,  $\Gamma_k$  is the containment component of the fibre amplifier at  $\lambda_k$ ,  $\sigma_k^a$  is the cross-sectional area for absorption,  $\sigma_k^e$  is the cross-sectional area for emission, and  $\tau$  is the spontaneous existence time of the higher order.

Pedersen et al. (1990)'s correspondence, which should be read along with the paper by Bjarklev et al. (1990), reported a design for measuring power, including amplified spontaneous emission. Their design has no calculation for each ray.

Snyder and Love (1983) describe a method that uses Maxwell's equations for fibre. This is much simpler than the approach taken by Saleh et al. (1990), with the work for weakly guiding fibres based around Equation 2.7, where  $\mathbf{h}_t$  is the transverse magnetic field,  $\mathbf{e}_t$  is the transverse electric field,  $\hat{\mathbf{z}}$  is the unit vector parallel to the wave-guide axis,  $n_{co}$  is the refractive index of the wave-guide's unbounded uniform medium and  $\epsilon_0$  and  $\mu_0$  are the electric permittivity of free space and the magnetic permeability of free space constants respectively (Snyder and Love, 1983, pp 281). The electric ( $\mathbf{E}(x, y, z)$ ) and magnetic ( $\mathbf{H}(x, y, z)$ ) fields for bound modes are given by Equation 2.8 and Equation 2.9, where  $\beta$  is the propagation constant and  $t$  and  $z$  denote transverse and longitudinal ("z"-direction) components respectively in the wave-guide's Cartesian coordinate system (Snyder and Love, 1983, pp 282).

$$\mathbf{h}_t = \left( \frac{\epsilon_0}{\mu_0} \right)^{\frac{1}{2}} n_{co} \hat{\mathbf{z}} \times \mathbf{e}_t \quad (2.7)$$

$$\mathbf{E}(x, y, z) = \mathbf{e}(x, y) \exp(i\beta z) = (\mathbf{e}_t + \hat{\mathbf{z}}e_z) \exp(i\beta z) \quad (2.8)$$

$$\mathbf{H}(x, y, z) = \mathbf{h}(x, y) \exp(i\beta z) = (\mathbf{h}_t + \hat{\mathbf{h}}h_z) \exp(i\beta z) \quad (2.9)$$

Considering the application of the condition for weak guidance to the typical commercial grade step-profile fibre (see Snyder and Love (1983, Chapter 14)), Liu (2005) says the power in each mode ( $P$ ) is obtained by integrating the intensity ( $I = 2 \left( E_r H_\phi^* - E_\phi H_r^* \right)$  where  $E_\phi$ ,  $E_r$ ,  $H_\phi$  and  $H_r$  are the electric and magnetic fields (as above, but in cylindrical coordinates) defined as per Equations 2.12-2.15 and \* represents the complex conjugate) over the fibre cross section as described by Equation 2.10, where  $E$  and  $H$  are as previously defined,  $r$  is the radius coordinate and  $\phi$  is the angular coordinate for the fibre's cylindrical coordinate system across core and cladding (Liu, 2005, pp 125-126). Here,  $dA$  can be replaced as per Equation 2.11 (referenced later). In Equations 2.12-2.15,  $\beta$  is the propagation constant,  $\omega$  is the angular frequency,  $\mu_0$  is magnetic permeability of free space as previously defined,  $\eta = \frac{\omega\mu_0 C_m}{\beta A_m}$ ,  $A_m$  and  $C_m$  are fibre constants to be found for the particular mode,  $J_\nu$  is the Bessel function of order  $\nu$ , and the transverse spatial parameter of the guided mode field,  $h$  is given by Equation 2.16, where  $k_{co}^2 = \frac{\omega^2 n_{co}^2}{c^2}$  is the core wave number in terms of the angular frequency  $\omega$ , core refractive index  $n_{co}$  and speed of light in free space  $c$ .

$$P = 2 \int_{A_\infty} (E_r H_\phi^* - E_\phi H_r^*) dA \quad (2.10)$$

$$dA = r d\phi dr \quad (2.11)$$

$$E_\phi = \begin{cases} \frac{i\omega\mu_0}{h} J_1(hr) & TE_{0n} \text{ modes} \\ 0 & TM_{0n} \text{ modes} \\ -\frac{i\beta}{h} \left[ \frac{1+\eta}{2} J_{m-1}(hr) + \frac{1-\eta}{2} J_{m+1}(hr) \right] \sin(m\phi) & HE_{mn}, EH_{mn} \text{ modes} \end{cases} \quad (2.12)$$

$$E_r = \begin{cases} 0 & TE_{0n} \text{ modes} \\ -\frac{i\beta}{h} J_1(hr) & TM_{0n} \text{ modes} \\ \frac{i\beta}{h} \left[ \frac{1+\eta}{2} J_{m-1}(hr) - \frac{1-\eta}{2} J_{m+1}(hr) \right] \cos(m\phi) & HE_{mn}, EH_{mn} \text{ modes} \end{cases} \quad (2.13)$$

$$H_\phi = \begin{cases} 0 & TE_{0n} \text{ modes} \\ -\frac{i\omega\varepsilon_1}{h} J_1(hr) & TM_{0n} \text{ modes} \\ \frac{i\omega\varepsilon_1}{h} \left[ \frac{1+\eta\frac{\beta^2}{k_1^2}}{2} J_{m-1}(hr) - \frac{1-\eta\frac{\beta^2}{k_1^2}}{2} J_{m+1}(hr) \right] \cos(m\phi) & HE_{mn}, EH_{mn} \text{ modes} \end{cases} \quad (2.14)$$

$$H_r = \begin{cases} -\frac{i\beta}{h} J_1(hr) & TE_{0n} \text{ modes} \\ 0 & TM_{0n} \text{ modes} \\ \frac{i\omega\varepsilon_1}{h} \left[ \frac{1+\eta\frac{\beta^2}{k_1^2}}{2} J_{m-1}(hr) + \frac{1-\eta\frac{\beta^2}{k_1^2}}{2} J_{m+1}(hr) \right] \sin(m\phi) & HE_{mn}, EH_{mn} \text{ modes} \end{cases} \quad (2.15)$$

$$h^2 = k_{co}^2 - \beta^2 \quad (2.16)$$

On the other hand, Snyder and Love (1983, pp292-293) define the modal power  $\tilde{P}$  for a weakly guiding waveguide by Equation 2.17.

$$\tilde{P} = \begin{cases} |a|^2 \frac{n_{co}}{2} \left( \frac{\varepsilon_0}{\mu_0} \right)^{\frac{1}{2}} \int_{A_\infty} \mathbf{e}_t^2 dA & \text{arbitrary} \\ |a|^2 \frac{n_{co}}{2} \left( \frac{\varepsilon_0}{\mu_0} \right)^{\frac{1}{2}} \int_{A_\infty} \Psi^2 dA & \text{non circular} \\ \pi \rho^2 |a|^2 n_{co} \left( \frac{\varepsilon_0}{\mu_0} \right)^{\frac{1}{2}} \int_0^\infty F_l^2 R dR & \text{circular} \end{cases} \quad (2.17)$$

In this equation,  $\tilde{\cdot}$  denotes zero order, or weak guidance, fields,  $\varepsilon_0$  and  $\mu_0$  are constants as previously defined,  $n_{co}$  is the core refractive index,  $a$  is the modal amplitude coefficient,  $\mathbf{e}_t$  is the modal field as previously defined (see also Section 3.2.1),  $\Psi$  is the solution of the scalar wave equation (see Section 3.2.2),  $l = 0, 1, 2, \dots$  and  $F_l$  is a fibre variable that satisfies Equation 2.18 (see Snyder and Love (1983, pp 287-288)).

$$\left\{ \frac{d^2}{dr^2} + \frac{1}{r} \frac{d}{dr} + k^2 n^2(r) - \frac{l^2}{r^2} - \tilde{\beta}^2 \right\} F_l = 0 \quad (2.18)$$

The differences between Equation 2.10 and Equation 2.17, principally  $\frac{1}{2} n_{co} \sqrt{\frac{\varepsilon_0}{\mu_0}}$ , relates to the constants and variables being built into the constituent components of Equation 2.10.

Both Snyder and Love (1983) and Liu (2005) observe that not all of the power is in the core and provide the ratio either in terms of the V parameter (normalised frequency) or as a straight ratio. Snyder

and Love (1983, pp 319) express it as per Equation 2.19 (where  $\tilde{\eta}$  is the fraction of power in the core,  $V$  is the fibre parameter,  $\tilde{U}$  and  $\tilde{W}$  are the scalar mode parameters for the core and cladding, and  $K$  is the modified Bessel function of the second kind of order  $m$ ), and equivalently Liu (2005, pp 134) expresses it as per Equation 2.20 (where  $\Gamma_{mn}$  is the fraction of power in the core for the particular ( $LP$ ) mode ( $mn$ ) in question or the confinement factor as he calls it,  $\rho$  is the core radius,  $h$  is the transverse spatial parameter of the guided mode field in the core region and the eigenvalue  $\gamma$  is the transverse spatial decay parameter of the mode field in the cladding region defined by Equation 2.21 where  $k_{cl}^2 = \frac{\omega^2 n_{cl}^2}{c^2}$  is the cladding wave number for the angular frequency  $\omega$ , cladding refractive index  $n_{cl}$  and speed of light in free space  $c$ , and  $\beta$  is the propagation constant).

$$\tilde{\eta} = \frac{\tilde{U}^2}{V^2} \left\{ \frac{\tilde{W}^2}{U^2} + \frac{K_m(\tilde{W})}{K_{m-1}(\tilde{W})K_{m+1}(\tilde{W})} \right\} \quad (2.19)$$

$$\Gamma_{mn} = 1 - \frac{h^2 \rho^2}{V^2} \left[ 1 - \frac{K_m^2(\gamma \rho)}{K_{m-1}(\gamma \rho)K_{m+1}(\gamma \rho)} \right] \quad (2.20)$$

Equating the variables and differences in nomenclature, these two equations are the same.

$$\gamma^2 = \beta^2 - k_{cl}^2 = \beta^2 - \frac{\omega^2 n_{cl}^2}{c^2} \quad (2.21)$$

## 2.4 Power Measurement

Shaklan (1991) has reported a method where a section of a fibre's cladding was stripped using hydrofluoric acid and then re-clad with index matching paraffin oil, causing the modes to spatially diffract through leakage out of the etched section. As per Figure 2.1, the far-field modal rings can be observed leaving the bottom of a glass container housing the paraffin oil and forming against a back plate, consequential to a laser being shone down the fibre from the far end. A collimated laser beam is shone up through the paraffin oil into the side of the fibre to inject a single mode. According to Shaklan, it does not need to be conical to improve selectivity, just so long as it is directed along the cone. The objective of this was to study the effect of side launching a single mode on the rest of the modes in a few-mode (up to about 15 modes) fibre. Shaklan (1991) talks about measuring the power of the modes but his report has no discussion about how this could be achieved.

Andermahr et al. (2008b)'s design uses a mode-selective 3-mirror ring resonator and a polarisation analysis. The 3-mirror ring resonator is used for mode analysis. The polarisation analysis instrument is a quarter-wave plate and a polarising beam splitter. The quarter wave plate is put in front of the polarising beam splitter and the ring resonator. The quarter wave plate is rotating and the height of each beam is measured. They energise a  $25\mu\text{m}$  core diameter fibre at an offset and phase that produces 2 modes. An interpretation of Andermahr et al.'s set-up is given at Figure 2.2. Earlier, Andermahr et al. (2008a) calculated, using a best fit curve, the power  $P$  of the total beam as per Equation 2.22, where  $S_0 \dots S_3$  are the Stokes parameters (determined from the polarising beam splitter and the quarter wave plate) and  $\alpha$  is the angle setting of the quarter-wave plate.

$$P(\alpha) = 0.5 \left[ \left( S_0 + \frac{S_1}{2} \right) + \left( \frac{S_1}{2} \right) \cos(4\alpha) + \left( \frac{S_2}{2} \right) \sin(4\alpha) - S_3 \sin(2\alpha) \right] \quad (2.22)$$

Using this set-up, for two-mode fibre pumped at 976nm and seeded at 1064nm, Andermahr et al.

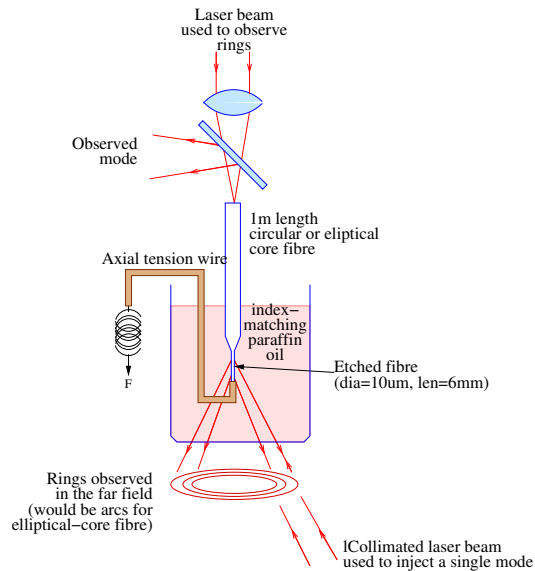


**Figure 2.1:** Modal separation and selection (Shaklan, 1991)

(2008b) observed that, under pumping, the fibre amplifier system's higher-order modes became more orthogonally polarised as pump power was increased, due to maximisation of the gain in the modes.

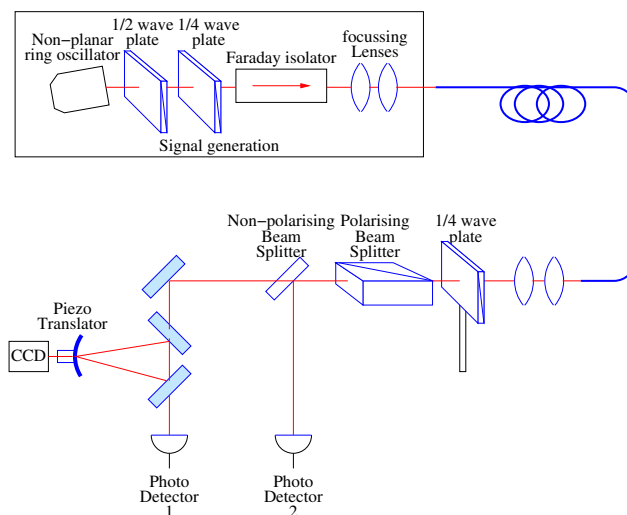


**Figure 2.2:** Interpretation of the description of the configuration used by Andermahr et al. (2008b)

Nicholson et al. (2008) produced a design for measuring the power of each higher-order mode in a few-mode fibre as well as providing a high quality image of the fibre modes. They analysed large mode area fibres with their system, providing better accuracy in determining beam quality than would be obtained by the traditional  $M^2$  parameter measurement. Measuring partially coherent transverse mode contents for bulk optics requires only measuring the transverse illumination intensity profile. As shown in Figure 2.3, Nicholson et al.'s machine had a Ytterbium based broadband optical source, the test fibre, 2 lenses for the image, a polariser instrument, a single-mode probe fibre, an x-y plane scanning platform, an optical spectrum analyser and a computer for information analysis.

On the space locations where 2 different modes overlap, there will be interference patterns caused by phase delay differences between the modes (where "phase delay" is consistently referred to by Nicholson et al. (2008) as "group delay"). There will be a spectral interference pattern from propagation of the broadband source in the fibre and there will be a spatial interference pattern between the fundamental mode and the higher-order mode. The amplitude of the interference fringes is dependent on the relative local amplitudes of the fields. Analysis of the modes is by plotting the Fourier transform of the optical spectrum

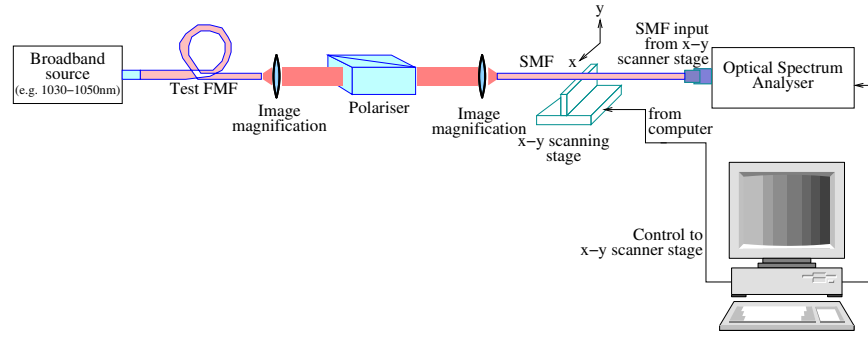


**Figure 2.3:** Spatially and spectrally resolved imaging set-up (Nicholson et al., 2008)

at each pixel and then the amplitudes of the Fourier transforms are summed. The  $x$  axis of the Fourier transform is proportional to the group delay difference between the modes and the length of fibre.

Nicholson et al. (2009) revised their original calculations and results in their 2008 paper by eliminating simplifying assumptions around the frequency independence of scattering into higher order modes. Nicholson et al. (2009) go on to report two equations (see equation 2.23 and equation 2.24) for the power at the overlap, which essentially analyses the intensity of the electric field and assumes that there is a slowly varying static (power spectrum) component ( $I_1(x, y, \omega)$ ) of the fundamental mode (compared to the interference beat frequencies) and a fast oscillating component ( $J(x, y, \omega)$ ) by interference between the 2 electric fields, consequently a low pass Fourier filter can be used for extracting the static component. The other component contains information on all mode fields at the place of measure. The component of interest is accessed by using a Fourier band pass filter at the group delay of the beat frequency of interest.

$$I(x, y, \omega) \simeq I_1(x, y, \omega) + 2\Re \left\{ \sqrt{I_1(x, y, \omega)} E_2(x, y, \omega) \right\} \quad (2.23)$$

$$J(x, y, \omega) \equiv \frac{I(x, y, \omega) - I_1(x, y, \omega)}{2\sqrt{I_1(x, y, \omega)}} \simeq \Re \left\{ \tilde{E}_2(x, y, \omega) \right\} \quad (2.24)$$

In Equation 2.23, the electric field is a function of spatial position and frequency,  $\tilde{E}(x, y, \omega) = \tilde{E}_1(x, y, \omega) + \tilde{E}_2(x, y, \omega)$  where  $\tilde{E}_1(x, y, \omega)$  is the field of the primary mode and  $E_2$  is the other mode that is small when compared to  $E_1$ .  $I$  is the intensity of the relevant mode and  $\Re$  represents the real part. Their analysis defines the power of the higher-order modes relative to the fundamental mode.

The authors explain that their equations break down when multi-path interference is 0dB because the assumption of small power in the higher-order modes completely breaks down.

## 2.5 Far-Field Profiling and Analysis

Gambling et al. (1976a) reported on a process to determine the modal intensity based on analysis of the far-field pattern of a fibre. The research seemed to have stopped after a short while and Campos et al. (1984) think this is because the technology at the time did not allow for easy detection of the first minimum at 40-70dB below the first maximum. The far-field pattern of the  $HE_{11}$  mode is a function of  $\rho$  and  $\Delta n$  (where  $\Delta n = n_{co} - n_{cl}$  is the refractive index difference of the core and cladding and  $\rho$  is the fibre core's radius), just like with multimode fibres. For weak guidance,  $\Delta n \ll n_{co}$  and with reference to Figure 2.4, the normalised far-field distribution in polar coordinates,  $\psi(r, \theta, \phi)$  is given by Equation 2.25, where

$V^2 = U^2 + W^2$ ,  $U$  and  $W$  are arguments of the Bessel and modified Hankel functions as defined above and  $\alpha = k\rho \sin \theta$  (Gambling et al., 1976a,b).

$$|\psi|^2 = \begin{cases} \left[ \frac{U^2 W^2}{(U^2 - \alpha^2)(W^2 + \alpha^2)} \left\{ J_0(\alpha) - \alpha J_1(\alpha) \frac{J_0(U)}{U J_1(U)} \right\} \right]^2 & ; U \neq \alpha \\ \left[ \frac{U^2 W^2}{2V^2} \frac{1}{U J_1(U)} \left\{ J_0^2(\alpha) + J_1^2(\alpha) \right\} \right]^2 & ; U = \alpha \end{cases} \quad (2.25)$$

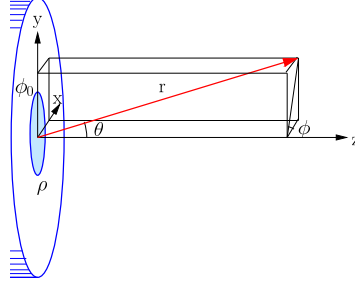


**Figure 2.4:** Spherical coordinate system and its relationship to the fibre for far-field calculations (Gambling et al., 1976a)

From far-field measurements taken by Gambling et al. (1976a), the core diameters were calculated and, for the few tests taken, were in good agreement with core diameters measured through etching.

Given that, in the near-field, the  $LP_{01}$  single-mode is purely transversal in the scalar approximation, Freude and Richter (1986) note the Fourier transform interconnection relation to the easily measured far-field. An alternative to performing the Fourier transform numerically is to use linear fitting to expand the data into a series of Gauss-Laguerre functions, based on the assumption that longitudinal components are negligibly small when compared to transversal amplitudes, so can be treated in a scalar approximation (Freude and Sharma, 1985). Freude and Sharma (1985) claim this method is also less sensitive to noise.

In addition to measuring intensity in the far-field for a single-mode fibre, the Mode Field Diameter (MFD) can also be measured based on the intensity readings (Michtchenko and Nava, 2006). The mode field diameter, which defines the irradiance power distribution per unit area for light entering or exiting the fibre, is derived from an intensity profile that is measured through the use of a photo detector. Michtchenko and Nava (2006) describe the far-field intensity profile for single mode fibre by Equation 2.26, where  $\psi(\theta)$  is the pattern of intensity in angle  $\theta$ ,  $\psi(0)$  is the maximum intensity at  $0^\circ$  and, for the far field angle,  $\sin \theta_f = \frac{\lambda}{\omega_0}$  for wavelength  $\lambda$  and half of the angular distribution  $d_f = 2\omega_0$ .

$$|\psi(\theta)|^2 = |\psi(0)|^2 e^{\frac{-2 \sin^2 \theta}{\sin^2 \theta_f}} \quad (2.26)$$

Michtchenko and Nava (2006) state that the condition  $r \geq z_R = \frac{\pi w^2}{\lambda}$  (where  $z_R$  is Relley's radius and  $w$  is the characteristic radius of the mode field) must be fulfilled to define the angular distribution. Working through a series of steps including the application of the Bessel function of the first kind of order 0 and Hankel transformation, they arrive at Equation 2.27 for interpreting the near field from the far field.

$$E(\rho') = 2\pi \int_0^\infty E_H(q) J_0(2\pi q \rho') q dq \quad (2.27)$$

where  $q = \sin \theta / \lambda$ ,  $E(\rho')$  is the near field and, in relation to the far field,  $E_f(r, \theta)$ , the Hankel transformation  $E_H(\rho) = -j\lambda r \exp(jkr) E_f(r, \theta)$ . Their experimental arrangement, involving a rotation table and a scanning photo-detector, is outlined in Figure 2.5.

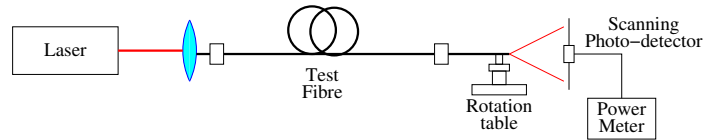


**Figure 2.5:** *The set-up for measuring the far-field intensity partner (Michtchenko and Nava, 2006)*

Michtchenko and Nava (2006) produced some intensity distribution results for the fundamental mode showing noise further out from the the centre, suggesting more than the fundamental mode being present. They claim the results were poor due to bending, join and splicing losses. They also produced a result curve for a new length of SMF-28 that appeared to have a good fit of the experimental profile to that calculated.

Microwave antennas under similar circumstances, for instance at the end of a waveguide, produce similar profile patterns to optical fibre ends (Gambling et al., 1976a). There is a common practice of using far-field approximations for half-power beam width and high power measurements (Rodriguez, 2008, sl 5-7). Quoting the 'famous' power-to-field relation of  $E(v/m) = \frac{\sqrt{30P_t G_t}}{r}$  and aperture size equation of  $D_0 = 20 \log_{10} \left( 0.81 \left[ 4\pi \left( \frac{a \cdot b}{\lambda^2} \right) \right] \right)$  (where  $a$  and  $b$  are the aperture dimensions,  $r$  is the radius of the average half-power field spherically around the antenna,  $P_t$  is the total power,  $G_t$  is the total gain and  $E$  is the field), Rodriguez (2008) warns that the near-field pattern is different, with the far-field being an approximation and the measurement point is important in terms of closeness to near field. Rodriguez (2008) also notes the  $S_{11}$  parameter (where  $S_{11} = \frac{P_{refl}}{P_{in}}$ ) must be considered for microwave antenna transmission, since there is some reflection back to the generator with microwave horns. At a glass-air interface, there is a 4 per cent reflection that must be accounted for in the analysis (Snyder and Love, 1983, pp 68).

## CHAPTER 3: THEORY

### 3.1 Foundation Mathematics

This section outlines the formulae that form the basis of the development of the theory. It does not include Maxwell's equations and other relevant equations covered in Chapter 2, but it does include the basic equations for power calculations. There are a number of alternative sources that can be referenced for these equations and their development in addition to those cited, including Kreyszig (1972); Snyder and Love (1983).

#### 3.1.1 Power Calculation

The general formula for power in a periodic system, known as Parseval's power theorem, is premised on power of a periodic signal being proportional to the sum of the squared amplitudes of all harmonic components of that signal, described by Equation 3.1 (Haykin, 1978, pp 9).

$$P = \sum_{n=-\infty}^{\infty} c_n c_n^* = \sum_{n=-\infty}^{\infty} |c_n|^2 \quad (3.1)$$

In Equation 3.1,  $c_n$  is the  $n^{\text{th}}$  harmonic component of a periodic signal,  $g_p(t)$  such that  $|c_n|$  is the amplitude of that  $n^{\text{th}}$  harmonic component.

### 3.2 Fraction of Power Curves

#### 3.2.1 Weak Guidance

A fibre is 'weakly guiding' if  $n_{co} \simeq n_{cl}$ , that is, if the difference between core and cladding refractive indices,  $\Delta \left( = \frac{n_{co}^2 - n_{cl}^2}{2n_{co}^2} \right)$ , approaches 0. This condition results in  $\beta \simeq kn_{co}$  and the solutions to the eigenvalue equations are virtually independent of  $\Delta$  and so is not sensitive to the fibre's polarisation properties (Snyder and Love, 1983, pp 227,259). Given that  $\Delta \ll 1$ ,  $|e_t| \gg |e_z|$  and  $|\mathbf{h}_t| \gg |h_z|$ , so the modes are nearly Transverse Electro-Magnetic (TEM) waves (Snyder and Love, 1983, pp 259). In spite of the term 'weakly guiding', such fibres are strong guides of light with very low loss (Snyder and Love, 1983, pp 281).

The weak guidance approximation simplifies the derivation of the vector modal fields in a weakly guiding step profile fibre. It relies on solutions of the scalar wave equation and not the vector wave equation, which simplifies calculations significantly (Snyder and Love, 1983, pp 281).

Supposing that, for a uniform medium (which is more or less what a weakly guiding fibre is) of refractive index  $n_{co}$ , which is more or less 'free space', then the modal fields are found from Maxwell's equations with a propagation constant of  $\beta = n_{co}k$ , longitudinal components being  $e_z = h_z = 0$ , and the transverse electric ( $\mathbf{e}_t$ ) and magnetic ( $\mathbf{h}_t$ ) fields of the Transverse Electro-magnetic (TEM) waves being related by Equation 3.2 (Snyder and Love, 1983, pp 281).

$$\mathbf{h}_t = \left( \frac{\epsilon_0}{\mu_0} \right)^{\frac{1}{2}} n_{co} \hat{\mathbf{z}} \times \mathbf{e}_t \quad (3.2)$$

Here,  $\hat{\mathbf{z}}$  is the unit vector for the fibre z-axis,  $\varepsilon_0$  is the electric permittivity of free space and  $\mu_0$  is the magnetic permeability of free space. Such a waveguide has no polarisation properties (Snyder and Love, 1983, pp 281). If the media were not uniform, then the modal fields would obey the vector wave equation and its polarisation effects would be governed by the  $\nabla_t \ln n^2$  terms. However, for a very small difference between core and cladding refractive index, the change in phase with polarisation of the electric field is small, the wave is still totally internally reflected, and the fields satisfy the scalar wave equation discussed in Section 3.2.2 (Snyder and Love, 1983, pp 282).

Following on from this, in the weak guidance approximation,  $\beta \simeq kn_{co} \simeq kn_{cl}$ , so the modes are nearly TEM and Equation 3.2 is approximately correct for the transverse fields (Snyder and Love, 1983, pp 283). The consequence of ignoring the polarisation effects contained in the  $\nabla_t \ln n^2$  term is that  $\mathbf{e}_t$  is defined by Equation 3.3, where  $\hat{\mathbf{x}}$  and  $\hat{\mathbf{y}}$  are the unit vectors for their respective axes.  $\Psi$  can then denote  $e_x$  or  $e_y$  and be satisfied by the scalar wave equation discussed in Section 3.2.2 (Snyder and Love, 1983, pp 283).

$$\mathbf{e}_t(x, y) = e_x(x, y) \hat{\mathbf{x}} + e_y(x, y) \hat{\mathbf{y}} \quad (3.3)$$

### 3.2.2 Scalar Wave Equation

By referring the components of  $\mathbf{E}_j$  and  $\mathbf{H}_j$  to fixed Cartesian directions, the vector wave equations that are the source-free solutions of Maxwell's equations can be simplified to those of Equation 3.4 (Snyder and Love, 1983, pp 221).

$$\begin{aligned} \{\nabla_t^2 + k^2 n^2 - \beta_j^2\} \mathbf{e}_j &= -\{\nabla_t + i\beta_j \hat{\mathbf{z}}\} \{\mathbf{e}_{tj} \cdot \nabla_t \ln n^2\} \\ \{\nabla_t^2 + k^2 n^2 - \beta_j^2\} \mathbf{h}_j &= -\{(\nabla_t \ln n^2) \times (\{\nabla_t + i\beta_j \hat{\mathbf{z}}\} \times \mathbf{h}_j)\} \end{aligned} \quad (3.4)$$

If you assume a step-index profile, then all the terms involving  $\nabla_t \ln n^2$  in Equation 3.4 vanish everywhere except in the core-cladding interface, so this equation can be simplified further to a scalar format (Snyder and Love, 1983, pp 223).

Snyder and Love (1983) describe a method that uses Maxwell's equations for fibre arranged with cylindrical coordinates  $(r, \phi, z)$  with  $\Psi(r, \phi)$  denoting either the x-polarised electric field or the y-polarised electric field, as per Figure 3.1, where  $\nabla_t^2$  is the transverse Laplace operator,  $\beta$  is the propagation constant,  $k = \frac{2\pi}{\lambda}$  is the free space wave number and  $n$  is the refractive index profile. The transverse Laplace operator in the scalar wave equation of Equation 3.5 (Snyder and Love, 1983, pp 223, 283, 641) has the differential form of Equation 3.6.

$$(\nabla_t^2 + k^2 n^2 - \beta^2) \Psi = 0 \quad (3.5)$$

$$\nabla_t^2 = \frac{\partial^2}{\partial r^2} + \frac{1}{r} \frac{\partial}{\partial r} + \frac{1}{r^2} \frac{\partial^2}{\partial \phi^2} \quad (3.6)$$

### 3.2.3 Calculation of V Parameter

The V parameter determines the number of modes that a fibre can support. This information is required for the different tests in the few-mode fibre experiments that are used to validate the final design.

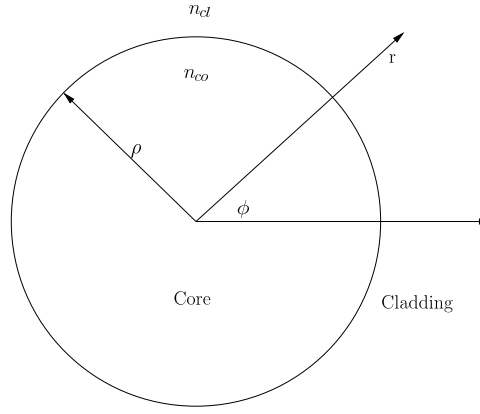


**Figure 3.1:** Fibre bound modes

As detailed at Appendix D in Section D.1, the eigenvalue equation for the fibre is written as Equation 3.7.

$$U \frac{J_{v+1}(U)}{J_v(U)} = W \frac{K_{v+1}(W)}{K_v(W)} \quad (3.7)$$

The well known Equation 3.8 can be similarly demonstrated (Love, 2009b, sl 1-3). Using numerical methods, a plot of  $U$  against  $V$  can be generated from Equation 3.7 and Equation 3.8 as shown in Figure 3.2.  $U$  and  $W$  are given by Equation 3.9 and Equation 3.10, where  $\rho$  is the core radius,  $k = \frac{2\pi}{\lambda}$  is the free space wave number,  $\beta$  is the propagation constant,  $n_{co}$  is the core refractive index and  $n_{cl}$  is the cladding refractive index.

$$V^2 = U^2 + W^2 \quad (3.8)$$

$$U = \rho (k^2 n_{co}^2 - \beta^2)^{\frac{1}{2}} \quad (3.9)$$

$$W = \rho (\beta^2 - k^2 n_{cl}^2)^{\frac{1}{2}} \quad (3.10)$$

### 3.2.4 Modal Power Curves

Substituting for  $R = \frac{r}{\rho}$  and for  $\tilde{U}$  and  $V$  into Equation 2.18 results in Equation 3.11 (Snyder and Love, 1983, pp 303). For a step profile fibre,  $f(R) = 0$ ;  $0 \leq R < 1$  for the core and  $f(R) = 1$ ;  $1 < R < \infty$  for the cladding.

$$\left\{ \frac{d^2}{dR^2} + \frac{1}{R} \frac{d}{dR} - \frac{l^2}{R^2} + \tilde{U}^2 - V^2 f(R) \right\} F_l(R) = 0 \quad (3.11)$$

The intensity  $I$ , or power density, is defined by Equation 3.12, where  $a$  is the modal amplitude (and modal power is given by  $|a|^2 N$ ) and  $F_l$  is given by Equation 3.13 (Snyder and Love, 1983, pp 311,313-319). For the fundamental and  $HE_{1m}$  modes, set  $l = 0$  (to give  $F_0$ ) in Equation 3.12.

$$I = \frac{|a|^2}{2} \left( \frac{\epsilon_0}{\mu_0} \right)^{\frac{1}{2}} n_{co} F_l^2 \quad (3.12)$$

## circular step-profile waveguide

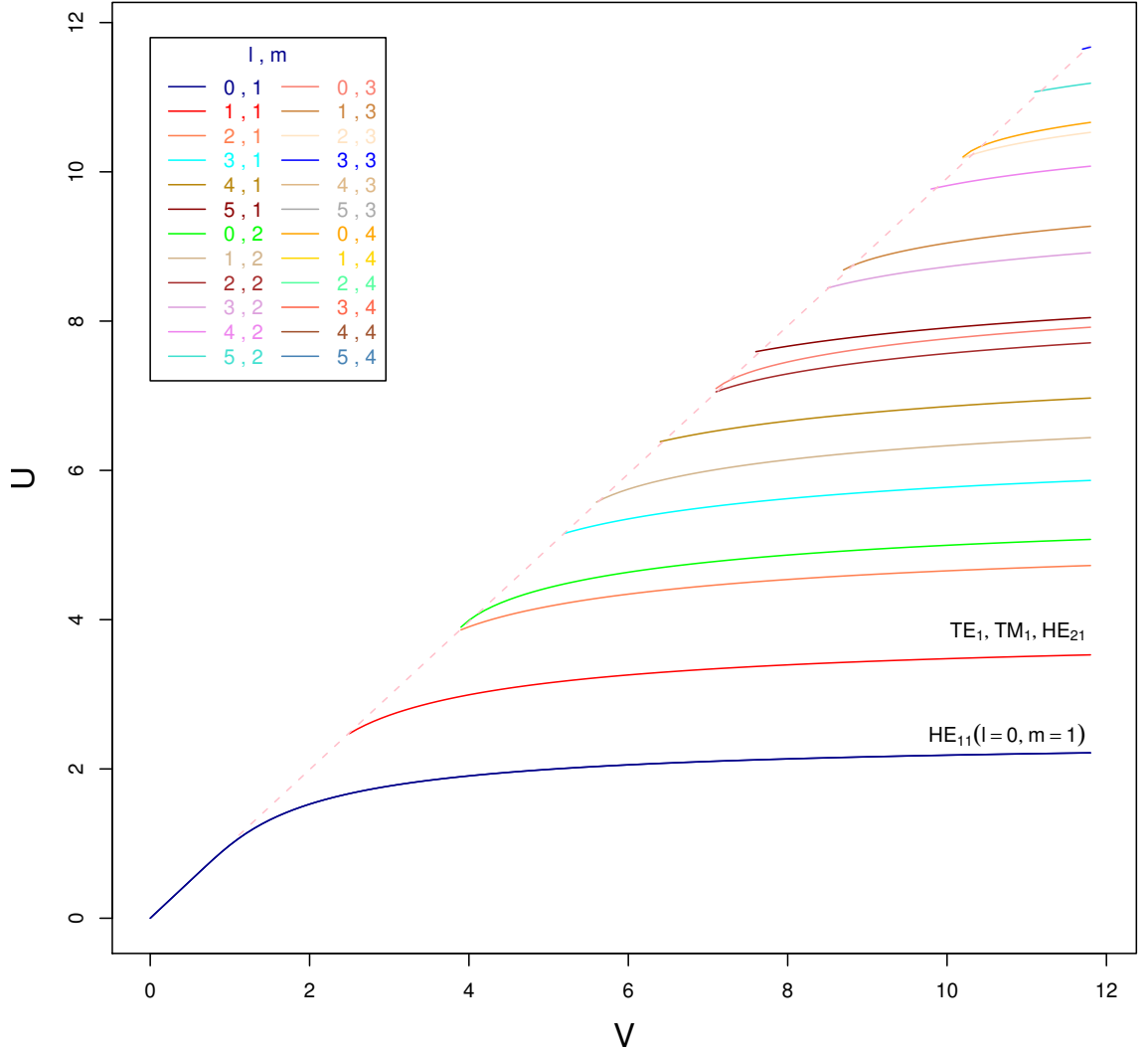


**Figure 3.2:**  $U$  against  $V$  Plot of the Eigenvalues for a step profile fibre using the weak guidance approximation for the  $HE_{lm}$ ,  $TE_{lm}$ ,  $EH_{lm}$  (as appropriate) modes (Snyder and Love, 1983, pp 254,320)

$$F_l = \begin{cases} \frac{J_l(UR)}{J_l(U)} & R \leq 1 \\ \frac{K_l(WR)}{K_l(W)} & R > 1 \end{cases} \quad (3.13)$$

These equations are utilised in Section D.2 at Appendix D.

In addition, by combining Equations 3.8 to 3.10,  $W$  and  $U$  are defined by Equation 3.14.

$$W^2 + U^2 = k^2 \rho^2 (n_{co}^2 - n_{cl}^2) \quad (3.14)$$

## 3.3 Power in the Modes

### 3.3.1 Total Power in Each Mode

The amplification can be modelled with modes. Referring to Figure 3.3, the source electric field,  $E_s$  is applied to the calculation using a normalised fibre radius (as per Snyder and Love (1983, pp 249) where  $R = \frac{r}{\rho}$ ) with  $R = 1$  (that is, at the boundary between the core and the cladding). From Snyder and Love (1983), given that as per Equation 2.11  $dA = r d\phi dr$ , we have Equation 3.15, where the denominator can be ignored for the purposes of the amplification. From this, the amplitude is calculated as per Equation 3.16.

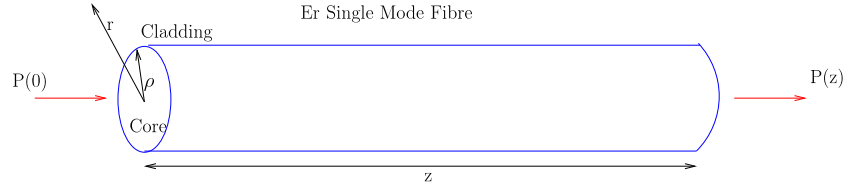


**Figure 3.3:** Parameter arrangement for the analysis of power in the modes in a length of amplifying fibre

$$\Psi_m = \frac{a_m J_m(U_m R) dA}{J_m(U_m)} \quad (3.15)$$

$$a_m = \frac{\int_{A_{co}} E_s J_m(U_m R) dA}{\int_{A_{\infty}} J_m^2(U_m R) dA} \quad (3.16)$$

In Equations 3.15 and 3.16,  $a_m$  is the amplitude of the  $m^{th}$  mode,  $J_m$  is the Bessel function of the first kind for the  $m^{th}$  mode,  $U_m$  is the core modal parameter, and  $A$  is the area.

In examining this equation, it is important to note that not all the power is in the core (see Snyder and Love (1983, pp 315-316)). This will need to be taken into account during the measurement of power.

The gain is represented by the application of amplification as per Equation 3.17, where the gain coefficient,  $\gamma$ , is calculated for a trial at Equation 3.18.

$$P(z) = P(0) \exp(+\gamma z) \quad (3.17)$$

$$\gamma_1 = \eta_1 \frac{2\pi}{\lambda} n_{(i)}; \quad n_{(i)} < 0 \quad (3.18)$$

Here, the fraction of power in the core,  $\eta$ , for a weakly guiding step profile fibre is given by Equation 3.19 (Snyder and Love, 1983, pp 313) and  $n_{(i)}$  is the (complex) refractive index that describes the fibre gain.

$$\eta = \frac{U^2}{V^2} \left[ \frac{W^2}{U^2} + \frac{K_0^2(W)}{K_1^2(W)} \right] \quad (3.19)$$

From this, a cut-back experiment can be conducted and the measured gain can be related to the ideal via Equation 3.20.

$$dB = 10 \log_{10} \frac{P(z)}{P(0)} = 10 \log_{10} \exp(\gamma \eta z) = 10 \gamma z \eta \log_{10} e \quad (3.20)$$

For the second run, using Equation 3.17 (that is,  $P_2(z) = P_2(0)e^{\gamma_2 z}$ ), the gain coefficient can be worked out from equation 3.18 as  $\gamma_2 = \eta_2 \frac{2\pi}{\lambda} n_{(i)}$ .

### 3.3.2 Mode Intensity Profile

While previous researchers caution that the far field is different to the near field (see Section 2.5 above), it might be reasonable to use the near field model and match the amplitude variables to approximately match the profiles. The far-field intensity profile is effectively a simplification of the near-field, and radiation from a fibre end, which is effectively a source point optical antenna, is an out-going spherical wave with a directional weighting function (Elliott, 2003, pp 28-29). Using a goniometric radiometer or similar intensity measurement tool, it is straight forward to measure the far field at the end of a fibre. Calibrating against total power from a power meter, this approach should be accurate enough to determine the relative power in each mode.

The analysis is based on Equation 3.21, as outlined in Section 2.3, being correct. Here,  $P$  is the power,  $r$  and  $\phi$  are the polar coordinates of a point on the end of the fibre,  $I(r, \phi)$  is the intensity at that point and the integral is taken over the entire area  $A$ . Then, by approximately matching the intensity profiles, the total relative intensity values in each mode is known and therefore the total power for each mode can be known.

$$P = \int_{A_\infty} I(r, \phi) dA = \int_0^\infty \int_0^{2\pi} I(r, \phi) r d\phi dr \quad (3.21)$$

The total intensity profile  $I_T(r, \phi)$  is assumed to be the sum of the individual intensity profiles  $I_m(r, \phi)$  for each mode  $m$  that is modified by an amplitude scaling factor for that mode  $a'_m = \sqrt{\frac{n_{co}}{2}} \left(\frac{\epsilon_0}{\mu_0}\right)^{\frac{1}{4}} a_m$  (where  $a_m$  is the intensity amplitude) and a length-dependent phase factor as per Equation 3.22. For instance, in Figure 3.4 which deals with two modes, Figure 3.4a is made up by summing the fundamental mode of Figure 3.4b and the second mode of Figure 3.4c plus the phase factor of Figure 3.4d.

$$I_T(r, \phi) = \sum_{m=1}^n |a'_m|^2 I_m(r, \phi) + 2 \sum_{m=1}^n \sum_{k=m+1}^n a'_m \sqrt{I_m(\phi, r)} a'_k \sqrt{I_k(\phi, r)} \cos((\beta_m - \beta_k) z) \quad (3.22)$$

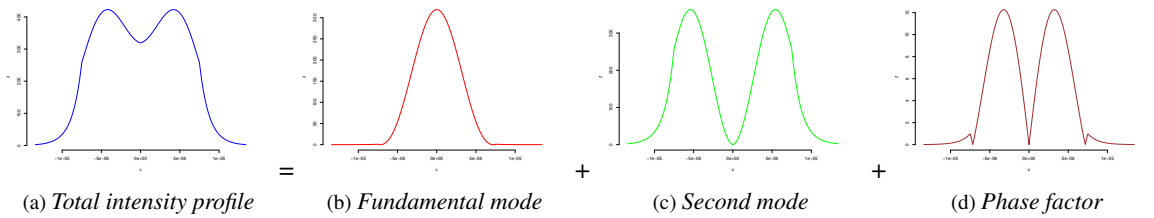


**Figure 3.4:** Intensity profile for two modes (an elevation view)

As intensity needs to be analysed as a function of both  $r$  (or  $R = \frac{r}{\rho}$ ) and  $\phi$ , Equation 3.15 or a derivative is not quite adequate, but Liu (2005, pp 133) offers a formula as per Equation 3.23, where  $J_m$  is the Bessel function of order  $m$  for mode  $m$ ,  $K_m$  is the modified Bessel function of order  $m$  for mode  $m$ ,  $\beta$  is the propagation constant,  $\rho$  is the core radius, the transverse spatial parameter of the guided mode field,  $h$ , is given by Equation 3.24, the transverse spatial decay parameter of the mode field in the cladding region,  $\gamma$  is defined by Equation 3.25, and  $k$  is the free space wave number,  $n_{co}$  is the core refractive index and  $n_{cl}$  is the cladding refractive index.

$$I_m(r, \phi) = \begin{cases} \frac{1}{J_m^2(hr)} J_m^2(hr) \cos^2(m\phi) & r < \rho \\ \frac{1}{K_m^2(\gamma\rho)} K_m^2(\gamma r) \cos^2(m\phi) & r > \rho \end{cases} \quad (3.23)$$

$$h^2 = (kn_{co})^2 - \beta^2 = k^2 n_{co}^2 - \beta^2 = \frac{U^2}{\rho^2} \quad (3.24)$$

$$\gamma^2 = \beta^2 - (kn_{cl})^2 = \beta^2 - k^2 n_{cl}^2 = \frac{W^2}{\rho^2} \quad (3.25)$$

Combining Equations 3.21 to 3.25 results in Equation 3.26, where  $\varphi$  is given by Equation 3.27.

$$P = \int_{A_\infty} \left( \sum_{m=1}^n \left\{ \frac{n_{co}}{2} \left( \frac{\varepsilon_0}{\mu_0} \right)^{\frac{1}{2}} |a_m|^2 \left[ \begin{cases} \frac{J_m^2(U \frac{r}{\rho})}{J_m^2(U)} \cos^2(m\phi) & r < \rho \\ \frac{K_m^2(W \frac{r}{\rho})}{K_m^2(W)} \cos^2(m\phi) & r > \rho \end{cases} \right] + \varphi \right\} \right) dA \quad (3.26)$$

$$\varphi = 2 \sum_{m=1}^n \sum_{k=m+1}^n \left( \frac{n_{co}}{2} \left( \frac{\varepsilon_0}{\mu_0} \right)^{\frac{1}{2}} a_m a_k \cdot \left[ \begin{cases} \left( \frac{J_m^2(U \frac{r}{\rho})}{J_m^2(U)} \frac{J_k^2(U \frac{r}{\rho})}{J_k^2(U)} \cos^2(m\phi) \cos^2(k\phi) \right)^{\frac{1}{2}} & r < \rho \\ \left( \frac{K_m^2(W \frac{r}{\rho})}{K_m^2(W)} \frac{K_k^2(W \frac{r}{\rho})}{K_k^2(W)} \cos^2(m\phi) \cos^2(k\phi) \right)^{\frac{1}{2}} & r > \rho \end{cases} \cos((\beta_m - \beta_k) z) \right] \right) \quad (3.27)$$

The full derivation of Equations 3.21 to 3.26 is provided in Section D.2 at Appendix D.

For a fibre excited by a known wavelength  $\lambda = \frac{2\pi c}{\omega}$  (where  $\omega$  is the angular frequency and  $c$  is the free space speed of light),  $n_{co}$ ,  $n_{cl}$  and  $\rho$  are known. Given that  $kn_{cl} < \beta \leq kn_{co}$  and given the approximation  $\beta \simeq kn_{co} \simeq kn_{cl}$  (and that  $n_{co} > n_{cl}$  and  $k = \frac{2\pi}{\lambda}$ ) for weakly guiding fibre (Snyder and Love, 1983, pp 283), one can assume that Equation 3.28 is adequate for providing a first approximation of  $\beta$  and that variation of  $\beta$  between a few modes has a negligible effect on power measurement (which is probably not strictly true, but its variation should round up into any calibration constants used).

$$\beta \simeq k \left( n_{cl} + \frac{n_{co} - n_{cl}}{2} \right) = \frac{2\pi}{\lambda} \frac{n_{cl} + n_{co}}{2} \quad (3.28)$$

As the fibre output may be twisted in an angle  $\alpha$  compared to the input injection of the modes, then, ignoring any potential variation in the mode caused by the fibre bending and stress induced polarisation that Randel et al. (2011) asserts takes place, Equation 3.22 is modified to Equation 3.29.

$$I_T(r, \phi) = \sum_{m=1}^n I_m(r, (\phi + \alpha)) + \varphi \quad (3.29)$$

### 3.3.3 Stability of Relative Mode Orientation

Randel et al. (2011) asserted that the orientation of the modes would be random and subject to fluctuation, since that is what was observed by Gordon and Kogelnik (2000) to take place in the two transverse modes (Snyder and Love, 1983, pp 284-286) that make up the fundamental  $LP_{01}$  mode. Gordon and

Kogelnik (2000), in reviewing the fundamental concepts of polarisation mode dispersion theory, explain that the modes couple with each other down the fibre through random changes in birefringence along the fibre length. Other literature researched also talked about bend birefringence in the fundamental modes (e.g. Song (2012)), but information on other higher order modes was not readily found. These modes are transverse and they are modulated with exactly the same signal.

That does not mean that there would be coupling or time-varying random changes in orientation between the fundamental  $LP_{01}$  mode and the second  $LP_{11}$  mode or any of the higher order linearly polarised modes. The more likely situation is as follows:

*Proposition 1:* In few-mode fibre, for bend radii greater than that which strips the higher order mode into the cladding, the polarisation does not appreciably affect mode orientation.

Indeed, there should be an effect on power level. While the experiments run to validate the theory in Section 3.3.2 validate this theorem, the fibre lengths are far too short to validate any effect on power level or over any great distance.

## CHAPTER 4: SYSTEM DESIGN

### 4.1 Specifications, Metrics and Functional Analysis

Specifications and metrics for the fibre mode power measurement device are contained in Appendix A. The design contained herein only takes the system to early prototype and is not intended to develop it into a production ready system.

The function diagram of the device for mode power measurement in fibre is at Figure 4.1.

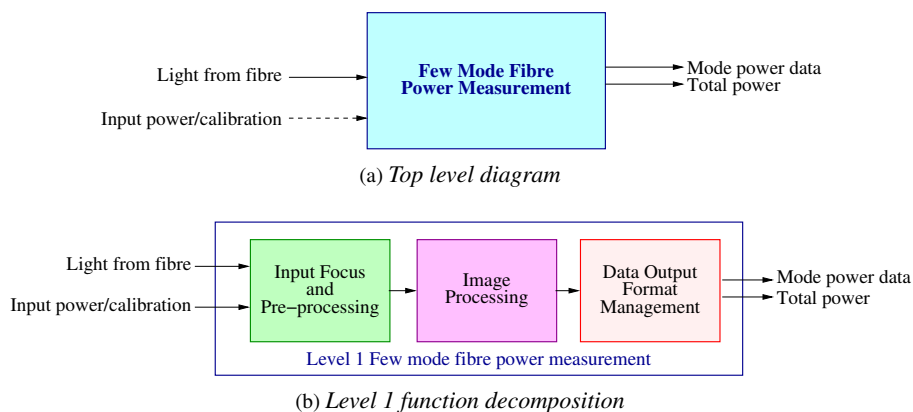


**Figure 4.1:** Function diagram of the fibre mode power measurement device

### 4.2 Concept Generation and Screening

#### 4.2.1 Power Level Detection Selection

The Image Focus and Pre-processing and the Image processing functional blocks can be considered together for the purposes of concept generation and screening, with the final selection being broken back out into its two constituent components for detailed design.

There are two readily available choices of device, with the possibility of fabrication of other techniques. Table 4.1 outlines the advantages and disadvantages of each with the Goniometric Radiometer Imaging option being selected as worthy of further investigation. Details of the concept generation and screening are contained at in Section B.1 at Appendix B.

#### 4.2.2 Data Output Format Management Selection

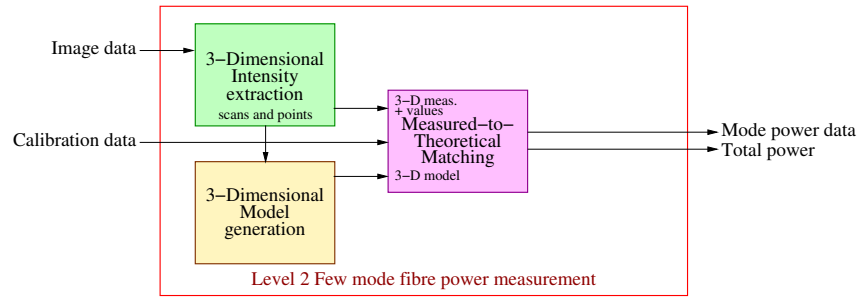
The Data Output Format Management is broken down into the sub-functions of Figure 4.2. These sub-functions are then constructed based on considered options and available requirements.

##### 4.2.2.1 3-Dimensional Intensity Extraction

The role of the 3-Dimensional Intensity Extraction function is to take the output from the goniometric radiometer in the 3 dimensional scan .prw file format and convert it into two .csv format files, one as the 3-dimensional measured values in polar coordinates centred at the fibre end, the other as control variables. The

**Table 4.1:** Alternatives for Power Level Detection

Option	Advantages	Disadvantages
Nicholson's $S^2$ Imaging	Previously demonstrated to work. Simple equipment configuration. Includes phase information.	Primitive power scanning approach. X-Y scanner not readily available. Likely resolution (and therefore accuracy) limits. Absolute power level determination may be problematic. Software processing of measurements required.
Modified $S^2$ Imaging using DataRay	Based on a demonstrated technique. No moving parts in imaging, therefore better repeatability. Includes phase information.	Limited by the resolution of the camera. Absolute power level determination may be problematic. Significant software processing of image required, which then needs to be translated into measurements to be processed.
Goniometric Radiometer Image Processing	Straight forward measurement using an off-the-shelf tool.	Requires post analysis from the output of proprietary software. Requires conversion of intensity distribution measurements into power amplitude.

**Figure 4.2:** Function Diagram for the Level 2 Data Output Format Management function decomposition

control variables are the number of scans and the number of points, the intensity profile centre offset from the polar coordinate centre (as distance from the centre in both polar coordinates and Cartesian coordinates and as the polar coordinates of the offset point), and the maximum intensity at the centre of the intensity profile. It assumes that the centre of the intensity profile is at the peak point in the case of a single mode profile or at the point mid-way between the two peaks in the case of a two mode profile.

For two modes, the two peaks are found by checking two halves of the profile for separated peaks, then looking through  $90^\circ$  if none was found there. The identified peaks are checked to be proper peaks (as opposed to bumps on the fundamental mode of a single mode plot) by using the cosine rule to ensure there is a minimum distance between them. For a line between two peaks at  $A(t, \theta)$  and  $B(s, \psi)$ , the calculation of the radius  $r$  component of a point  $P(r, \phi)$  for any angle  $\phi$  along that line is from Equation 4.1.

$$r = \frac{(s \cos \psi - t \cos \theta) t \sin \theta - (s \sin \psi - t \sin \theta) t \cos \theta}{(s \cos \psi - t \cos \theta) \sin \phi - (s \sin \psi - t \sin \theta) \cos \phi} \quad (4.1)$$

Full details of the mathematics can be found in Section B.2 at Appendix B.

### 4.2.2.2 3-Dimensional Model Generation

The approach taken to the results analysis is to prepare a theoretical profile and map the measured results onto that model, adjusting the model's parameters to achieve a match. The value of those parameters then defines the power levels in each mode.

As alluded to in the literature review and also as implied in the theory, there are a couple of alternative approaches to defining the power profile. One is to start with the equations of Snyder and Love (1983) to produce an equation that describes the profile, at least in the near field and preferably in the far-field. The other is to start with the equation provided by Liu (2005), approximate any unknown parameters, then adjust to match the far-field measurements. Both approaches are based on the same theory and will lead to the same outcome, but deal with the amalgamation of variable terms in the formulae in slightly different ways. Table 4.2 outlines the advantages and disadvantages of each approach. For expediency, use of the equation by Liu (2005) (detailed in Section 3.3.2 above) has been selected as the quickest to initially proceed with. Details of the concept generation and screening are contained at in Section B.3 at Appendix B.

**Table 4.2:** *Alternatives for Power Modelling*

Option	Advantages	Disadvantages
Modification of Snider and Love's approach for profiling	Well understood base equations for power. One of the authors is on hand to guide development. Power level formulae for fundamental and second mode available.	Power level by mode not in format suitable for plotting. Considerable work required to manipulate it into a form that can be used to map into the far field results of the goniometric radiometer.
Use Liu's power formula and adapt to far field measured values	Formula for near field readily available in a directly usable format.	Formula not in a form that maps directly into the far field results of the goniometric radiometer. A few of the variables are unknown and will need to be approximated. Does not provide a consolidated view of the power profile.

In addition to a straight match of the model to the measured result, the model also needs to take into account deviation from theoretical outcomes due to environmental factors. Apart from the angular orientation of the modes with respect to the goniometric radiometer being difficult to determine in advance of measurement taking, the modes may vary in relation to each other and may not propagate on the central z-axis of the fibre, for instance due to variations in the core-cladding refractive index profile from one side of the fibre to the other. This may result in modes being offset with respect to each other, making, for instance, the second mode to have peaks at two different heights (Hewlett, 2012, pers. comm.). This variation affects the power level calculation. Mathematics for the offset model correction are also contained in Section B.3 at Appendix B.

## 4.3 System Construction

The Implementation of the software to process the output from the Goniometric Radiometer, satisfying the sub-functions of the Data Output Format Management function, is in the source code at Listing E.1 in Appendix E for the 3-Dimensional Intensity Extraction function and in the source code at Listing E.2 and Listing E.3 in Appendix E for the 3-Dimensional Model Generation function.

A block diagram of the total system, including a mapping back to the Level 0, 1 and 2 functions, is at Figure 4.3. Figure 4.4 shows key components of the system, namely the Photon Inc. Goniometric

Radiometer with the constructed face plate and launch jig, a typical snapshot of the Photon Inc. Goniometric Radiometer viewer software, a snippet of output from the 3-dimensional intensity extraction software and a typical plot of modelled and measured intensity that is output from the intensity profile matching software.

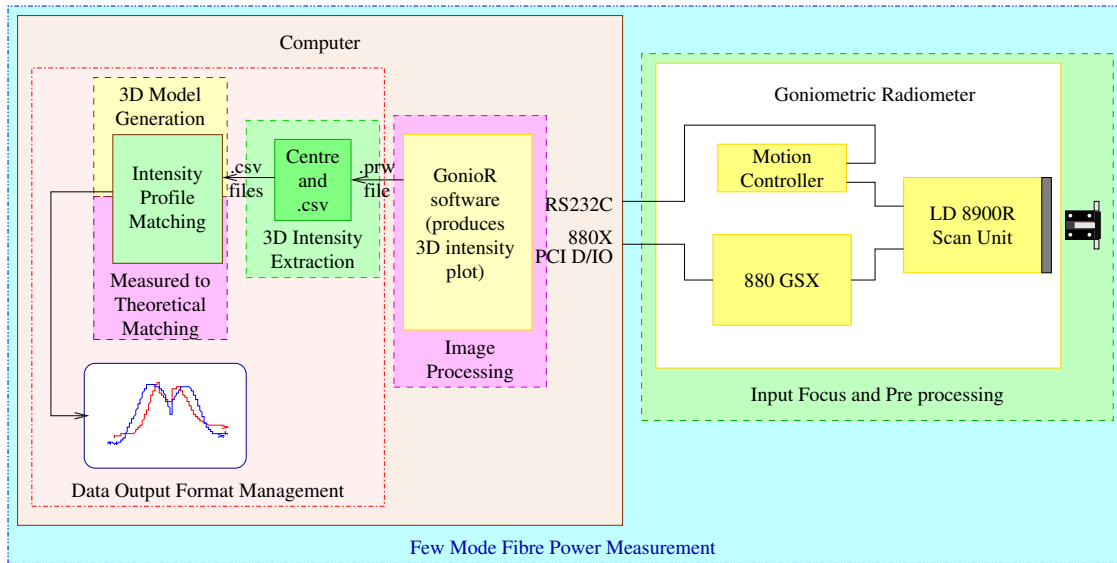
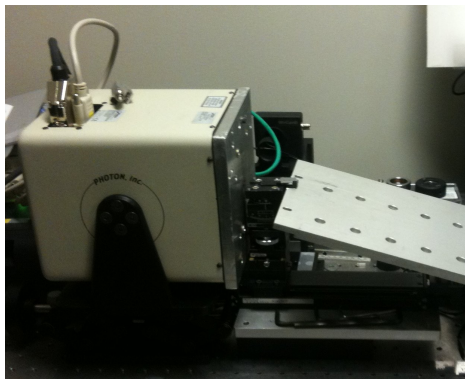
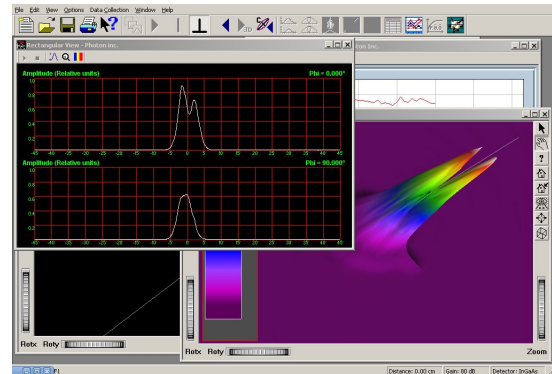


**Figure 4.3:** Total System Block Diagram, showing how hardware and software within hardware maps on to the functional decomposition.



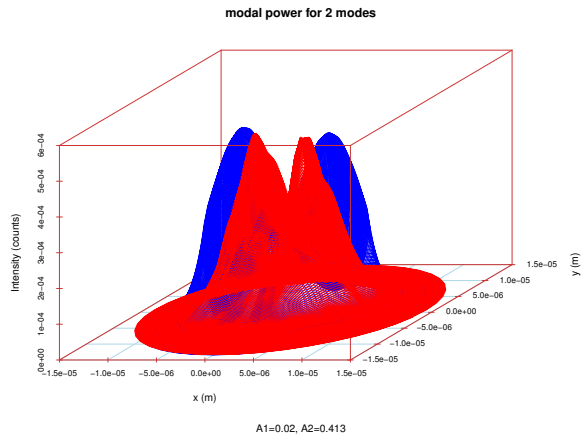
(a) Goniometric radiometer and its face plate and fibre launch jig.



(b) Typical goniometric radiometer software image

.csv file:	.par file:
phi.r.z	20
0.00000, 0.00000, 26802.89063	3241
0.15708, 0.00000, 27555.98438	-0.96504
0.31416, 0.00000, 30828.03516	-4.86947
0.47124, 0.00000, 25914.79492	-0.15097
0.62832, 0.00000, 26149.82422	0.95316
0.78540, 0.00000, 25269.77930	24
0.94248, 0.00000, 23916.83008	32
1.09956, 0.00000, 21880.31055	24602.41406
1.25664, 0.00000, 23221.99023	-2.96406
1.41372, 0.00000, 25613.14063	
1.57080, 0.00000, 29115.99023	
<snip>	

(c) Typical 3D intensity extraction snippet



(d) Typical intensity profile matching output, where red is the measured and blue is the modelled intensity

**Figure 4.4:** As-built test system key components

## 4.4 System Testing

To test the effectiveness of the power measurement system, for non-amplified signal, the system is set up to measure the power in a 2-mode fibre as per Figure 4.5, where the fibre is put through a bend radius test. For an amplified signal, the system is set up to measure the power in a 2-mode fibre length containing a segment of gain fibre as per Figure 4.6, and is also put through a bend radius test.

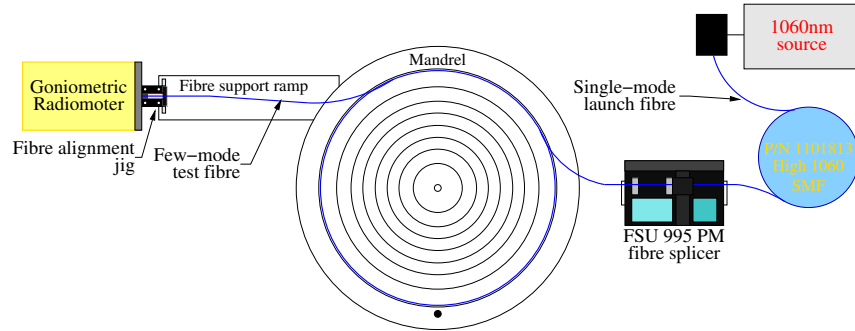


**Figure 4.5:** Layout of the system for a bend radius test of 2-mode fibre, showing up to the Goniometric Radiometer interface to the system.

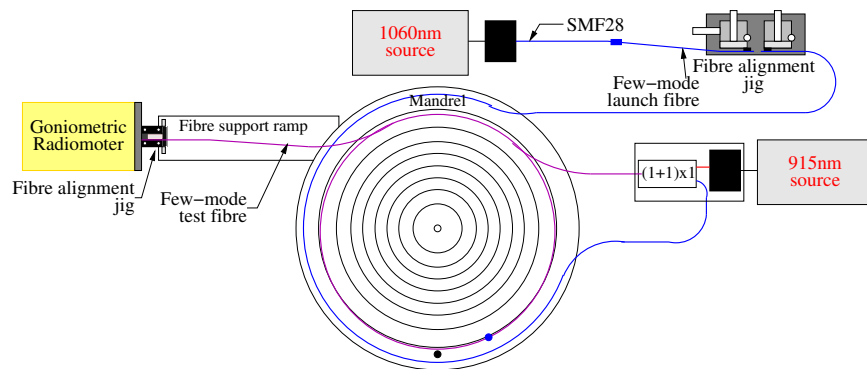
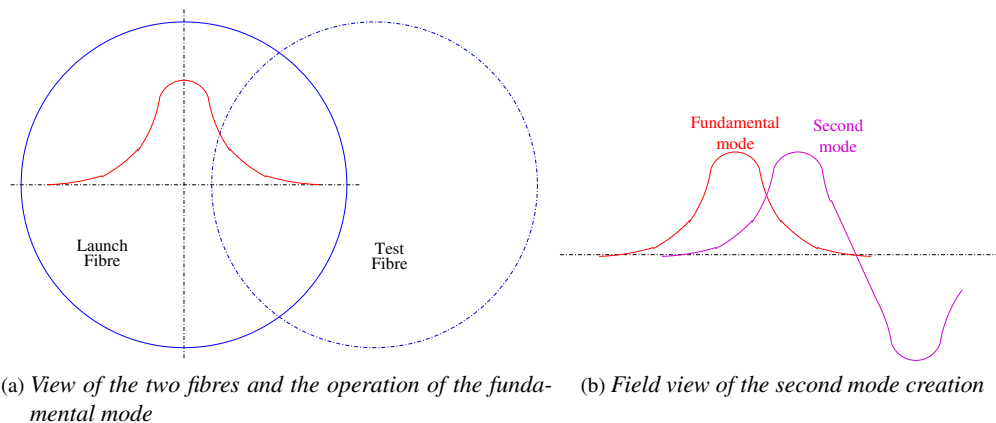


**Figure 4.6:** Layout of the system for a bend radius test of 2-mode fibre undergoing few-mode power amplification, showing up to the Goniometric Radiometer interface to the system.

To generate the second mode, as shown in Figure 4.5 and Figure 4.6, the test fibre is offset from a launch fibre in the fibre alignment jig. With reference to Figure 4.7a, the principle occurring is the offset of the fundamental mode is exciting the second mode, as shown in Figure 4.7b.



(a) View of the two fibres and the operation of the fundamental mode

(b) Field view of the second mode creation

**Figure 4.7:** Second Mode Creation in the fibre alignment jig

## CHAPTER 5: MODAL AMPLITUDE

### 5.1 Un-amplified Few-Mode Fibre

#### 5.1.1 Power Level Detection

The concept being tested here is to form a near-field model of the modal profile at the end of the fibre and then map the far-field measured value onto the near-field model. If a calibrated model matches over a range, then the concept could be deemed successful.

The design chosen is constrained by the dynamic range of the goniometric radiometer. Fortunately its dynamic range is very wide, with the ability to adjust the sensitivity from 0dB to 139dB for the InGaAs detector that it uses. This has enabled the detection of signals in the nano Watt range, with an 18nW signal being successfully detected and profiled. With regard to high power, the goniometric radiometer was purchased with a polarising mirror to cut the input power down by at least a half. Other attenuators could also be calibrated and then deployed into the optical circuit at entry to the goniometric radiometer to achieve a similar outcome.

The system designed will vary the phase variation of the model to align with that of the goniometric radiometer. However, When the centre of each of the modes varies relative to each other, the model needs to adjust to reflect that offset as discussed in Section 4.2.2.2. The consequence of not doing so is it would not match difference in amplitude; a feature visible in Figure 5.1 for example.

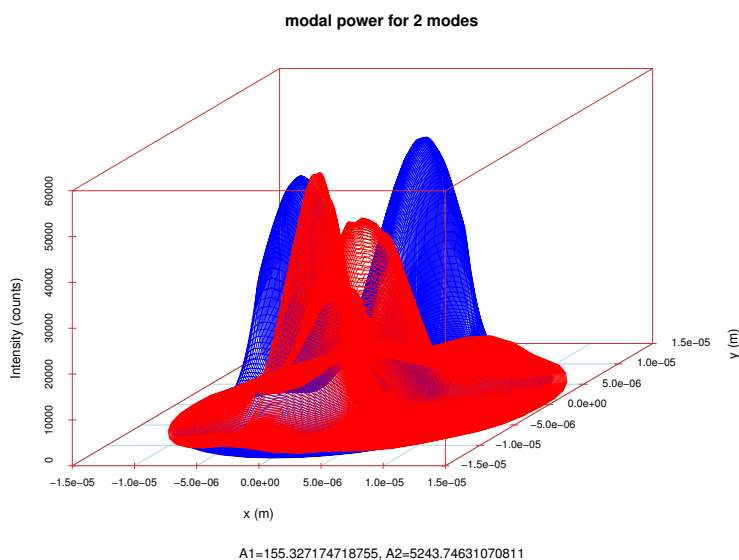


**Figure 5.1:** Run 7 on 3.7m LMA-YDF-15/123, one of the two mode tests made prior to the power amplification test, showing the effect of the centre of the modes being offset

The current system design only identifies and models 2 modes. Expanding the modelling beyond 2 modes is not difficult; the algorithm handles any number of modes. However, the software that converts the output from the Photon Inc. Goniometric Radiometer viewer software into Comma Separated Value (CSV) format and extracts key parameters, namely the 3D Intensity Extraction function, does need to be enhanced to handle more modes. The Measured to Theoretical Matching component of the Intensity Profile Matching software would also need to be enhanced to match more than two modes.

## 5.1.2 Power Level Consistency and Accuracy

During many of the tests, there was fluctuation in the intensity peak as measured by the goniometric radiometer, with the degree of fluctuation more or less proportional to the sensitivity gain setting in the goniometric radiometer. This fluctuation also appeared to be inversely proportional to the test fibre's bend radius. A consequence of this fluctuation is the intensity profile, being a snapshot in time, but taken as a sweep of angles over many seconds, did not represent the average intensity at each sample point. Therefore, the accuracy of the system in measuring the power in each mode would have been randomly affected by the degree of fluctuation.

The test bench in the later tests was located next to a power distribution board. The room contained a number of environmental chambers, which tended to cause variation in air-conditioning, which impacted both power load and air currents in the room, including over the test bench. Occasionally, plots of variation in the angular centroid as monitored by the goniometric radiometer software showed a periodic fluctuation.

Several different power meters were used at different phases of the testing and their calibration levels varied. This affected consistency between the different phases of the tests. However the main power level accuracy tests were consistently done in the last phases using the UDT 5370 Optimeter. A plot of measured against calculated values is at Figure 5.2. The original sample set had just 3 of the samples separated out to be used to calibrate against.

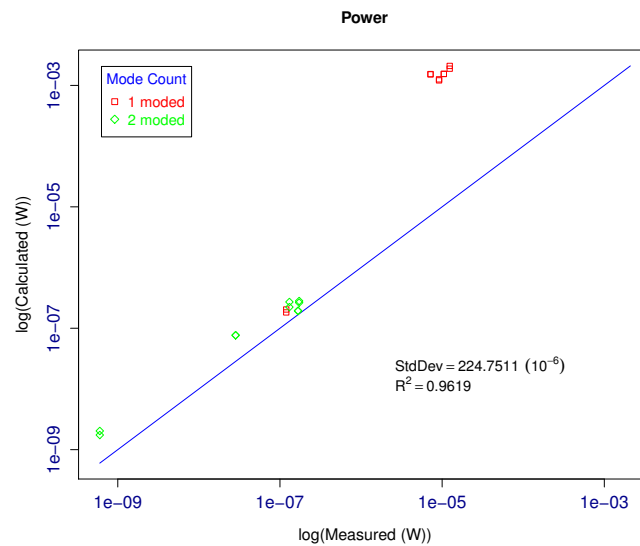


Figure 5.2: Power level accuracy test

With  $R^2 > 0.9$ , the fit is reasonable. In practice, a larger sample set would be used to calibrate against, which should make the accuracy tighter. The graph does not include error bars for the measured results, but they were seen to vary by between  $\pm 1\%$  and  $\pm 10\%$ . That variation was probably mostly due to the observed fluctuation. The graph implies, and the later power amplification tests suggest that, the results may be more accurate if separate calibration constants were used for the different number of modes.

## 5.1.3 Bend Radius Test

A bend radius test was done on LMA-GSF-15/123 few mode fibre, injecting one and two modes, and then on the LMA-GSF-15/123 few mode fibre joined to a length of LMA-YDF-15/130 Ytterbium doped few mode fibre with amplification applied. The results for both cases are graphed at Figure 5.3, where the power is

that calculated using the Intensity Profile Matching algorithm and the angle is relative to the goniometric radiometer's x-axis. Note that fibre orientation to the goniometric radiometer was not maintained in the amplified fibre suite of tests, resulting in the high variation in angle.

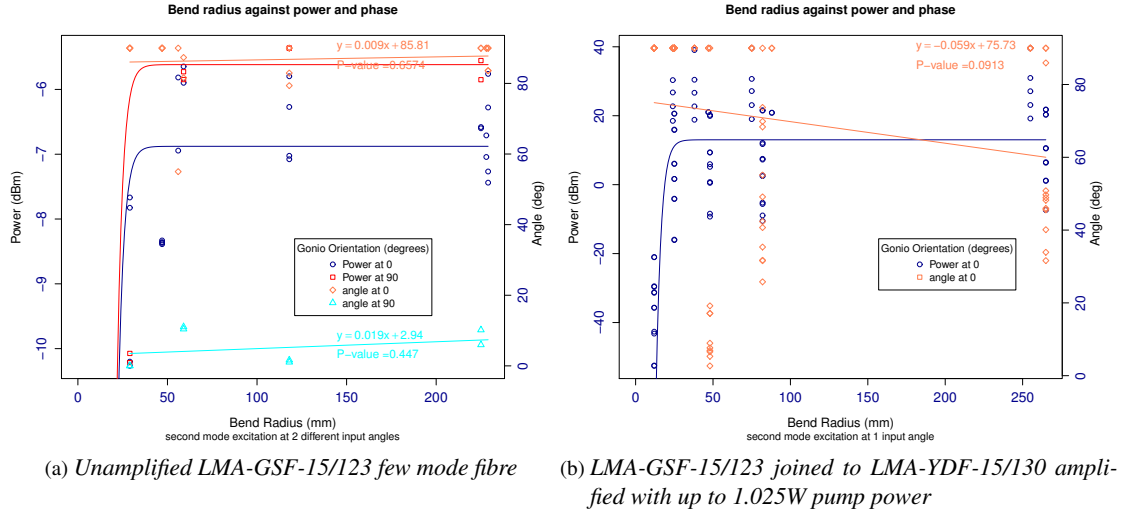


**Figure 5.3:** Bend radius tests

The second mode angles were quite linear with bend radius, with deviation of less than  $\pm 10^\circ$  for a particular orientation in the no amplification case of Figure 5.3a. This is discussed further in Section 5.2.

There was a considerable amount of variation in power levels for the no amplification case of Figure 5.3a, being in the order of just over 1dBm. This was likely due to signal level fluctuation between tests caused by interference sources in the industrial environment surrounding the test bench. Figure 5.3b includes all levels of pump power from 0W up to 1.025W, so amplitude varies for it, but it does show the consistency of the bend radius knee.

All results showed a consistent bend radius with bend loss occurring at less than 30mm, being around 20-25mm for the LMA-GSF-15/123 fibre and loss being consistently static for radii of 50mm or larger. This bend radius response was independent of the number of modes propagating and whether or not the fibre was charged with amplified signal.

At the bend knee, the power level dropped off sharply and was consistent irrespective of whether the fibre was carrying one or two modes. The calculated bend loss is derived from Equation 5.1, where  $\gamma$  is given by Equation 5.2 (Snyder and Love, 1983, pp 479), and for the LMA-GSF-15/123, which has  $NA = 0.08$  with  $n_{cl} = 1.4498$  for pure silica,  $n_{co} = \sqrt{NA^2 + n_{cl}^2} = 1.4519$ ,  $\Delta = \frac{n_{co}^2 - n_{cl}^2}{2n_{co}^2} = 0.001518$ , using the approximation of  $\beta \approx \frac{2\pi}{\lambda} \frac{1}{2} (n_{co} + n_{cl}) = 859958$  at  $\lambda = 1060nm$ ,  $V = \frac{2\pi\rho}{\lambda} NA = 3.55652$ ,  $k = \frac{2\pi}{\lambda} = 5927533$ ,  $U = \rho\sqrt{k^2 n_{co}^2 - \beta^2} = 2.5153$  and  $W = V^2 - U^2 = 2.5144$ . Using a bend loss  $R_b$  of between about 19 and 200, for the total  $z$  distance from the start of the bend to the end to be a single turn, this calculated bend loss is as per Figure 5.4.

$$loss(dB) = -10 \log \left( \frac{P(z)}{P(0)} \right) = -10 \log e^{-\gamma z} = (20 \log e) \gamma z = 8.686 \gamma z \quad (5.1)$$

$$\gamma = \sqrt{\frac{\pi\rho}{R_b} \frac{V^2 \sqrt{W}}{2\rho U^2}} \exp \left( -\frac{4}{3} \Delta \frac{R_b W^3}{\rho V^2} \right) \quad (5.2)$$

While the calculation and matching plot of Figure 5.4 deals with single mode fibre, for the two mode

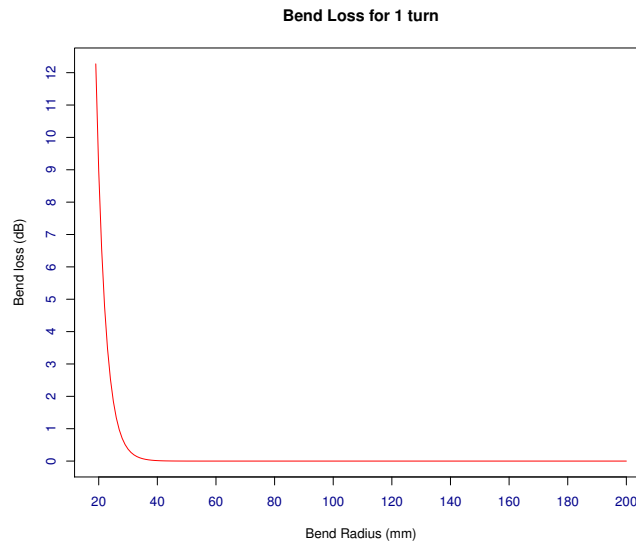


**Figure 5.4:** *Calculated bend loss for LMA-GSF-15/123*

fibre analysed here, the bend loss begins at a bend radius of around 30mm, which agrees with the measured results of Figure 5.3.

## 5.2 Short Distance Mode Orientation

In Section 3.3.3, it was proposed that, for short distances at least, the orientation of modes in few mode fibre is not noticeably affected by any birefringence introduced by bending. As part of the testing of the power meter software, tests were run on injecting the second mode at two different angles  $90^\circ$  apart. Results of tests indicate that this proposition is correct. This is quite visible in Figure 5.3, where the bend radius angles are relatively linear and are nearly  $90^\circ$  apart.

Further tests with longer fibre lengths need to be conducted, but if the proposition holds true for lengths less than 500m, then it may mean a potentially simple solution to few mode transmission within a data centre. This is important as complex solutions are expensive and data centres are sensitive to the price of Small Form-factor Pluggables (SFPs) due to the large numbers used.

## 5.3 Amplification of Few-Mode Fibre

Getting the fibre amplifier to work such that it amplified each mode proved to be difficult, with the primary issue being the very small power level in the seed signal. This was exacerbated by the approach taken to launch more than one mode into the test fibre. Providing better matching launch fibre to reduce mismatch of the fields between fibres did help by reducing signal loss by approximately 16dB. A more powerful seed signal was not available to alternatively manage the problem. Testing demonstrated that adequate seed signal is required in order for few-mode amplification to work.

Amplifying two modes through a 2m length of cladding pumped Ytterbium-doped fibre amplifier demonstrated a higher degree of amplification of the fundamental mode over the second mode, but with a strong second mode signal containing more than 60% of the total power, amplification of the fundamental mode is only 5% or  $\sim 2$ dB greater than for the second mode. This is because, just as amplification has a

logarithmic relation to pump power, so amplification is dependent on the incoming seed signal power, a situation suggested by the way rare-earth amplifiers work as described by Figure 1.2 on page 5.

Also, when comparing the degree of gain achieved out of the same amount of pump power for a single injected mode and two injected modes as shown in Figure 5.5, two modes did fare better than one mode. This is because, at least for the short lengths of test fibres used, more amplification takes place with two modes as the fields extend further into the cladding than with a single mode and the bulk of the fields therefore got greater power level exposure to pump power energy.

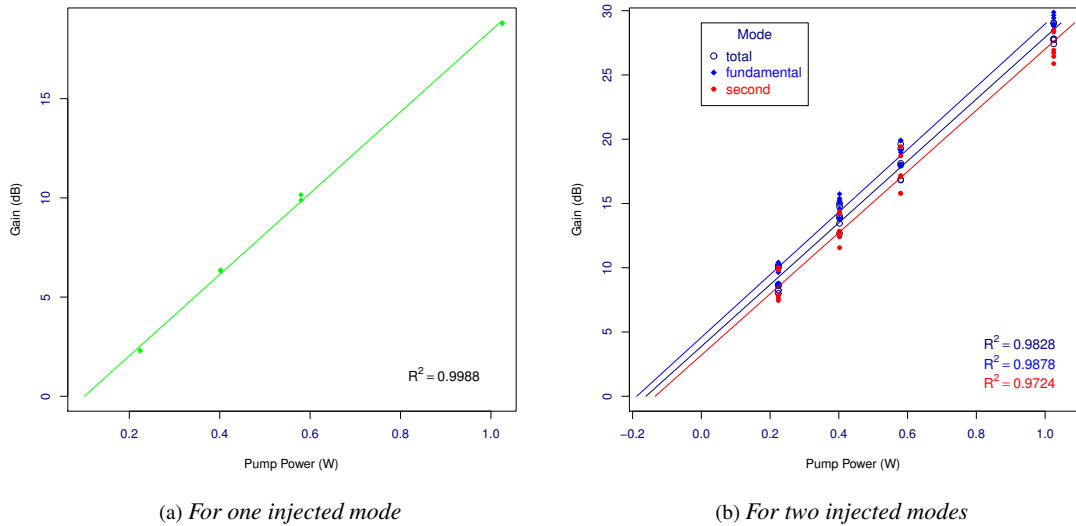


**Figure 5.5:** Ytterbium Doped Fibre Amplifier (YDFA) pump power to gain relationship

Given the measured length of the gain fibre is 2m, applying the formula of Equation 3.20, the gain coefficient for each pump power value for single- and for two-modes is plotted in Figure 5.6. This plot shows that the gain coefficient is linear with pump power, as implied in the formulae of Section 3.3.1, that is,  $\gamma \propto P_{pump}$  and therefore  $n_i \propto P_{pump}$  as is expected.

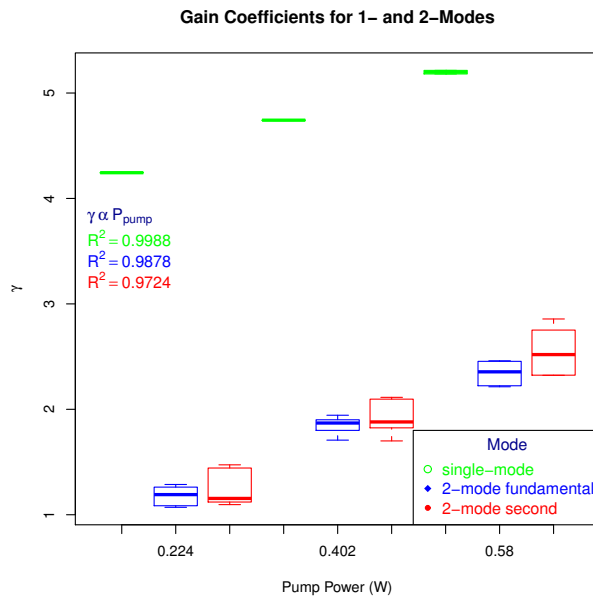


**Figure 5.6:** Gain Coefficient

# CHAPTER 6: CONCLUSIONS AND RECOMMENDATIONS

## 6.1 Outcomes

Testing on the approach of calculating the near-field model and then mapping it out to the far-field measured profile in order to determine the mode parameters works with an adequate degree of accuracy for the purposes of comparison of power in each of the modes, although the approach can do with some refinement. Therefore the technology devised here can be put to general use for purposes of measuring relative modal amplitudes in mode division multiplexing and in analysis of the quality of the output of power lasers.

Bend loss experiments demonstrated that, above the radius where power is stripped out of the core, bending does not noticeably affect the second mode any more than it does the fundamental mode. Further, the experiments demonstrated that, for two modes, the bend radius calculation for single mode provides an adequate guide for industry, a situation that is likely to exist for the higher order modes in general.

The observation that with higher initial amplitudes in the higher order modes, as was observed with 2-mode fibre, gives good amplification of those higher order modes means that there is an opportunity to exploit this feature in order to even out or otherwise control power amplification of the modes.

## 6.2 Further Work

Although the model has been built with more than two modes in mind, it currently handles just two modes. The model needs expanding to handle more than one mode. Further, the as the test results suggest separate calibration constants for the different number of modes may provide greater accuracy and help better account for the different propagation constants for the different modes, further investigation along that line should be conducted.

High power tests, that is more than milliwatts, were not conducted in the preparation of this thesis. AOFR's particular interests are in the area of high power modal analysis. The model needs validating for high power mode quantification and analysis.

In addition, testing done to support this thesis was plagued by losses caused by the apparatus used to inject more than one mode into a fibre. Although the fibre-air interface would have only contributed a small component of that loss, the interfaces do exist and provide an opportunity for further analysis of this important aspect of fibre technology. Further research should be conducted on the analysis and detail the four per cent reflection at the fibre-air interface and its consequential effects on the individual modes.

## REFERENCES

- ADVA, Feb 2011. Adva fsp 3000 data sheet. PDF, last accessed 23/05/2012.  
 URL [http://www.advaoptical.com/~media/Resources/Data%20Sheets/FSP\\_3000.ashx](http://www.advaoptical.com/~media/Resources/Data%20Sheets/FSP_3000.ashx)
- Andermahr, N., Theeg, T., Fallnich, C., 2008a. Novel approach for polarization-sensitive characterization of transversal modes in few-mode optical fibers. *Applied Physics B: Lasers and Optics* 91 (2), 353–357.  
 URL <http://www.springerlink.com/content/0167353268g42145/?p=78c29aa2e7a0433b8dc9e7f62128a00a&pi=24>
- Andermahr, N., Theeg, T., Fallnich, C., May 2008b. Novel approach for polarization-sensitive mode measurement and its application in few-mode fiber amplifier systems. In: *Lasers and Electro-Optics, 2008 and 2008 Conference on Quantum Electronics and Laser Science. CLEO/QELS 2008. Conference on. IEEE-Inst Electrical Electronics Engineers Inc*, pp. 1–2.
- Armitage, J., Wyatt, R., Ainslie, B., Craig-Ryan, S., 2 March 1989. Highly efficient 980 nm operation of a yb3+-doped silica fibre laser. *Electronics Letters* 25 (5), 298–299.
- Bassett, I., Canning, J., Argyros, A., 2004. Single mode fibre. Patent Application No. US2004/0151449 A1 filed 4/04/2003.
- Bjarklev, A., Hansen, S. L., Povlsen, J. H., 1990. Large signal modeling of an erbium doped fiber amplifier. In: DIGONNET, M. (Ed.), *Fiber Laser Sources and Amplifiers*. Vol. 1171 of *Proceedings of The Society of Photo-Optical Instrumentation Engineers (SPIE)*. Soc Photo Opt Instrumentat Engineers, SPIE - Int Soc Optical Engineering, Bellingham, pp. 118–129, conf On Fiber Laser Sources and Aplifiers, Boston, MA, SEP 06-08, 1989.
- Byron, K., Pitt, G., Dec 1985. Limits to power transmission in optical fibres. *Electronics Letters* 21 (19), 850–852.
- Campos, A., Srivastava, R., Roversi, J., August 1984. Characterization of single-mode fibers from wavelength dependence of modal field and far field. *Lightwave Technology, Journal of* 2 (4), 334–340.  
 URL <http://ieeexplore.ieee.org/stamp/stamp.jsp?tp=&arnumber=1073622>
- Carpenter, L. L., Jul 1974. Method of forming a light focusing fiber waveguide. US Patent No. 3823995.
- CorActive, 2011. Coractive active double clad fibers for high-power lasers and amplifiers. PDF, last accessed 24/06/2012.  
 URL [http://www.coractive.com/pdf/brochures/ActiveDCF\\_BR0006r09.pdf](http://www.coractive.com/pdf/brochures/ActiveDCF_BR0006r09.pdf)
- Corning, Jul 2011. Corning smf-28 ull optical fibre. PDF, last accessed 21/05/2012.  
 URL <http://www.corning.com/WorkArea/showcontent.aspx?id=41243>
- Corning, 2012. Optical fiber timeline. HTML.  
 URL <http://www.corning.com/opticalfiber/innovation/discovery/timeline.aspx>
- Curtiss, L. E., Hirschowitz, B., Peters, C. W., Jan 1957. A long fiberscope for internal medical examinations. *Journal of the Optical Society of America* 47 (1), 117–117, 41st Meeting of the Optical Society of America.
- Davis, C., Murphy, T., July 2011. Fiber-optic communications [in the spotlight]. *Signal Processing Magazine, IEEE* 28 (4), 152–150.

- Elliott, R. S., 2003. *Antenna Theory and Design*, revised Edition. IEEE Press Series on Electromagnetic Wave Theory. IEEE Press/John Wiley & Sons, Inc., Los Angeles, USA, original edition published in 1981.
- Fermann, M., Hanna, D., Shepherd, D., Suni, P., Townsend, J., 1 Sep 1988. Efficient operation of an yb-sensitised er fibre laser at 1.56  $\mu\text{m}$ . *Electronics Letters* 24 (18), 1135–1136.  
URL <http://ieeexplore.ieee.org/stamp/stamp.jsp?tp=&arnumber=19590>
- Fleisch, D., 2008. *A Student's Guide to Maxwell's Equations*. Cambridge University Press, The Edinburgh Building, Cambridge CB2 8RU, UK.
- Freude, W., Richter, H., 28 Aug 1986. Refractive-index profile determination of single-mode fibres by far-field power measurements at 1300 nm. *Electronics Letters* 22 (18), 945–947.  
URL <http://ieeexplore.ieee.org/stamp/stamp.jsp?tp=&arnumber=4256851>
- Freude, W., Sharma, A., Jun 1985. Refractive-index profile and modal dispersion prediction for a single-mode optical waveguide from its far-field radiation pattern. *Lightwave Technology, Journal of* 3 (3), 628–634.  
URL <http://ieeexplore.ieee.org/stamp/stamp.jsp?tp=&arnumber=1074231>
- Gambling, W., Payne, D., Matsumura, H., Dyott, R., September 1976a. Determination of core diameter and refractive-index difference of single-mode fibres by observation of the far-field pattern. *Microwaves, Optics and Acoustics, IEE Journal on* 1 (1), 13–17.  
URL <http://ieeexplore.ieee.org/stamp/stamp.jsp?tp=&arnumber=4807415>
- Gambling, W., Payne, D., Matsumura, H., Dyott, R., 14 Oct 1976b. Routine characterisation of single-mode fibres. *Electronics Letters* 12 (21), 546–547.  
URL <http://ieeexplore.ieee.org/stamp/stamp.jsp?tp=&arnumber=4240131&isnumber=4240129>
- Gloge, D., 1971. Weakly guiding fibers. *Applied Optics* 10 (10), 2252–2258.
- Gordon, J., Kogelnik, H., 25 Apr 2000. Pmd fundamentals: Polarization mode dispersion in optical fibers. *Proceedings Of The National Academy Of Sciences Of The United States of America* 97 (9), 4541–4550.
- Hanna, D., Percival, R., Perry, I., Smart, R., Suni, P., Townsend, J., Tropper, A., Jun 1988a. Continuous-wave oscillation of a monomode ytterbium-doped fibre laser. In: *All-Fibre Devices*, IEE Colloquium on. IEEE, pp. 14/1–14/4.  
URL <http://ieeexplore.ieee.org/stamp/stamp.jsp?tp=&arnumber=209401>
- Hanna, D., Percival, R., Perry, I., Smart, R., Suni, P., Townsend, J., Tropper, A., 18 Aug 1988b. Continuous-wave oscillation of a monomode ytterbium-doped fibre laser. *Electronics Letters* 24 (17), 1111–1113.  
URL <http://ieeexplore.ieee.org/stamp/stamp.jsp?tp=&arnumber=191771>
- Haykin, S., 1978. *Communication Systems*. John Wiley & Sons Inc.
- Hecht, J., 2004. *City of light : the story of fiber optics*, rev. and expanded ed Edition. The Sloan technology series. Oxford University Press, New York, USA.
- Hecht, J., N.D. A short history of fiber optics. HTML, reproduced from *Fiber Optics Technician's Handbook*, by Jim Hayes, Delmar Publishers, Albany, New York. Last Accessed 22/05/2012.  
URL <http://www.sff.net/people/jeff.hecht/history.html>
- Hewlett, S., 26 Sep 2012. Effects of core-cladding interface on modes. Personal communication.

- Huang, C., Chang, C., Jheng, D., Hsu, K., Huang, S., Huang, D., April 2012. Direct side pumping of double-clad fiber laser by laser diode array through the use of subwavelength grating coupler. *Photonics Journal, IEEE* 4 (2), 411–421.  
URL <http://ieeexplore.ieee.org/stamp/stamp.jsp?tp=&arnumber=6144685>
- I-Tech, 2012. Cisco oc3/stm1 sfp, single-mode fibre, intermediate reach sfp-oc3-ir1=. HTML, last accessed 24/05/2012 - price AUD636.00 inc GST.  
URL [http://www.itech.com.au/products/108221\\_CISCO\\_OC3\\_\\_STM1\\_SFP\\_\\_Single\\_mode.aspx](http://www.itech.com.au/products/108221_CISCO_OC3__STM1_SFP__Single_mode.aspx)
- Ip, E., Bai, N., Huang, Y.-K., Mateo, E., Yaman, F., Li, M.-J., Bickham, S., Ten, S., Linares, J., Montero, C., Moreno, V., Prieto, X., Tse, V., Chung, K. M., Lau, A., Tam, H.-Y., Lu, C., Luo, Y., Peng, G.-D., Li, G., Sept. 2011. 88x3x112-gb/s wdm transmission over 50 km of three-mode fiber with inline few-mode fiber amplifier. In: *Optical Communication (ECOC), 2011 37th European Conference and Exhibition on*. pp. 1–3.
- Jachetta, J., Oct 2008. Fiber-optic transport. *Broadcast Engineering* 50 (10), 12,14–19, last accessed 5/05/2012.  
URL <http://search.proquest.com/docview/218618539?accountid=8330>
- Kao, K. C., Hockham, G. A., July 1966. Dielectric-fibre surface waveguides for optical frequencies. *Electrical Engineers, Proceedings of the Institution of* 113 (7), 1151–1158.
- Kapron, F., Keck, D., Maurer, R., 1970. Radiation losses in glass optical waveguides. *Applied Physics Letters* 17 (10), 423–&.
- Keck, D. B., Jul 2000. Optical fiber spans 30 years. *Lightwave Magazine (reprint)* -, 1–3, last accessed 21/05/2012.  
URL <http://www.corning.com/WorkArea/linkit.aspx?LinkIdentifier=id&ItemID=10941>
- Keck, D. B., Schultz, P. C., Jan 1973. Method of producing optical waveguide fibers. US Patent No. 3711262.
- Koebele, C., Salsi, M., Charlet, G., Bigo, S., Sep 15 2011a. Nonlinear effects in mode-division-multiplexed transmission over few-mode optical fiber. *Photonics Technology Letters, IEEE* 23 (18), 1316–1318.
- Koebele, C., Salsi, M., Sperti, D., Tran, P., Brindel, P., Mardoyan, H., Bigo, S., Boutin, A., Verluise, F., Sillard, P., Astruc, M., Provost, L., Cerou, F., Charlet, G., 15 Aug 2011b. Two mode transmission at 2x100gb/s, over 40km-long prototype few-mode fiber, using lcos-based programmable mode multiplexer and demultiplexer. *Optics Express* 19 (17), 16593–16600, last accessed 21/11/2011.  
URL <http://www.opticsinfobase.org/viewmedia.cfm?uri=oe-19-17-16593&seq=0>
- Kreyszig, E., 1972. *Advanced Engineering Mathematics*, 3rd Edition. John Wiley & Sons Inc., Ohio State University, Columbus, Ohio.
- Liu, J.-M., 2005. *Photonic Devices*. Cambridge University Press, The Edinburgh Building, Cambridge CB2 8RU, UK.
- Love, J., Riesen, N., 1 Feb 2012. Single-, few-, and multimode y-junctions. *Lightwave Technology, Journal of* 30 (3), 304–309.  
URL <http://ieeexplore.ieee.org/xpl/articleDetails.jsp?arnumber=6105499>

- Love, J. D., 2009a. Lecture-04-02/03/09. WebCT, last accessed 15 March 2009.  
URL [http://webct.anu.edu.au/SCRIPT/PHYS3060\\_Sem\\_1\\_2009/scripts/student/serve\\_tree.pl?3619134969++START++\\_homepage#](http://webct.anu.edu.au/SCRIPT/PHYS3060_Sem_1_2009/scripts/student/serve_tree.pl?3619134969++START++_homepage#)
- Love, J. D., 2009b. Lecture-07-11/03/09. WebCT, last accessed 24 April 2009.  
URL [http://webct.anu.edu.au/SCRIPT/PHYS3060\\_Sem\\_1\\_2009/scripts/student/serve\\_tree.pl?3619134969++START++\\_homepage#](http://webct.anu.edu.au/SCRIPT/PHYS3060_Sem_1_2009/scripts/student/serve_tree.pl?3619134969++START++_homepage#)
- Love, J. D., Sep 2011. Engn6613 lecture-18-28/09/11. PDF, last accessed 28/09/2011.  
URL <http://wattlecourses.anu.edu.au/mod/resource/view.php?id=331068>
- Marcuse, D., Dec 1993. Bend loss of slab and fiber modes computed with diffraction theory. *Quantum Electronics, IEEE Journal of* 29 (12), 2957–2961.
- Mears, R., Reekie, L., Poole, S., Payne, D., 15 Aug 1985. Neodymium-doped silica single-mode fibre lasers. *Electronics Letters* 21 (17), 738–740.
- Mears, R., Reekie, L., Poole, S., Payne, D. N., 30 Jan 1986. Low-threshold tunable cw and q-switched fibre laser operating at 1.55  $\mu\text{m}$ . *Electronics Letters* 22 (3), 159–160.  
URL <http://ieeexplore.ieee.org/stamp/stamp.jsp?tp=&arnumber=4256297>
- Michtchenko, A., Nava, M., Sept. 2006. Far field technique applied in single mode optical fibers for studying of modal field diameter. In: *Electrical and Electronics Engineering, 2006 3rd International Conference on. IEEE*, pp. 1–3.  
URL <http://ieeexplore.ieee.org/stamp/stamp.jsp?tp=&arnumber=4017957>
- Nicholson, J. W., Yablon, A. D., Fini, J. M., Mermelstein, M. D., Jan. 2009. Measuring the modal content of large-mode-area fibers. *Selected Topics in Quantum Electronics, IEEE Journal of* 15 (1), 61–70, sponsored by IEEE Photonics Society.
- Nicholson, J. W., Yablon, A. D., Ramachandran, S., Ghalimi, S., 12 May 2008. Spatially and spectrally resolved imaging of modal content in large-mode-area fibers. *Optics Express* 16 (10), 7233–7243.
- Nicol, D. R., Harvey, J. T., Svoboda, V., Donaghy, F. A., Storey, C. H., Ballinger, K. R., Jul 1978. A 2 km optical fiber communication trial. *Communications, IEEE Transactions on* 26 (7), 1061–1067, last accessed 20/05/2012.  
URL <http://ieeexplore.ieee.org/stamp/stamp.jsp?tp=&arnumber=1094173>
- Ogilvie, G., Esdaile, R., Kidd, G., 2 Nov 1972. Transmission loss of tetrachloroethylene-filled liquid-core-fibre light guide. *Electronics Letters* 8 (22), 533–534.
- Openreach, Jan 2012. Fsp 3000 overview slides. PDF, last accessed 23/05/2012.  
URL <https://www.openreach.co.uk/orpg/home/products/ethernet-services/opticalspectrumaccess/downloads/FSP%203000%20overview%20slides.pdf>
- Paschotta, R., Feb 2012. Encyclopedia of laser physics and technology - fiber amplifiers. HTML, last accessed 10/03/2012.  
URL [http://www.rp-photonics.com/fiber\\_amplifiers.html](http://www.rp-photonics.com/fiber_amplifiers.html)
- Paschotta, R., Nilsson, J., Tropper, A., Hanna, D., Jul 1997. Ytterbium-doped fiber amplifiers. *Quantum Electronics, IEEE Journal of* 33 (7), 1049–1056.  
URL <http://ieeexplore.ieee.org/stamp/stamp.jsp?tp=&arnumber=594865>
- Pask, H., Archambault, J., Hanna, D., Reekie, L., Russell, P., Townsend, J., Tropper, A., 26 May 1994. Operation of cladding-pumped yb<sup>3+</sup>-doped silica fibre lasers in 1  $\mu\text{m}$  region. *Electronics Letters* 30 (11), 863–865.  
URL <http://ieeexplore.ieee.org/stamp/stamp.jsp?tp=&arnumber=287471>

- Pedersen, B., Dybdal, K., Hansen, K., Bjarklev, A., Povlsen, J. H., Vendeltoft-Pommer, H., Larsen, C. C., Dec 1990. Detailed theoretical and experimental investigation of high-gain erbium-doped fiber amplifier. *Photonics Technology Letters, IEEE* 2 (12), 863–865.
- Petermann, K., 25 Oct 1979. Wavelength-dependent transmission at fibre connectors. *Electronics Letters* 15 (22), 706–708.
- Poole, C. D., Wang, S., 15 Oct 1993. Bend-induced loss for the higher-order spatial mode in a dual-mode fiber. *Optics Letters* 18 (20), 1712–1714.
- Poole, S., Payne, D., Fermann, M., 15 Aug 1985. Fabrication of low-loss optical fibres containing rare-earth ions. *Electronics Letters* 21 (17), 737–738.
- R Development Core Team, 2010. *R: A Language and Environment for Statistical Computing*. R Foundation for Statistical Computing, Vienna, Austria.  
URL <http://www.R-project.org>
- Randel, S., Ryf, R., Sierra, A., Winzer, P. J., Gnauck, A. H., Bolle, C. A., Essiambre, R.-J., Peckham, D. W., McCurdy, A., Lingle, Jr., R., Aug 15 2011. 6x56-gb/s mode-division multiplexed transmission over 33-km few-mode fiber enabled by 6x6 mimo equalization. *Optics Express* 19 (17), 16697–16707, last accessed 21/11/2011.  
URL <http://www.opticsinfobase.org/viewmedia.cfm?uri=oe-19-17-16697&seq=0>
- Renaud, C., Selvas-Aguilar, R., Nilsson, J., Turner, P., Grudinin, A., Aug. 1999. Compact high-energy q-switched cladding-pumped fiber laser with a tuning range over 40 nm. *Photonics Technology Letters, IEEE* 11 (8), 976–978.  
URL <http://ieeexplore.ieee.org/stamp/stamp.jsp?tp=&arnumber=775318>
- Riesen, N., Love, J., Jun 2011. Dispersion equalisation in few-mode fibres. *Optical and Quantum Electronics* 42, 577–585.  
URL <http://www.springerlink.com/content/v387455562k30508/>
- Riesen, N., Love, J., Arkwright, J., 1 March 2012. Few-mode elliptical-core fiber data transmission. *Photonics Technology Letters, IEEE* 24 (5), 344–346.  
URL <http://ieeexplore.ieee.org/xpl/articleDetails.jsp?arnumber=6097024>
- Rodriguez, V., Aug. 2008. Half power beamwidth and high power measurements: The dangers of using far field approximations in the near field. In: *Electromagnetic Compatibility, 2008. EMC 2008. IEEE International Symposium on. IEEE, Detroit, MI, U.S.A.*, pp. 1–6.  
URL <http://ieeexplore.ieee.org/stamp/stamp.jsp?tp=&arnumber=4652224>
- Router-Switch, 2012. Glc-sx-mm. HTML, last accessed 24/05/2012 - price AUD209.34.  
URL <http://www.router-switch.com/glc-sx-mm-p-1747.html>
- Saleh, A. A. M., Jopson, R. M., Evankow, J. D., Aspell, J., Oct 1990. Modeling of gain in erbium-doped fiber amplifiers. *Photonics Technology Letters, IEEE* 2 (10), 714–717.
- Shaklan, S., 20 Oct 1991. Selective mode injection and observation for few-mode fiber optics. *Applied Optics* 30 (30), 4379–4383.
- Snyder, A. W., Dec 1969a. Asymptotic expressions for eigenfunctions and eigenvalues of a dielectric or optical waveguide. *Microwave Theory and Techniques, IEEE Transactions on* 17 (12), 1130–1138.  
URL <http://ieeexplore.ieee.org/stamp/stamp.jsp?tp=&arnumber=1127112>

- Snyder, A. W., Dec 1969b. Excitation and scattering of modes on a dielectric or optical fiber. *Microwave Theory and Techniques, IEEE Transactions on* 17 (12), 1138 – 1144.  
URL <http://ieeexplore.ieee.org/stamp/stamp.jsp?tp=&arnumber=1127113>
- Snyder, A. W., Love, J. D., 1983. *Optical waveguide theory*. Chapman and Hall, London; New York, reprint available from Kluwer Academic Publishers.
- Sommer, R., Deluca, R., Burke, G., 5 Aug 1976. New glass system for low-loss optical waveguides. *Electronics Letters* 12 (16), 408 –409, Corning Glass Works.
- Song, K. Y., Jun 2012. Effects of induced birefringence on Brillouin dynamic gratings in single-mode optical fibers. *Opt. Lett.* 37 (12), 2229–2231.  
URL <http://ol.osa.org/abstract.cfm?URI=ol-37-12-2229>
- Tucker, R. S., Oct 2005. Photonics down under. In: *Lasers and Electro-Optics Society, 2005. LEOS 2005. The 18th Annual Meeting of the IEEE. IEEE*, pp. 43–44, also in *IEEE Lasers & Electro-Optics Society Newsletter, Vol 20, No 1, Feb 2006*, pg 14-20.  
URL <http://photonicsociety.org/newsletters/feb06/leos0206.pdf>
- Ulrich, K. T., Eppinger, S. D., 2004. *Product Design and Development*, 3rd Edition. McGraw-Hill/Irwin, ISBN-13: 978-0-07-247146-5.
- Zorn, J. C., Nov 2009. Michigan discovery: Fiber optics for the transmission of images. HTML, last accessed 20/05/2012.  
URL <https://lsa-cms1.lsa.umich.edu/umich/v/index.jsp?vgnextoid=4dd418dcccfb4210VgnVCM100000a3b1d38dRCRD&vgnnextchannel=cf8820ffcbcfc11020ffcbcfc1109db1d38dRCRD&vgnnextfmt=print&vgnnextrefresh=1>

# APPENDIX A: DETAILED CUSTOMER NEEDS AND METRICS

## A.1 Customer Needs

The customer statements, for processing into interpreted needs, were gleaned from discussions with the supervisors.

The interpreted needs were then organised into a hierarchy, ready for ranking. The interpreted needs were ranked using key ANU and AOFR stakeholders from lowest to highest in order of importance. The ranking was scaled to a 1 to 5 scale with 5 being most important and 1 being least important. The guideline applied is from Ulrich and Eppinger (2004, pg 67). For quick visual analysis, a 3 star rating was also applied.

Table A.1 details the customer statements after collection into like statements. The table also shows the interpreted needs relating to each statement and allocates each interpreted need a primary need for summarising into a hierarchy.

**Table A.1:** *Customer statements and interpreted needs*

The device must be able to measure the power in the modes of ordinary data transmission cladding pumped fibre amplifier.	The device shall be capable of measuring power in individual modes at levels of between 3nW and 10 mW (-55 to 10 dBm).	The device can measure power in individual modes
The device must be able to measure the power in the modes of a cladding pumped laser.	The device shall be capable of measuring power in individual modes at levels of up to at least 1 kW.	The device can measure power in individual modes
The device must be capable of being prototyped using equipment available at AOFR.	The device shall be constructed using either a LD8900R Goniometric Radiometer or a UCD 12 camera.	The device can be prototyped using available parts and instruments.
The device must be able to work with Erbium doped fibres.	The device shall be capable of measuring modal power from single and few-mode erbium doped fibres.	The device can measure the modal power in common fibre types.
The device must be able to work with standard weakly guiding glass fibres.	The device shall be capable of measuring modal power from single and few-mode silica fibres.	The device can measure the modal power in common fibre types.
The device needs to tell the relative difference in power between the modes.	The device shall be capable of presenting the power of each mode as a percentage of the total power measured.	The device can measure power in individual modes.
The results need to be repeatable.	The device shall have a measurement tolerance for the modes of better than 5% variation against total power measured.	The device has an accuracy level enabling its use in commercial applications.

Customer Statement	Interpreted Need	Primary Need(s)
The results need to be explainable through a mathematical model.	A theory for the few-mode power amplification needs to be developed, upon which the device shall be based.	The device operation matches sound theory.
It would be useful if the device could tell how much power is sloshing around in the cladding.	The device shall be capable of measuring relative power from cladding modes.	The device can measure power in individual modes.
It needs to be designed and prototyped by September.	The device shall be designed and demonstrated to work within 5 months from design analysis commencement.	The project budget and schedule shall be met.

The results of the assignment of order of importance to interpreted needs is shown in Table A.2. This table shows the ranked needs in hierarchical order. The importance ratings for the level 1 items in the interpreted needs hierarchy are shown in Table A.3.

**Table A.2: Interpreted Needs Hierarchy**

	***	<b>The device can measure power in individual modes.</b>	5
1	***	The device shall be capable of measuring power in individual modes at levels of between 3 nW and 10 mW (-55 to 10 dBm).	5
2	***	The device shall be capable of measuring power in individual modes at levels of up to at least 1 kW.	5
3	***	The device shall be capable of presenting the power of each mode as a percentage of the total power measured.	5
4	***	The device shall be capable of measuring relative power from cladding modes.	5
		<b>The device can be prototyped using available parts and instruments.</b>	1
5		The device shall be constructed using either a LD8900R Goniometric Radiometer or a UCD 12 camera.	1
	**	<b>The device can measure the modal power in common fibre types.</b>	3
6	**	The device shall be capable of measuring modal power from single and few-mode erbium doped fibres.	3
7	**	The device shall be capable of measuring modal power from single and few-mode silica fibres.	3
	***	<b>The device has an accuracy level enabling its use in commercial applications.</b>	5
8	***	The device shall have a measurement tolerance for the modes of better than 5% variation against total power measured.	5
	**	<b>The device operation matches sound theory.</b>	3
9	**	A theory for the few-mode power amplification needs to be developed, upon which the device shall be based.	3
10		The project budget and schedule shall be met.	2
		The device shall be designed and demonstrated to work within 5 months from design analysis commencement.	2

**Table A.3:** *Importance Ratings for Primary Customer Needs*

<b>Primary Customer Need</b>	<b>Importance</b>
The device can measure power in individual modes.	5
The device can be prototyped using available parts and instruments.	1
The device can measure the modal power in common fibre types.	3
The device has an accuracy level enabling its use in commercial applications.	5
The device operation matches sound theory.	3

# APPENDIX B: DESIGN DETAILS

## B.1 Concept Selection of Power Detector

If we consider the Image Focus and Pre-processing and the Image processing functional blocks together for the purposes of the initial concept generation and screening, then take the selection from that and separate it back out into its two constituent components for detailed design, the fundamental process for measurement can be more effectively selected.

A concept classification tree is shown at Figure B.1. A pictorial description of the design of each option for each of the functional blocks is shown in Table B.1.

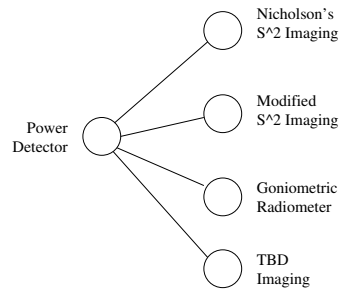


Figure B.1: Classification tree for the power detector

Table B.1: Option design for each of the functional blocks

Option	Image Focus and Pre-processing	Image Processing
Nicholson's $S^2$ Imaging		
Modified $S^2$ Imaging		
Goniometric Radiometer		

Details of the options are as follows:

$S^2$  Imaging The Spatially and Spectrally resolved imaging approach proffered by Nicholson et al. (2008) involves raster scanning the optical intensity of a magnified image of the fibre output with an

optical spectrum analyser, via a polariser to ensure the mode polarisation is known, to determine the power level.

- Polariser is used to ensure the polarisation states of the modes are aligned to the single-mode fibre end face.
- The polariser is rotated to fully characterise the multi-path interference.
- Modes are orthogonal, which means the beam must be sampled point wise to observe interference between the modes.
- A Fourier transform is done of the spectrum (power against wavelength) at each point.
- The points are scanned at  $20 \times 20$  or  $30 \times 30$  pixel resolution with a mode field diameter of  $4.8\mu m$ .
- The final result is

$$A(D_{grp}) = \sum_{x=0, y=0}^{\infty} f(P(x, y, \omega))$$

Modified  $S^2$  is a modification of the the  $S^2$  Imaging approach whereby the  $x - y$  scanning stage is replaced by a high resolution CCD arrangement and possibly a tunable source as opposed to a broadband source for faster imaging and image processing. It otherwise has the same aspects and considerations as the  $S^2$  Imaging approach.

LD8900R is a Goniometric Radiometer based approach whereby the intensity of the modal image, taken and presented in 3 dimensions, is processed into a power level equivalent. This concept assumes that there is a direct relationship between the intensity measurement made by the LD8900R and the power level in each mode.

Design considerations are outlined in Table 4.1 at Section 4.2 above with a preliminary concept selection against metrics detailed in Table B.2 and with specific comparison against customer needs detailed in Table B.3, where the concept scoring matrix approach was used.

**Table B.2:** Concept screening for the Power Detector

Selection Criteria		Concepts		
		$S^2$ Imaging	Mod $S^2$ Imaging	Gon. Rad
1	Total power level accuracy at 1mW in Er doped fibre	0	0	+
2	Total power level accuracy at 1W in Er doped fibre	+	+	0
3	Total power level maximum in Er doped fibre	0	0	-
5	Total power level accuracy at 1mW in Yb doped fibre	0	0	+
6	Total power level accuracy at 1W in Yb doped fibre	+	+	0
7	Total power level maximum in Yb doped fibre	0	0	-
9	Total power level accuracy at 1mW in Corning fibre	0	+	+
10	Total power level accuracy at 1W in Corning fibre	+	+	0
11	Total power level maximum in Corning fibre	0	0	-
13	Relative power levels for each mode when compared to total measured power	-	0	+
14	Price of prototype construction, not including available components or tools	-	+	+
15	Schedule variance at the end of project	-	+	+
	Sum +s	3	6	6
	Sum 0s	6	6	3
	Sum -s	-3	0	-3
	Net score	0	6	3
	Rank	3	1	2
	Continue?	Maybe	Y	Y

**Table B.3:** Match rating for the power detector against interpreted customer needs (1=much worse, 3=same, 5=much better)

No.	Need	Imp.	Weight	$S^2$ Imaging	Mod $S^2$ Imaging	Gon. Rad
1	The device shall be capable of measuring power in individual modes at levels of between 10 and 100 mW.	5	15%	2	3	5
2	The device shall be capable of measuring power in individual modes at levels of up to at least 1 kW.	5	15%	1	3	4
3	The device shall be capable of measuring modal power at 1550nm wavelength.	5	15%	3	3	3
4	The device shall be capable of measuring modal power at 1060nm wavelength.	5	15%	3	3	3
7	The device shall be constructed using either a LD8900R Goniometric Radiometer or a UCD 12 camera.	1	3%	1	3	3
8	The device shall be capable of measuring modal power from single and few-mode erbium doped fibres.	3	9%	3	3	3
9	The device shall be capable of measuring modal power from few-mode Ytterbium doped fibres.	3	9%	4	3	3
10	The device shall be capable of measuring modal power from single and few-mode silica fibres.	3	9%	3	3	4
13	The device shall be designed and demonstrated to work within 5 months from design analysis commencement.	3	9%	3	3	4
Total Score			100%	2.58	3	3.64
Rank				3	2	1
Continue?				No	No?	Yes

## B.2 Concept Generation of 3-Dimensional Intensity Extraction

### B.2.1 Intensity Extraction

The Goniometric Radiometer has a hemispherical detection structure with 3241 detectors evenly spaced between  $\pm 1.32653rad$ .  $0rad$  is treated as vertical. This device sweeps through  $180^\circ(\pi rad)$ , taking 10, 20, 50, 100 and 200 scans. As it covers nearly a full half circle, it effectively sweeps the full  $360^\circ$ .

The Goniometric Radiometer software can output the data for a 3-dimensional sweep into a binary file with a '.prw' extension. This file contains the actual number of scans taken, the number of measurement points (presumably always 3241), an array of the angles of each of the 3241 detectors and the measured intensity, in counts, arranged in sets of scans with each containing a set of measurement points.

The approach taken to reading in and formatting up the data for matching to the model is as follows:

1. Read in the number of scans and the number of measurement points (these are 2 byte unsigned integers).
2. Read in the measurement point angles into an array (these are IEEE 754 floating point numbers).
3. Read in the intensity data (these are IEEE 754 floating point numbers) into an array of scans by angles.
4. Translate the intensity data into a polar coordinate arrangement for easy processing, in the format of  $(\phi, r, z)$ .
5. Perform calculations on the data to determine the maxima for the fundamental and second modes (other modes not handled at this stage) and calculate the offset from  $(0, 0)$  of the data centre (to

account for slight misalignment of the fibre to the detectors). Output this data to a text file for further processing by the 3-Dimensional Model Generation and the Measured-to-Theoretical Matching functions.

6. Output the intensity data, in  $(\phi, r, z)$  format, to a comma separated value file for further processing by the Measured-to-Theoretical Matching function.

## B.2.2 Mode Intensity Maxima and Minima Detection

This approach is only designed to work for one or two modes. It would need further considerable work to deal with more than 2 modes. The concept adopted is to split the measured data into 2 parts, look for peaks in each part, rotate if more than one peak is not detected, then if still one peak is detected, it is single moded. The maximum intensity detected is the value output as is the position of this peak. Otherwise the fibre is assumed to be two moded.

A line is drawn between the two peaks and the minima point along that line is found. This point is assumed to be the centre of the fibre. Given the equation of the line  $r = f(\phi)$ , for increasing angle  $(\phi)$  from the peak with the smallest angle out to the peak with the largest angle, calculate  $r$  and determine if it is the point of minimum. Save the minimum for passing on to the other functions.

The calculation of the radius, given the polar coordinates of the two peaks, being  $A(t, \theta) = A(x_1, y_1)$  and  $B(s, \psi) = B(x_2, y_2)$ , then for a point  $P(r, \phi) = P(x, y)$ , is calculated in accordance with Figure B.2, using Equations B.1, B.2 and B.3 for the line and Equation B.4 for the slope of the line and the indicial Equation B.5 for the line given a point on the line.

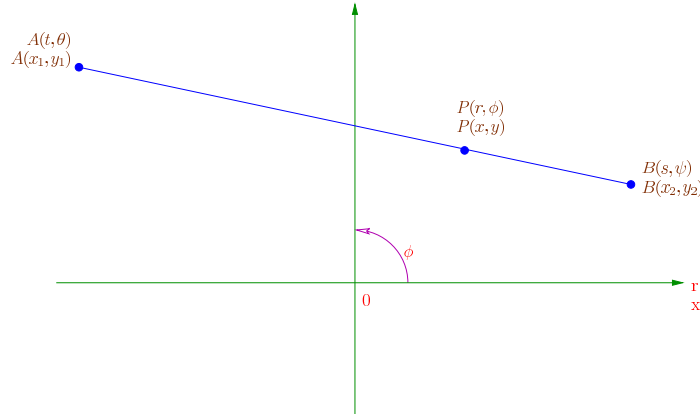


**Figure B.2:** Calculation of  $r = f(\phi)$  for a line in polar coordinate system

$$A(t, \theta) : \begin{cases} x_1 = t \cos \theta \\ y_1 = t \sin \theta \end{cases} \quad (\text{B.1})$$

$$B(s, \psi) : \begin{cases} x_2 = s \cos \psi \\ y_2 = s \sin \psi \end{cases} \quad (\text{B.2})$$

$$P(r, \phi) : \begin{cases} x = r \cos \phi \\ y = r \sin \phi \end{cases} \quad (\text{B.3})$$

$$m = \frac{y_2 - y_1}{x_2 - x_1} \quad (\text{B.4})$$

$$y - y_1 = m(x - x_1) \quad (\text{B.5})$$

Substituting Equation B.1 into Equation B.5 results in Equation B.6.

$$y - t \sin \theta = m(x - t \cos \theta) \quad (\text{B.6})$$

Substituting Equation B.1 and Equation B.2 into Equation B.4 results in Equation B.7.

$$m = \frac{s \sin \psi - t \sin \theta}{s \cos \psi - t \cos \theta} \quad (\text{B.7})$$

Substituting Equation B.7 into Equation B.6 results in Equation B.8.

$$y - t \sin \theta = \frac{(s \sin \psi - t \sin \theta)(x - t \cos \theta)}{s \cos \psi - t \cos \theta} \quad (\text{B.8})$$

Substituting Equation B.3 into Equation B.8 results in Equation B.9, which works through Equations B.10 to B.13 (at Equation B.12 the denominators cancel provided that  $s \cos \psi - t \cos \theta \neq 0$ ), resulting in Equation B.14 for  $r$ .

$$r \sin \phi - t \sin \theta = \frac{(s \sin \psi - t \sin \theta) r \cos \phi}{s \cos \psi - t \cos \theta} - \frac{(s \sin \psi - t \sin \theta) t \cos \theta}{s \cos \psi - t \cos \theta} \quad (\text{B.9})$$

$$r \sin \phi - \frac{(s \sin \psi - t \sin \theta) r \cos \phi}{s \cos \psi - t \cos \theta} = t \sin \theta - \frac{(s \sin \psi - t \sin \theta) t \cos \theta}{s \cos \psi - t \cos \theta} \quad (\text{B.10})$$

$$\frac{(s \cos \psi - t \cos \theta) r \sin \phi - (s \sin \psi - t \sin \theta) r \cos \phi}{s \cos \psi - t \cos \theta} = \frac{(s \cos \psi - t \cos \theta) t \sin \theta - (s \sin \psi - t \sin \theta) t \cos \theta}{s \cos \psi - t \cos \theta} \quad (\text{B.11})$$

$$(s \cos \psi - t \cos \theta) r \sin \phi - (s \sin \psi - t \sin \theta) r \cos \phi = (s \cos \psi - t \cos \theta) t \sin \theta - (s \sin \psi - t \sin \theta) t \cos \theta \quad (\text{B.12})$$

$$r((s \cos \psi - t \cos \theta) \sin \phi - (s \sin \psi - t \sin \theta) \cos \phi) = (s \cos \psi - t \cos \theta) t \sin \theta - (s \sin \psi - t \sin \theta) t \cos \theta \quad (\text{B.13})$$

$$r = \frac{(s \cos \psi - t \cos \theta) t \sin \theta - (s \sin \psi - t \sin \theta) t \cos \theta}{(s \cos \psi - t \cos \theta) \sin \phi - (s \sin \psi - t \sin \theta) \cos \phi} \quad (\text{B.14})$$

To ensure that the measured peaks are not just the same peak with little bumps on it, which a computer algorithm would otherwise find even when the detection algorithm is working from the centre (where peaks

should be concentrated) outwards, the distance between the peaks is detected. If they are too close, say within two per cent of the total radius, then they are assumed to be the same peak. The distance between the peaks is calculated, using the polar coordinate notation of Figure B.3, using the Cosine rule as Equation B.15.

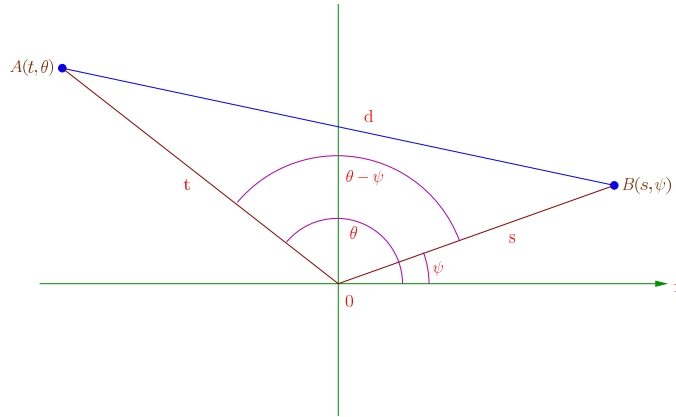


Figure B.3: Calculation of the distance,  $d$ , between two points

$$d = \sqrt{t^2 + s^2 - 2st \cos(\theta - \psi)} \tag{B.15}$$

## B.3 Concept Selection of Power Profile Formula

### B.3.1 Formula Selection

The two readily available options for the choice of the formula and the surrounding parameters that will need to be accounted for or approximated are to enhance the formulae from Snyder and Love (1983) or to use the formulae from Liu (2005) and apply approximations and enhancements to it using formulae from Snyder and Love (1983). A concept classification tree is at Figure B.4.

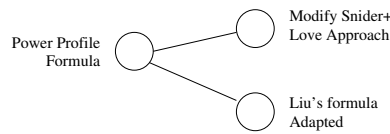


Figure B.4: Classification tree for the power profile formula

Details of the options are as follows:

Derive from S+L Use formulae of Snyder and Love (1983, pp 311, 319) for  $I = \sum |a_n|^2 |\psi_n|^2 + \phi$ , where  $\psi_1 = \frac{J_0(U_1 R)}{J_0(U)}$ ,  $\psi_2 = \frac{J_1(U_2 R)}{J_1(U)}$  and  $\phi = 2ke \{ a_1 \psi_1 a_2^* \psi_2^* e^{j(\Delta\beta z)} \}$  for each mode and rework into the intensity profile formula. Expand the formula to yield the intensity profile. Match the intensity profile to that measured and integrate the intensity profile to provide the power.

Liu+ Use the intensity formula,  $I(\phi, r)$ , of Liu (2005, pp 133), approximating an expression for  $\beta$  from Snyder and Love (1983, pp 283) given that it is part way between  $kn_{cl}$  and  $kn_{co}$  ( $\beta$  is the propagation constant, where  $k = \frac{2\pi}{\lambda}$  is the free space wave number,  $n_{cl}$  is the cladding refractive index,  $n_{co}$  is the core refractive index and  $\lambda$  is the wavelength) so assume it is half way in between, and use the Liu (2005, pp 122) definitions of  $k_{co}^2 = \frac{\omega^2 n_{co}^2}{c^2}$  where  $\omega = \frac{2\pi c}{\lambda}$  is

the angular frequency (and  $c$  is the speed of light in a vacuum) and  $k_{cl}^2 = \frac{\omega^2 n_{cl}^2}{c^2}$  to determine  $h$  and  $\gamma$ .

Considerations for the two options are outlined in Table 4.2 at Section 4.2 above with concept selection assessment against metrics detailed in Table B.4 and with comparison against customer needs detailed in Table B.5, where the concept scoring matrix approach was used.

**Table B.4:** Concept screening for the power profile formula

Selection Criteria		Concepts	
		Derive from S+L	Liu+
1	Total power level accuracy at 1mW in Er doped fibre	0	0
2	Total power level accuracy at 1W in Er doped fibre	0	0
4	Relative power levels difference when compared to calculated – Er fibre	0	0
5	Total power level accuracy at 1mW in Yb doped fibre	0	0
6	Total power level accuracy at 1W in Yb doped fibre	0	0
8	Relative power levels difference when compared to calculated – Yb fibre	0	0
9	Total power level accuracy at 1mW in Corning fibre	0	0
10	Total power level accuracy at 1W in Corning fibre	0	0
12	Relative power levels difference when compared to calculated – Corning fibre	0	0
13	Relative power levels for each mode when compared to total measured power	0	0
15	Schedule variance at the end of project	-	0
	Sum +s	0	0
	Sum 0s	10	11
	Sum -s	1	0
	Net score	-1	0
	Rank	2	1
	Continue?	Maybe	Yes

**Table B.5:** Match rating for the power profile formula against interpreted customer needs (1=much worse, 3=same, 5=much better)

No.	Need	Imp.	Weight	Derive from S+L	Liu+
5	The device shall be capable of presenting the power of each mode as a percentage of the total power measured.	5	33%	3	3
11	The device shall have a measurement tolerance for the modes of better than 5% variation against total power measured.	4	27%	3	3
12	A theory for the few mode power amplification needs to be developed, upon which the device shall be based.	3	20%	3	3
13	The device shall be designed and demonstrated to work within 5 months from design analysis commencement.	3	20%	3	5
		Total score	100%	3	3.4
		Rank		2	1
		Continue?		No	Yes

A retrofit of all derivations into a format similar to that typically used by Snyder and Love (1983) can be done at a later stage, after the concept is validated in the early prototype.

### B.3.2 Offsetting for Mode Position Variation

Modes may be offset relative to each other. This can occur for a number of possible reasons, related to the refractive index profile across the fibre. If the boundary between the refractive index of the core and cladding is not uniform (that is, not the same on one side as on the other), then the modes may not share a common centre. The following equations provide the calculation for the offset.

Figure B.5 shows the reference points for the calculation. The point  $P(r, \theta)$  needs to be calculated as if the centre  $T(s, \alpha)$  was actually at  $O(0, 0)$ , that is as if  $s = 0$  and as if  $\alpha = 0$ , thereby ensuring that the translated  $P'(p, \phi)$  is calculated relative to the mode it is dealing with (the second mode in the example).

Using the cosine rule, the length  $p$  is determined using Equation B.16.

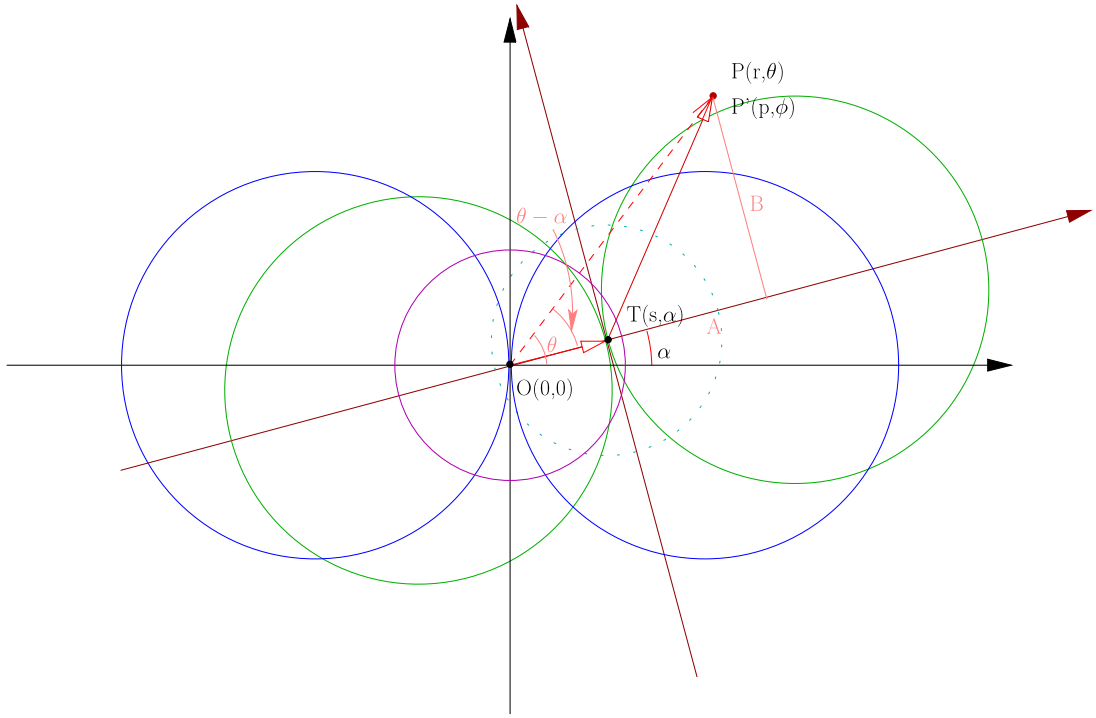


**Figure B.5:** Translation of a mode from the origin to an offset (second mode shown shifted here)

$$p = \sqrt{r^2 + s^2 - 2rs \cos(\theta - \alpha)} \quad (\text{B.16})$$

Given Equation B.17 and Equation B.18, the angle  $\phi$  is determined using Equation B.19.

$$\cos(\theta - \alpha) = \frac{s + A}{r} \implies A = r \cos(\theta - \alpha) - s \quad (\text{B.17})$$

$$\sin(\theta - \alpha) = \frac{B}{r} \implies B = r \sin(\theta - \alpha) \quad (\text{B.18})$$

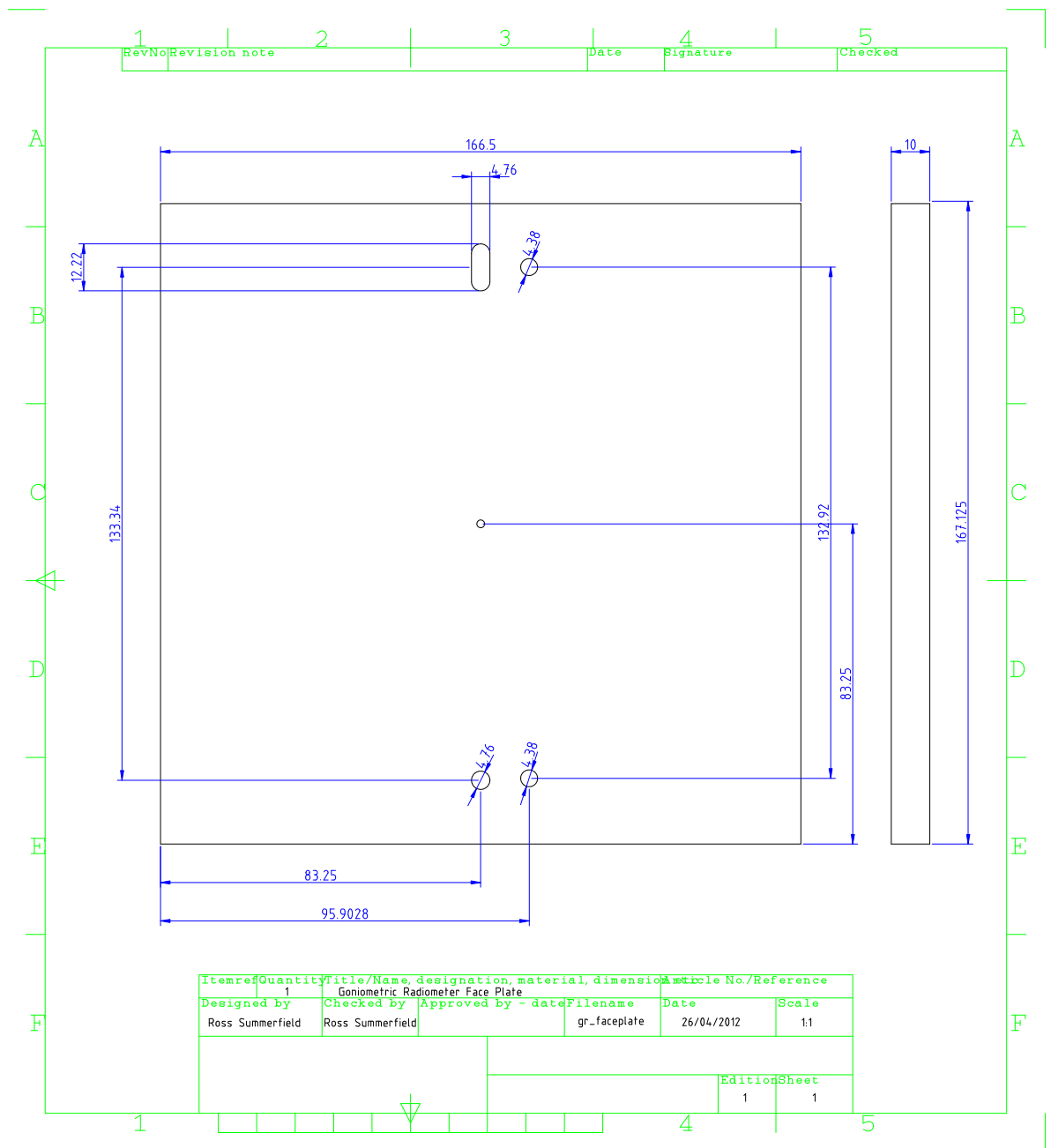
$$\tan(\phi) = \frac{B}{A} = \frac{r \sin(\theta - \alpha)}{r \cos(\theta - \alpha) - s} \implies \phi = \arctan\left(\frac{r \sin(\theta - \alpha)}{r \cos(\theta - \alpha) - s}\right) \quad (\text{B.19})$$

The reverse conversion is given by Equation B.20 for the radius  $r$  and by Equation B.21 for the angle  $\theta$ .

$$r = \sqrt{s^2 + p^2 - 2sp \cos(\pi - \phi)} \quad (\text{B.20})$$

$$\theta = \arctan\left(\frac{p \sin(\phi)}{p \cos(\phi) + s}\right) + \alpha \quad (\text{B.21})$$

# APPENDIX C: DESIGN DRAWINGS



## APPENDIX D: DETAILED EQUATION DEVELOPMENT

The following sections detail development of equations used in Chapter 3. Much of the information is generally available in published literature but detailed here as supporting information for completeness.

### D.1 Eigenvalue Equations Weakly Guiding Fibre

Substituting in the normalised radial coordinate,  $R = \frac{r}{\rho}$  (such that  $r = R\rho$ ) as per Snyder and Love (1983, pp 249), Equation 3.6 simplifies to Equation D.1 (in agreement with Love (2009b, sl 7)).

$$\nabla_t^2 = \frac{1}{\rho^2} \left\{ \frac{\partial^2}{\partial R^2} + \frac{1}{R} \frac{\partial}{\partial R} + \frac{1}{R^2} \frac{\partial^2}{\partial \phi^2} \right\} \quad (\text{D.1})$$

Substituting Equation D.1 into Equation 3.5 gives Equation D.2, which, after multiplying both sides through by  $\rho^2$ , rearranges to D.3. Given that  $U^2 = \rho^2 (k^2 n_{co}^2 - \beta^2)$  (Snyder and Love, 1983, pp 294), this is the same result as (12-11a) for the core in Snyder and Love (1983, pp 249). Also, given that  $W^2 = \rho^2 (\beta^2 - k^2 n_{cl}^2) \Rightarrow W^2 = -\rho^2 (k^2 n_{cl}^2 - \beta^2)$  (Snyder and Love, 1983, pp 294), this is the same result as (12-11b) for the cladding in Snyder and Love (1983, pp 249).

$$\left( \frac{1}{\rho^2} \left\{ \frac{\partial^2}{\partial R^2} + \frac{1}{R} \frac{\partial}{\partial R} + \frac{1}{R^2} \frac{\partial^2}{\partial \phi^2} \right\} + k^2 n^2 - \beta^2 \right) \Psi = 0 \quad (\text{D.2})$$

$$\left\{ \frac{\partial^2}{\partial R^2} + \frac{1}{R} \frac{\partial}{\partial R} + \frac{1}{R^2} \frac{\partial^2}{\partial \phi^2} + \rho^2 (k^2 n^2 - \beta^2) \right\} \Psi = 0 \quad (\text{D.3})$$

From Figure 3.1, it can be seen that  $n$  is symmetric about the  $z$  axis and is independent of  $\phi$ . The separation of variables can then be used to solve Equation D.3, using the assumption that  $\Psi(R, \phi) = F(R)G(\phi)$  and substituting it in, gives Equations D.4 to D.7 (which agrees with Love (2009b, sl 8)).

$$\left\{ \frac{\partial^2 FG}{\partial R^2} + \frac{1}{R} \frac{\partial FG}{\partial R} + \frac{1}{R^2} \frac{\partial^2 FG}{\partial \phi^2} + \rho^2 (k^2 n^2(R) - \beta^2) FG \right\} = 0 \quad (\text{D.4})$$

$$\frac{R^2}{FG} \left\{ \frac{\partial^2 FG}{\partial R^2} + \frac{1}{R} \frac{\partial FG}{\partial R} + \rho^2 (k^2 n^2(R) - \beta^2) FG \right\} + \frac{R^2}{R^2 FG} \frac{\partial^2 FG}{\partial \phi^2} = 0 \quad (\text{D.5})$$

$$\frac{R^2}{F} \left\{ \frac{\partial^2 FG}{G \partial R^2} + \frac{1}{R} \frac{\partial FG}{G \partial R} + \rho^2 (k^2 n^2(R) - \beta^2) \frac{FG}{G} \right\} + \frac{R^2}{R^2 G} \frac{\partial^2 FG}{F \partial \phi^2} = 0 \quad (\text{D.6})$$

$$\frac{R^2}{F} \left\{ \frac{\partial^2 F}{\partial R^2} + \frac{1}{R} \frac{\partial F}{\partial R} + \rho^2 (k^2 n^2(R) - \beta^2) F \right\} + \frac{1}{G} \frac{\partial^2 G}{\partial \phi^2} = 0 \quad (\text{D.7})$$

Now, since  $F(R)$  is a function of  $R$  only and  $G(\phi)$  is a function of  $\phi$  only, the differential terms are not partial for their respective parts; that is, Equation D.7 can be written as D.8.

$$\frac{R^2}{F} \left\{ \frac{d^2 F}{dR^2} + \frac{1}{R} \frac{dF}{dR} + \rho^2 (k^2 n^2(R) - \beta^2) F \right\} + \frac{1}{G} \frac{d^2 G}{d\phi^2} = 0 \quad (\text{D.8})$$

By setting  $G$  as per the following in Equation D.9 where  $v$  is a constant, so that the result would be a harmonic equation with sine and cosine solutions for odd and even functions of  $\phi$  (Love, 2009b, sl 8), then double differentiation generally gives Equation D.10 (in either case).

$$G = \begin{cases} \sin(v\phi) \\ \cos(v\phi) \end{cases} \quad (\text{D.9})$$

$$\frac{d^2 G}{d\phi^2} = -v^2 G \quad (\text{D.10})$$

Substituting into Equation D.8 results in Equation D.11, which as  $G$  must be single valued as  $\phi$  varies, so  $v$  is a non-negative integer.

$$\frac{R^2}{F} \left\{ \frac{d^2 F}{dR^2} + \frac{1}{R} \frac{dF}{dR} + \rho^2 (k^2 n^2(R) - \beta^2) F \right\} - v^2 = 0 \quad (\text{D.11})$$

$$\frac{R^2}{F} \left\{ \frac{d^2 F}{dR^2} + \frac{1}{R} \frac{dF}{dR} + \rho^2 (k^2 n^2(R) - \beta^2) F \right\} = v^2 \quad (\text{D.12})$$

Equation D.11 can be restated as Equation D.12. Then multiplying both sides by  $\frac{F}{R^2}$  results in Equation D.13. This can be restated as Equation D.14.

$$\left\{ \frac{d^2 F}{dR^2} + \frac{1}{R} \frac{dF}{dR} + \rho^2 (k^2 n^2(R) - \beta^2) F \right\} = \frac{v^2 F}{R^2} \quad (\text{D.13})$$

$$\left\{ \frac{d^2 F}{dR^2} + \frac{1}{R} \frac{dF}{dR} + \rho^2 (k^2 n^2(R) - \beta^2) F \right\} - \frac{v^2 F}{R^2} = 0 \quad (\text{D.14})$$

Then, putting  $\frac{v^2 F}{R^2}$  inside the brackets and finally drawing the differentiated term outside of the brackets results in Equation D.15 (in agreement with Love (2009b, sl 8)).

$$\left\{ \frac{d^2}{dR^2} + \frac{1}{R} \frac{d}{dR} - \frac{v^2}{R^2} + \rho^2 (k^2 n^2(R) - \beta^2) \right\} F = 0 \quad (\text{D.15})$$

Given that the core mode parameter,  $U = \rho (k^2 n_{co}^2 - \beta^2)^{\frac{1}{2}}$  (Snyder and Love, 1983, pp 294) and noting that, for a step profile weakly guiding fibre,  $n(R) = n_{co}$ , so that  $U^2 = \rho^2 (k^2 n^2(R) - \beta^2)$ , then substituting that into Equation D.15 results in Equation D.16.

$$\left\{ \frac{d^2}{dR^2} + \frac{1}{R} \frac{d}{dR} - \frac{v^2}{R^2} + U^2 \right\} F = 0 \quad (\text{D.16})$$

Multiplying Equation D.16 by  $R^2$  gives Equation D.17, and then setting  $s = UR$  or  $R = \frac{s}{U}$ , results in Equation D.18, which, bearing in mind that  $U$  is a constant, simplifies to Equation D.19 (in agreement with Love (2009b, sl 9)).

$$\left\{ R^2 \frac{d^2}{dR^2} + \frac{R^2}{R} \frac{d}{dR} - \frac{v^2 R^2}{R^2} + U^2 R^2 \right\} F = 0 \quad (\text{D.17})$$

$$\left\{ R^2 \frac{d^2}{d\left(\frac{s}{U}\right)^2} + R \frac{d}{d\frac{s}{U}} - v^2 + s^2 \right\} F = 0 \quad (\text{D.18})$$

$$\left\{ s^2 \frac{d^2}{ds^2} + s \frac{d}{ds} + (s^2 - v^2) \right\} F = 0 \quad (\text{D.19})$$

Equation D.19 is Bessel's equation (Kreyszig, 1972, pp 125) with a solution of the general form  $F(R) = C_1 J_\nu(s) + C_2 Y_\nu(s)$  where  $J_\nu$  is a Bessel function of the first kind of order  $\nu$ ,  $Y_\nu$  is a Bessel function of the second kind and  $C_1$  and  $C_2$  are constants (Kreyszig, 1972; Love, 2009b, pp 133; sl 9).

The solution of  $F(R)$  is bounded throughout the core. On the fibre axis,  $R = 0$ ,  $s = U \times 0 = 0$ ,  $Y(s)$  is singular and so  $C_2 = 0$ . Therefore,  $F(R)$  satisfies Equation D.20. Then substituting back for  $s = UR$  results in Equation D.21.

$$F(R) = C_1 J_\nu(s) \quad (\text{D.20})$$

$$F(R) = C_1 J_\nu(UR) \quad (\text{D.21})$$

The core mode field solution  $\Psi(R, \phi) = F(R)G(\phi)$ , by substituting in Equation D.21 and D.9, is therefore Equation D.22 (as per Love (2009b, sl 9)).

$$\Psi(R, \phi) = C_1 J_\nu(UR) \begin{cases} \sin(v\phi) \\ \cos(v\phi) \end{cases} \quad (\text{D.22})$$

Given that the cladding mode parameter,  $W = \rho (\beta^2 - k^2 n_{cl}^2)^{\frac{1}{2}}$  (Snyder and Love, 1983, pp 294) and noting that, for a step profile weakly guiding fibre,  $n(R) = n_{cl}$ , so that  $-W^2 = -\rho^2 (\beta^2 - k^2 n^2(R)) = \rho^2 (k^2 n^2(R) - \beta^2)$ , then substituting that into Equation D.15 results in Equation D.23.

$$\left\{ \frac{d^2}{dR^2} + \frac{1}{R} \frac{d}{dR} - \frac{v^2}{R^2} - W^2 \right\} F = 0 \quad (\text{D.23})$$

Multiplying Equation D.23 by  $R^2$  gives Equation D.24, and then setting  $s = WR$  or  $R = \frac{s}{W}$ , results in Equation D.25, which, bearing in mind that  $W$  is a constant, simplifies to Equation D.26 (in agreement with Love (2009b, sl 10)).

$$\left\{ R^2 \frac{d^2}{dR^2} + \frac{R^2}{R} \frac{d}{dR} - \frac{v^2 R^2}{R^2} - W^2 R^2 \right\} F = 0 \quad (\text{D.24})$$

$$\left\{ R^2 \frac{d^2}{d\left(\frac{s}{U}\right)^2} + R \frac{d}{d\frac{s}{U}} - v^2 - s^2 \right\} F = 0 \quad (\text{D.25})$$

$$\left\{ s^2 \frac{d^2}{ds^2} + s \frac{d}{ds} - (s^2 + v^2) \right\} F = 0 \quad (\text{D.26})$$

Equation D.26 is the modified Bessel equation (Snyder and Love, 1983, pp 713) with a solution of the general form  $F(R) = C_1 I_\nu(s) + C_2 K_\nu(s)$  where  $I_\nu$  is the modified Bessel function of the first kind of

order  $\nu$ ,  $K_\nu$  is the modified Bessel function of the second kind and  $C_1$  and  $C_2$  are constants (Love, 2009b, sl 10).

The solution of  $F(R)$  is bounded throughout the cladding from  $1 \leq R \leq \infty$ . On the fibre axis, as  $R \rightarrow \infty$ ,  $s \rightarrow \infty$ , since  $I_\nu(s)$  is singular and so  $C_1 = 0$ . Therefore,  $F(R)$  satisfies Equation D.27. Then substituting back for  $s = WR$  results in Equation D.28.

$$F(R) = C_2 K_\nu(s) \quad (\text{D.27})$$

$$F(R) = C_2 K_\nu(WR) \quad (\text{D.28})$$

The cladding mode field solution  $\Psi(R, \phi) = F(R)G(\phi)$ , by substituting in Equation D.28 and D.9, is therefore Equation D.29 (as per Love (2009b, sl 10)).

$$\Psi(R, \phi) = C_2 K_\nu(WR) \begin{cases} \sin(v\phi) \\ \cos(v\phi) \end{cases} \quad (\text{D.29})$$

For the core-cladding interface, there must be continuity for the scalar wave equation and all first derivatives. This means that there is continuity at  $R = 1$  for  $\Psi(R, \phi)$ ,  $\frac{\partial \Psi(R, \phi)}{\partial R}$  and  $\frac{\partial \Psi(R, \phi)}{\partial \phi}$ . As both the core and cladding solutions for  $\Psi(R, \phi)$  have a dependence on  $\phi$ , the requirement for the partial derivatives is satisfied. Combining Equation D.22 and Equation D.29 gives Equation D.30 and dividing through both sides by the common variables results in Equation D.31 for continuity of  $\Psi(R, \phi)$ .

$$C_1 J_\nu(UR) \begin{cases} \sin(v\phi) \\ \cos(v\phi) \end{cases} = C_2 K_\nu(WR) \begin{cases} \sin(v\phi) \\ \cos(v\phi) \end{cases} \quad (\text{D.30})$$

$$C_1 J_\nu(U) = C_2 K_\nu(W) \quad (\text{D.31})$$

Differentiating Equation D.31 for the continuity of  $\frac{\partial \Psi(R, \phi)}{\partial R}$  results in Equation D.32.

$$C_1 U J'_\nu(U) = C_2 W K'_\nu(W) \quad (\text{D.32})$$

Dividing Equation D.32 by Equation D.31 results in the eigenvalue Equation D.33, eliminating the constants  $C_1$  and  $C_2$ .

$$\frac{U J'_\nu(U)}{J_\nu(U)} = \frac{W K'_\nu(W)}{K_\nu(W)} \quad (\text{D.33})$$

Using the recurrence relations as described by Snyder and Love (1983, pp 714), where for the variables in Equation D.33,  $m = \nu$  and  $z = U$ ;  $z = W$  respectively, the eigenvalue equation for the fibre is rewritten as Equation D.34 (Love, 2009b, sl 11). This equation is equivalent to the equation by Gloge described in Section 1.2.2.

$$U \frac{J_{\nu+1}(U)}{J_\nu(U)} = W \frac{K_{\nu+1}(W)}{K_\nu(W)} \quad (\text{D.34})$$

The well known Equation D.35 can be similarly demonstrated (Love, 2009b, sl 1-3). Using numerical methods, a plot of  $U$  against  $V$  can be generated from Equation D.34 and Equation D.35.

$$V^2 = U^2 + W^2 \quad (\text{D.35})$$

## D.2 Modal Power Distribution

In analysing the intensity at the fibre end face, the 4% internal reflection is ignored as only power out the far end of the fibre is of concern. The effect of the consequential backward propagating modes is also ignored on the basis that the effect is likely to be small when compared to the error in measurement. The intensity  $I_j$  for the  $j$ th forward propagating mode is given by Equation D.36, where  $a_j$  is the amplitude of the  $j$ th mode, and the power  $P_j$  in the  $j$ th mode is given by Equation D.37 (Snyder and Love, 1983, pp215-216).

$$I_j = \frac{1}{2} |a_j|^2 \Re \{ \mathbf{E}_j \times \mathbf{H}_j^* \cdot \hat{\mathbf{z}} \} = \frac{1}{2} |a_j|^2 \mathbf{e}_j \times \mathbf{h}_j^* \cdot \hat{\mathbf{z}} \quad (\text{D.36})$$

$$P_j = \int_{A_\infty} I_j dA = \frac{1}{2} |a_j|^2 \int_{A_\infty} \mathbf{e}_j \times \mathbf{h}_j^* \cdot \hat{\mathbf{z}} dA \quad (\text{D.37})$$

The Intensity for the fundamental mode  $I_0(R, \phi)$  is given by Equation D.38, where the normalised radius  $R$  is given by  $R = \frac{r}{\rho}$  and the profile is given by Figure D.1 (Snyder and Love, 1983, pp 313).

$$I_0(R, \phi) = \frac{|a_0|^2}{2} \left( \frac{\varepsilon_0}{\mu_0} \right)^{\frac{1}{2}} n_{co} F_0^2 = \frac{|a_1|^2 n_{co}}{2} \left( \frac{\varepsilon_0}{\mu_0} \right)^{\frac{1}{2}} \begin{cases} \left( \frac{J_0(UR)}{J_0(U)} \right)^2 & R \leq 1 \\ \left( \frac{K_0(WR)}{K_0(W)} \right)^2 & R > 1 \end{cases} \quad (\text{D.38})$$

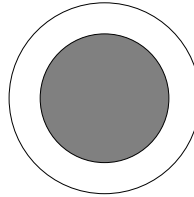


**Figure D.1:** Fundamental mode field profile

Noting that the fundamental mode is symmetric, so there is no  $\phi$  component in the equation, and given that the intensity for the second mode  $I_1(R, \phi)$  is given by Equation D.39 (Snyder and Love, 1983, pp 319) with the  $\phi$  component added in and where that  $\phi$  component is either sin or cos, the field profile is given by Figure D.2.

$$I_1(R, \phi) = \frac{|a_1|^2}{2} \left( \frac{\varepsilon_0}{\mu_0} \right)^{\frac{1}{2}} n_{co} F_1^2 \begin{matrix} \sin \\ \cos \end{matrix} (\phi) = \frac{|a_1|^2 n_{co}}{2} \left( \frac{\varepsilon_0}{\mu_0} \right)^{\frac{1}{2}} \begin{cases} \left( \begin{matrix} \frac{J_1(UR)}{J_1(U)} \sin \\ \cos \end{matrix} (\phi) \right)^2 & R \leq 1 \\ \left( \begin{matrix} \frac{K_1(WR)}{K_1(W)} \sin \\ \cos \end{matrix} (\phi) \right)^2 & R \geq 1 \end{cases} \quad (\text{D.39})$$

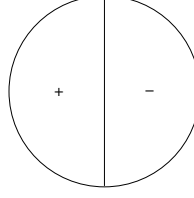


**Figure D.2:** Second mode field profile

By judicious choice so that the result is 1 for  $\phi = 0$  when  $m = 1$ , then choosing  $\cos(\phi)$ , which matches the desired result for intensity for the second mode, the total intensity for each mode  $m$  generally,  $I_{tm}(R, \phi)$  is given by Equation D.40.

$$I_{tm}(R, \phi) = \frac{|a_m|^2 n_{co}}{2} \left(\frac{\varepsilon_0}{\mu_0}\right)^{\frac{1}{2}} F_m^2 \cos(m\phi) = \frac{|a_m|^2 n_{co}}{2} \left(\frac{\varepsilon_0}{\mu_0}\right)^{\frac{1}{2}} \begin{cases} \left(\frac{J_m(UR)}{J_m(U)} \cos(m\phi)\right)^2 & R \leq 1 \\ \left(\frac{K_m(WR)}{K_m(W)} \cos(m\phi)\right)^2 & R \geq 1 \end{cases} \quad (\text{D.40})$$

Back substituting for  $R = \frac{r}{\rho}$  and rearranging the constants in Equation D.40 results in Equation D.41.

$$I_{tm}(R, \phi) = |a_m|^2 \frac{n_{co}}{2} \left(\frac{\varepsilon_0}{\mu_0}\right)^{\frac{1}{2}} \begin{cases} \left(\frac{1}{J_m(U)} J_m\left(\frac{U r}{\rho}\right) \cos(m\phi)\right)^2 & r < \rho \\ \left(\frac{1}{K_m(W)} K_m\left(\frac{W r}{\rho}\right) \cos(m\phi)\right)^2 & r > \rho \end{cases} \quad (\text{D.41})$$

Considering the basic intensity for a mode is related to the total intensity for a mode via  $I_{tm}(R, \phi) = I_m(R, \phi) \left|a'_m\right|^2$  and rolling the constant  $\frac{n_{co}}{2} \left(\frac{\varepsilon_0}{\mu_0}\right)^{\frac{1}{2}}$  in with the intensity amplitude  $|a_m|^2$  such that  $a'_m = \sqrt{\frac{n_{co}}{2}} \left(\frac{\varepsilon_0}{\mu_0}\right)^{\frac{1}{4}} a_m$ , then Equation D.41 can be rewritten for just  $I_m(R, \phi)$  as Equation D.42, with a few other refinements resulting from combination and multiplication out.

$$I_m(R, \phi) = \begin{cases} \frac{J_m^2\left(\frac{U r}{\rho}\right)}{J_m^2(U)} \cos^2(m\phi) & r < \rho \\ \frac{K_m^2\left(\frac{W r}{\rho}\right)}{K_m^2(W)} \cos^2(m\phi) & r > \rho \end{cases} \quad (\text{D.42})$$

Given that the core mode parameter,  $U = \rho(k^2 n_{co}^2 - \beta^2)^{\frac{1}{2}}$  and the cladding mode parameter,  $W = \rho(\beta^2 - k^2 n_{cl}^2)^{\frac{1}{2}}$  (Snyder and Love, 1983, pp 294), Liu's Equation D.43 and Equation D.44 are substituted into Equation D.42 to result in Equation D.45, which matches that of Liu (2005, pp 133).

$$h^2 = k^2 n_{co}^2 - \beta^2 = \frac{\omega^2 n_{co}^2}{c^2} - \beta^2 \Rightarrow h = (k^2 n_{co}^2 - \beta^2)^{\frac{1}{2}} = \frac{U}{\rho} \Rightarrow U = h\rho \quad (\text{D.43})$$

$$\gamma^2 = \beta^2 - k^2 n_{cl}^2 = \beta^2 - \frac{\omega^2 n_{cl}^2}{c^2} \Rightarrow \gamma = (\beta^2 - k^2 n_{cl}^2)^{\frac{1}{2}} = \frac{W}{\rho} \Rightarrow W = \gamma\rho \quad (\text{D.44})$$

$$I_m(\phi, r) = \begin{cases} \frac{1}{J_m^2(hr)} J_m^2(hr) \cos^2(m\phi) & r < \rho \\ \frac{1}{K_m^2(\gamma r)} K_m^2(\gamma r) \cos^2(m\phi) & r > \rho \end{cases} \quad (\text{D.45})$$

Field energy in a circular waveguide flows in the longitudinal direction, with the exception of evanescent fields. The power of a mode is obtained by integrating the intensity of that mode over the the entire

cross section of that waveguide, and consequently the longitudinal components  $\varepsilon_z$  and  $\mathcal{H}_z$  do not contribute to the mode's intensity or power, so the intensity is only a function of the  $(x, y)$  components (Liu, 2005, pp 62). Assuming a circular step index fibre, power  $P$  in a mode  $\nu$  is therefore given by Equation D.46 (Liu, 2005, pp 126). Splitting out the constants and reworking for total power, this is equivalent to Equation D.47.

$$P_\nu = \int_{r=0}^{\infty} \int_{\phi=0}^{2\pi} I_\nu r d\phi dr \quad (\text{D.46})$$

$$P = \int_{A_\infty} I_T(\phi, r) dA = \int_0^{\infty} \int_0^{2\pi} I_T(\phi, r) r d\phi dr \quad (\text{D.47})$$

Extrapolating from Equation D.36, and noting that the field is given by Equation D.48 for mode  $j$  (as per Equation 2.8) (Snyder and Love, 1983, pp 211), intensity for mode  $j$  is given by the square of the modulus of the field as in Equation D.49, total intensity is given by the sum of the fields as per Equation D.50 for  $m$  modes.

$$E_j = \mathbf{e}_j \exp(i\beta_j z) \equiv a_j \Psi_j e^{i\beta_j z} \quad (\text{D.48})$$

$$I_j = |E_j|^2 \quad (\text{D.49})$$

$$I_T = \left| \sum_{j=1}^m E_j \right|^2 \quad (\text{D.50})$$

Expanding Equation D.50 for two modes, for example, results in Equation D.51, where  $\beta_n$  is the propagation constant of the  $n^{\text{th}}$  mode (1 or 2 in this case) and  $z$  is the length of the fibre, by using the fact that  $|z| = \sqrt{zz^*} \Rightarrow |z|^2 = (\sqrt{zz^*})^2 = zz^*$  and that  $(z_1 + z_2)^* = z_1^* + z_2^*$  (see for example Kreyszig (1972, pp 465)), and this equation then expands from Equation D.52 to Equation D.53, assuming no loss in the waveguide.

$$I_T = |a_1 \Psi_1 e^{i\beta_1 z} + a_2 \Psi_2 e^{i\beta_2 z}|^2 = (a_1 \Psi_1 e^{i\beta_1 z} + a_2 \Psi_2 e^{i\beta_2 z}) (a_1^* \Psi_1^* (e^{i\beta_1 z})^* + a_2^* \Psi_2^* (e^{i\beta_2 z})^*) \quad (\text{D.51})$$

$$I_T = a_1 \Psi_1 (e^{i\beta_1 z}) a_1^* \Psi_1^* (e^{i\beta_1 z})^* + a_1 \Psi_1 (e^{i\beta_1 z}) a_2^* \Psi_2^* (e^{i\beta_2 z})^* + a_2 \Psi_2 (e^{i\beta_2 z}) a_1^* \Psi_1^* (e^{i\beta_1 z})^* + a_2 \Psi_2 (e^{i\beta_2 z}) a_2^* \Psi_2^* (e^{i\beta_2 z})^* \quad (\text{D.52})$$

$$I_T = |a_1 \Psi_1|^2 |e^{i\beta_1 z}|^2 + |a_2 \Psi_2|^2 |e^{i\beta_2 z}|^2 + a_1 \Psi_1 (e^{i\beta_1 z}) a_2^* \Psi_2^* (e^{i\beta_2 z})^* + a_2 \Psi_2 (e^{i\beta_2 z}) a_1^* \Psi_1^* (e^{i\beta_1 z})^* \quad (\text{D.53})$$

Noting that  $e^z = e^x (\cos y + i \sin y)$  (Kreyszig, 1972, pp 481), then  $z = 0 + iy \Rightarrow e^z = e^{iy} = 1 (\cos y + i \sin y)$  and  $|e^{iy}| = \sqrt{(\cos^2 y + \sin^2 y)} = 1$ , which leads to  $(e^{i\beta_1 z}) (e^{i\beta_1 z})^* = |e^{i\beta_1 z}|^2 = 1$ . Substituting that into Equation D.53 results in Equation D.54, reducing and simplifying to Equation D.59.

$$I_T = |a_1\Psi_1|^2 \times 1 + |a_2\Psi_2|^2 \times 1 + a_1\Psi_1 a_2^* \Psi_2^* (e^{i\beta_1 z}) (e^{i\beta_2 z})^* + a_1^* \Psi_1^* a_2 \Psi_2 (e^{i\beta_1 z})^* (e^{i\beta_2 z}) \quad (\text{D.54})$$

$$I_T = |a_1|^2 |\Psi_1|^2 + |a_2|^2 |\Psi_2|^2 + a_1 \Psi_1 a_2^* \Psi_2^* e^{i\beta_1 z} e^{-i\beta_2 z} + a_1^* \Psi_1^* a_2 \Psi_2 e^{-i\beta_1 z} e^{i\beta_2 z} \quad (\text{D.55})$$

$$I_T = |a_1|^2 |\Psi_1|^2 + |a_2|^2 |\Psi_2|^2 + a_1 \Psi_1 a_2^* \Psi_2^* e^{i\beta_1 z - i\beta_2 z} + a_1^* \Psi_1^* a_2 \Psi_2 e^{i\beta_2 z - i\beta_1 z} \quad (\text{D.56})$$

$$I_T = |a_1|^2 |\Psi_1|^2 + |a_2|^2 |\Psi_2|^2 + a_1 \Psi_1 a_2^* \Psi_2^* e^{i\beta_1 z - i\beta_2 z} + a_1^* \Psi_1^* a_2 \Psi_2 e^{-i(\beta_1 z - i\beta_2 z)} \quad (\text{D.57})$$

$$I_T = |a_1|^2 |\Psi_1|^2 + |a_2|^2 |\Psi_2|^2 + a_1 \Psi_1 a_2^* \Psi_2^* e^{i\beta_1 z - i\beta_2 z} + a_1^* \Psi_1^* a_2 \Psi_2 e^{-i(\beta_1 z - i\beta_2 z)} \quad (\text{D.58})$$

$$I_T = |a_1|^2 |\Psi_1|^2 + |a_2|^2 |\Psi_2|^2 + a_1 \Psi_1 a_2^* \Psi_2^* e^{i(\beta_1 - \beta_2)z} + a_1^* \Psi_1^* a_2 \Psi_2 e^{-i(\beta_1 - \beta_2)z} \quad (\text{D.59})$$

Noting that  $z = x + iy \Rightarrow z = r(\cos y + i \sin y) = r e^{i\theta}$  (Kreyszig, 1972, pp 482), Equation D.59 is rewritten as Equation D.60.

$$I_T = |a_1|^2 |\Psi_1|^2 + |a_2|^2 |\Psi_2|^2 + a_1 \Psi_1 a_2^* \Psi_2^* (\cos((\beta_1 - \beta_2)z) + i \sin((\beta_1 - \beta_2)z)) + a_1^* \Psi_1^* a_2 \Psi_2 (\cos((\beta_1 - \beta_2)z) - i \sin((\beta_1 - \beta_2)z)) \quad (\text{D.60})$$

Rearranging the sine and cosine terms in Equation D.60 results in Equation D.61, simplifying to Equation D.62

$$I_T = |a_1|^2 |\Psi_1|^2 + |a_2|^2 |\Psi_2|^2 + a_1 \Psi_1 a_2^* \Psi_2^* \cos((\beta_1 - \beta_2)z) + a_1^* \Psi_1^* a_2 \Psi_2 \cos((\beta_1 - \beta_2)z) + a_1 \Psi_1 a_2^* \Psi_2^* i \sin((\beta_1 - \beta_2)z) - a_1^* \Psi_1^* a_2 \Psi_2 i \sin((\beta_1 - \beta_2)z) \quad (\text{D.61})$$

$$I_T = |a_1|^2 |\Psi_1|^2 + |a_2|^2 |\Psi_2|^2 + (a_1 \Psi_1 a_2^* \Psi_2^* + a_1^* \Psi_1^* a_2 \Psi_2) \cos((\beta_1 - \beta_2)z) + (a_1 \Psi_1 a_2^* \Psi_2^* - a_1^* \Psi_1^* a_2 \Psi_2) i \sin((\beta_1 - \beta_2)z) \quad (\text{D.62})$$

Given that the fibre does not have imaginary gain, the real part of the phase terms apply as per Equation

D.63.

$$\begin{aligned}
 I_T &= |a_1|^2 |\Psi_1|^2 + |a_2|^2 |\Psi_2|^2 + \\
 &\Re \{ (a_1 \Psi_1 a_2^* \Psi_2^* + a_1^* \Psi_1^* a_2 \Psi_2) \cos((\beta_1 - \beta_2) z) + \\
 &(a_1 \Psi_1 a_2^* \Psi_2^* - a_1^* \Psi_1^* a_2 \Psi_2) i \sin((\beta_1 - \beta_2) z) \}
 \end{aligned} \tag{D.63}$$

Given that  $z = x + iy$  and that  $z^* = x - iy$ , and so  $z + z^* = 2x$  and  $z - z^* = 2iy$ , then  $\Re\{z\} = x = \frac{1}{2}(z + z^*)$  (and  $\Im(z) = y = \frac{1}{2i}(z - z^*)$ ) (Kreyszig, 1972, pp 464). By setting  $z = a_1 \Psi_1 a_2^* \Psi_2^* = x + iy$  in Equation D.63, Equation D.64 results.

$$I_T = |a_1|^2 |\Psi_1|^2 + |a_2|^2 |\Psi_2|^2 + \Re \{ (2x) \cos((\beta_1 - \beta_2) z) + (2iy) i \sin((\beta_1 - \beta_2) z) \} \tag{D.64}$$

Then removing the imaginary component to just contain the real component in Equation D.64 results in Equation D.65.

$$I_T = |a_1|^2 |\Psi_1|^2 + |a_2|^2 |\Psi_2|^2 + 2a_1 \Psi_1 a_2^* \Psi_2^* \cos((\beta_1 - \beta_2) z) \tag{D.65}$$

As it is only the real component of the phase difference that is of interest, and noting that  $\Psi_2$  is real, Equation D.66 applies.

$$I_T = |a_1|^2 |\Psi_1|^2 + |a_2|^2 |\Psi_2|^2 + 2a_1 a_2 \Psi_1 \Psi_2 \cos((\beta_1 - \beta_2) z) \tag{D.66}$$

For 3 modes, Equation D.67 applies.

$$\begin{aligned}
 I_T &= |a_1 \Psi_1|^2 + |a_2 \Psi_2|^2 + |a_3 \Psi_3|^2 + \\
 &2a_1 \Psi_1 a_2 \Psi_2 \cos((\beta_1 - \beta_2) z) + 2a_1 \Psi_1 a_3 \Psi_3 \cos((\beta_1 - \beta_3) z) + \\
 &2a_2 \Psi_2 a_3 \Psi_3 \cos((\beta_2 - \beta_3) z)
 \end{aligned} \tag{D.67}$$

By extrapolation, for any number of modes, Equation D.68 applies.

$$I_T = \left| \sum_{j=1}^m a_m \Psi_m e^{i\beta_m z} \right|^2 = \sum_{j=1}^m |a_m|^2 |\Psi_m|^2 + 2 \sum_{j=1}^m \sum_{k=j+1}^m a_j \Psi_j a_k \Psi_k \cos((\beta_j - \beta_k) z) \tag{D.68}$$

In the general case, by substituting back in for intensity in terms of  $I_m(\phi, r) = |\Psi_m|^2$  as per Equation D.49, the total intensity  $I_T(\phi, r)$  is given by Equation D.69, where  $(\beta_m - \beta_k)$  is the difference between the propagation constants for each mode,  $z$  is the length of fibre and  $a'_m \sqrt{I_m(\phi, r)} a'_k \sqrt{I_k(\phi, r)}$  is an amplification constant.

$$I_T(\phi, r) = \sum_{m=1}^n |a'_m|^2 I_m(\phi, r) + 2 \sum_{m=1}^n \sum_{k=m+1}^n a'_m \sqrt{I_m(\phi, r)} a'_k \sqrt{I_k(\phi, r)} \cos((\beta_m - \beta_k)z) \quad (\text{D.69})$$

In Equation D.69,  $|a'_m|^2$  is given by Equation D.70, where  $\varepsilon_0$  is the electric permittivity of free space,  $\mu_0$  is the magnetic permeability of free space and  $a_m$  is the intensity amplitude related to mode  $m$ .

$$|a'_m|^2 = \frac{n_{co}}{2} \left( \frac{\varepsilon_0}{\mu_0} \right)^{\frac{1}{2}} |a_m|^2 \quad (\text{D.70})$$

Also in Equation D.69, the last term, relating to  $\Re \{a_m \Psi_m a_k^* \Psi_k^* \dots\}$ , is a phase component which is sinusoidal and proportional to the fibre length and the difference in the propagation constants between each mode.

Substituting Equation D.45 and Equation D.70 into Equation D.69 and substituting this into Equation D.47, the total power  $P$  is therefore given by Equation D.71 or equivalently by Equation D.72.

$$P = \int_{A_\infty} \left( \sum_{m=1}^n \left\{ \frac{n_{co}}{2} \left( \frac{\varepsilon_0}{\mu_0} \right)^{\frac{1}{2}} |a_m|^2 \left[ \begin{array}{l} \frac{1}{J_m^2(hr)} J_m^2(hr) \cos^2(m\phi) \quad r < \rho \\ \frac{1}{K_m^2(\gamma r)} K_m^2(\gamma r) \cos^2(m\phi) \quad r > \rho \end{array} \right] \right\} + \varphi \right) dA \quad (\text{D.71})$$

$$P = \int_{A_\infty} \left( \sum_{m=1}^n \left\{ \frac{n_{co}}{2} \left( \frac{\varepsilon_0}{\mu_0} \right)^{\frac{1}{2}} |a_m|^2 \left[ \begin{array}{l} \frac{J_m^2(U \frac{r}{\rho})}{J_m^2(U)} \cos^2(m\phi) \quad r < \rho \\ \frac{K_m^2(W \frac{r}{\rho})}{K_m^2(W)} \cos^2(m\phi) \quad r > \rho \end{array} \right] \right\} + \varphi \right) dA \quad (\text{D.72})$$

where, from Equation D.69,  $\varphi$  is given by Equation D.73, which elaborates to Equation D.75.

$$\varphi = 2 \sum_{m=1}^n \sum_{k=m+1}^n \frac{n_{co}}{2} \left( \frac{\varepsilon_0}{\mu_0} \right)^{\frac{1}{2}} a_m a_k \sqrt{I_m(\phi, r)} \sqrt{I_k(\phi, r)} \cos((\beta_m - \beta_k)z) \quad (\text{D.73})$$

$$\varphi = 2 \sum_{m=1}^n \sum_{k=m+1}^n \left( \frac{n_{co}}{2} \left( \frac{\varepsilon_0}{\mu_0} \right)^{\frac{1}{2}} a_m a_k \cdot \left[ \begin{array}{l} \left[ \begin{array}{l} \sqrt{\frac{J_m^2(U \frac{r}{\rho})}{J_m^2(U)} \cos^2(m\phi)} \sqrt{\frac{J_k^2(U \frac{r}{\rho})}{J_k^2(U)} \cos^2(k\phi)} \quad r < \rho \\ \sqrt{\frac{K_m^2(W \frac{r}{\rho})}{K_m^2(W)} \cos^2(m\phi)} \sqrt{\frac{K_k^2(W \frac{r}{\rho})}{K_k^2(W)} \cos^2(k\phi)} \quad r > \rho \end{array} \right] \cos((\beta_m - \beta_k)z) \end{array} \right) \quad (\text{D.74})$$

$$\varphi = 2 \sum_{m=1}^n \sum_{k=m+1}^n \left( \frac{n_{co}}{2} \left( \frac{\varepsilon_0}{\mu_0} \right)^{\frac{1}{2}} a_m a_k \cdot \left[ \begin{array}{l} \left[ \begin{array}{l} \sqrt{\frac{J_m^2(U \frac{r}{\rho})}{J_m^2(U)} \frac{J_k^2(U \frac{r}{\rho})}{J_k^2(U)} \cos^2(m\phi) \cos^2(k\phi)} \quad r < \rho \\ \sqrt{\frac{K_m^2(W \frac{r}{\rho})}{K_m^2(W)} \frac{K_k^2(W \frac{r}{\rho})}{K_k^2(W)} \cos^2(m\phi) \cos^2(k\phi)} \quad r > \rho \end{array} \right] \cos((\beta_m - \beta_k)z) \end{array} \right) \quad (\text{D.75})$$

# APPENDIX E: PSEUDO AND SOURCE CODE FOR GRAPH PRODUCTION AND AMPLIFICATION PROCESSING

## E.1 Goniometric Radiometer Data Extraction

**Listing E.1:** *Goniometric Radiometer .prw to CSV Conversion*

```

-----
— Goniometric Radiometer .prw to .csv conversion —
-----
— By Ross Summerfield
— Created 26/07/2012
— Reads in the .prw file , converts theta to r, then saves out
— the data in the format of phi, r, z
— (where phi = the theta in the data analysis routines)
with Ada.Text_IO; use Ada.Text_IO;
with Ada.Sequential_IO;
with Ada.Numerics;
with Ada.Command_Line;
with prw_maths;
procedure prw2csv is

    package angle_io is new Ada.Text_IO.Float_IO(float);
    package scan_io is new Ada.Text_IO.Integer_IO(natural);
    use Ada.Numerics, prw_maths.numeric, prw_maths;

    package prw_IO_sp is new Ada.Sequential_IO(byte);

    mode_arg : natural := 2;
    meas_arg : natural := 0;
    epsilon : constant float := 0.000000001;

    function File_Name return string is
        use Ada.Command_Line;
    begin
        if Argument_Count = 0 then
            return "LMA-GSF-15-123_b29";
        else
            if Argument_Count >= 2 then
                mode_arg:= Character'Pos(Argument(2)(1)) - Character'Pos('0');
            end if;
            if Argument(1)((Argument(1)'Length)-3) = '.' then
                return Argument(1)(1..(Argument(1)'Length)-4);
            else
                return Argument(1);
            end if;
        end if;
    end File_Name;

    function Number_of_Modes return positive is
    begin
        if meas_arg > 0 then
            return meas_arg;
        else
            return mode_arg;
        end if;
    end Number_of_Modes;

    procedure Translate(input : in out prw_IO_sp.File_Type;
                       output : in out Ada.Text_IO.File_Type;
                       parameters : in out Ada.Text_IO.File_Type) is
        large : constant positive := 3241;
        scale : constant float := 1.0;--but 0.0827;-- nom. scan distance=82.7mm

```

```

type theta_array is array (0..large) of float;
type data_array is array (positive range <>,positive range <>) of float;
type polar_coord is record — goniometric radiometer integer form
  r,
  theta : natural;
end record;
type pol_coord_array is array(positive range <>) of polar_coord;

— The array of thetas is used in finding the centre, since it
— is required to calculate the radius, r.
thetas : theta_array;
— The angle is also saved out for later use
alpha : float;
scans_count: positive := 20;

procedure Read_Integer(input : in out prw_IO_sp.File_Type;
  result : out natural) is
  — Read in 2 bytes in big endian order and turn it into
  — an integer number
  bytes : byte_array := (0,0,0,0);
begin
  prw_IO_sp.Read(input, bytes(0));
  prw_IO_sp.Read(input, bytes(1));
  result := natural(bytes(1)) * 16#100# + natural(bytes(0));
end Read_Integer;
procedure Read_Float(input : in out prw_IO_sp.File_Type;
  result : out float) is
  — Read in 4 bytes and turn it into a floating point number
  bytes : byte_array := (0,0,0,0);
begin
  for byte_num in 0..3 loop
    prw_IO_sp.Read(input, bytes(byte_num));
  end loop;
  — convert to float and load
  result := IEEE754toFloat(bytes);
end Read_Float;

function Radius(for_index : in positive) return float is
  — Here, we assume that for_index = 1 is r = 0.
  — At this point, the index into is 1621.
  offset : constant positive := (thetas'Last-thetas'First)/2;
begin
  return scale * Sin(thetas(for_index + offset) );
end Radius;

function Radius_Index(for_radius : in float) return positive is
  — Convert back to an integer radius: find closest entry
  — in thetas
  — Descale and convert r into the radius point for angle comparison.
  r : float := ArcSin(for_radius / scale);
  max_points : constant positive := (thetas'Last+1-thetas'First)/2;
begin
  for i in 2..thetas'Last - 1 loop
    if i = 2 then
      if Abs(r-thetas(i)) > Abs(r-thetas(i-1)) then
        return Abs(1-max_points+1);
      elsif Abs(r-thetas(i)) < Abs(r-thetas(i-1)) and
        Abs(r-thetas(i)) < Abs(r-thetas(i+1)) then
        return Abs(i-max_points+1);
      end if;
    elsif i = thetas'Last - 1 then
      if Abs(r-thetas(i)) > Abs(r-thetas(i+1)) then
        return Abs(thetas'Last-max_points+1);
      elsif Abs(r-thetas(i)) < Abs(r-thetas(i-1)) and
        Abs(r-thetas(i)) < Abs(r-thetas(i+1)) then
        return Abs(i-max_points+1);
      end if;
    else
      if Abs(r-thetas(i)) < Abs(r-thetas(i-1)) and
        Abs(r-thetas(i)) < Abs(r-thetas(i+1)) then
        — got it
        if Abs(i-max_points+1) > 0 then
          return Abs(i-max_points+1);
        else — could be 0 since thetas'last > 3241 and thetas(3250)=0
          return 1;
        end if;
      end if;
    end if;
  end loop;
end Radius_Index;

```

```

        end if;
    end if;
end loop;
— Did not find it if we got here — give default of ?
return Abs(integer(for_radius * float(max_points))+1);
end Radius_Index;

function Angle(theta : in natural) return float is
    max_scans : constant positive := scans_count * 2;
begin
    return 2.0 * pi / float(max_scans) * float(theta-1);
end Angle;

function Angle_Index(for_theta : in float) return natural is
    max_scans : constant positive := scans_count * 2;
    theta : float;
begin
    theta := (float(max_scans)*for_theta)/(2.0*pi) + 1.0;
    if theta < 1.0 then
        theta := 1.0;
    elsif theta > float(max_scans) then
        theta := float(max_scans);
    end if;
    return natural(theta);
end Angle_Index;

function To_Polar_Coord(from : in polar_coordinates) return polar_coord is
begin
    if from.r > 1.0 then
        return (Radius_Index(1.0), Angle_Index(from.theta));
    else
        return (Radius_Index(from.r), Angle_Index(from.theta));
    end if;
end To_Polar_Coord;

function Convert_To_Polar(from_scan_array : in data_array)
    return data_array is
    num_points : constant positive := from_scan_array'Last(1);
    num_scans : constant positive := from_scan_array'Last(2);
    max_points : constant positive := num_points / 2 + 1;
    max_scans : constant positive := num_scans * 2;
    result : data_array(1..max_points, 1..max_scans);
begin
    — point_number == radius, scan_number == angle
    for point_number in (num_points / 2)+1 .. num_points loop
        for scan_number in 1 .. num_scans loop
            — output the data collected — positive angles
            result(point_number-(num_points/2), scan_number) :=
                from_scan_array(point_number, scan_number);
            result(point_number-(num_points/2), scan_number+num_scans) :=
                from_scan_array(num_points-point_number+1, scan_number);
        end loop;
    end loop;
    return result;
end Convert_To_Polar;

function Find_Centre(for_intensity : in data_array)
    return pol_coord_array is — polar_coord is
    — assume intensity is arranged in polar coordinates (r, theta)
    — but assuming r and theta are normalised to sequential integers
    theta_range : constant positive := for_intensity'Last(2);
    half_theta : constant positive := theta_range / 2;
    max_points : constant positive := for_intensity'Last(1);
    type quadrant is (zero, ninety);
    type max_point is record
        pt : polar_coord;
        max : float;
    end record;

    procedure Find_Peaks(for_intensity : in data_array;
        offset : in polar_coordinates;
        test_angle : in quadrant;
        max_1, max_2: out max_point) is
        — Attempt to find the peaks (up to 2 modes) in the intensity plot
        offs : polar_coord;
    begin

```

```

max_1.max := 0.0;
max_2.max := 0.0;
if test_angle = zero then
  for r in for_intensity'Range(1) loop
    for theta in 1 .. (half_theta / 2) loop
      if offset.r = 0.0 and offset.theta = 0.0 then
        offs := (r, theta);
      else
        offs := To_Polar_Coord(Inverse_Offset(
                                coord=> (Radius(r), Angle(theta)),
                                by_amount => offset));
      end if;
      if for_intensity(offs.r, offs.theta) > max_1.max then
        max_1.max := for_intensity(offs.r, offs.theta);
        max_1.pt.r := offs.r;
        max_1.pt.theta := offs.theta;
      end if;
    end loop;
    for theta in 3 * theta_range / 4 + 1 .. theta_range loop
      if offset.r = 0.0 and offset.theta = 0.0 then
        offs := (r, theta);
      else
        offs := To_Polar_Coord(Inverse_Offset(
                                coord=> (Radius(r), Angle(theta)),
                                by_amount => offset));
      end if;
      if for_intensity(offs.r, offs.theta) > max_1.max then
        max_1.max := for_intensity(offs.r, offs.theta);
        max_1.pt.r := offs.r;
        max_1.pt.theta := offs.theta;
      end if;
    end loop;
    for theta in (half_theta/2)+1 .. 3 * theta_range / 4 loop
      if offset.r = 0.0 and offset.theta = 0.0 then
        offs := (r, theta);
      else
        offs := To_Polar_Coord(Inverse_Offset(
                                coord=> (Radius(r), Angle(theta)),
                                by_amount => offset));
      end if;
      if for_intensity(offs.r, offs.theta) > max_2.max then
        max_2.max := for_intensity(offs.r, offs.theta);
        max_2.pt.r := offs.r;
        max_2.pt.theta := offs.theta;
      end if;
    end loop;
  end loop;
else — test_angle = 90
  for r in for_intensity'Range(1) loop
    for theta in 1 .. half_theta loop
      if offset.r = 0.0 and offset.theta = 0.0 then
        offs := (r, theta);
      else
        offs := To_Polar_Coord(Inverse_Offset(
                                coord=> (Radius(r), Angle(theta)),
                                by_amount => offset));
      end if;
      if for_intensity(offs.r, offs.theta) > max_1.max then
        max_1.max := for_intensity(offs.r, offs.theta);
        max_1.pt.r := offs.r;
        max_1.pt.theta := offs.theta;
      end if;
    end loop;
    for theta in half_theta+1 .. theta_range loop
      if offset.r = 0.0 and offset.theta = 0.0 then
        offs := (r, theta);
      else
        offs := To_Polar_Coord(Inverse_Offset(
                                coord=> (Radius(r), Angle(theta)),
                                by_amount => offset));
      end if;
      if for_intensity(offs.r, offs.theta) > max_2.max then
        max_2.max := for_intensity(offs.r, offs.theta);
        max_2.pt.r := offs.r;
        max_2.pt.theta := offs.theta;
      end if;
    end loop;
  end loop;
end if;

```

```

        end loop;
    end loop;
end Find_Peaks;

function Calc_r(point_1, point_2 : polar_coord; phi : positive)
    return positive is — return r for phi
    s      : constant positive := point_1.r;
    psi    : constant positive := point_1.theta;
    t      : constant positive := point_2.r;
    theta  : constant positive := point_2.theta;
    phi_rad : constant float := 2.0*pi/float(theta_range)*float(phi-1);
    s_mm   : constant float := Radius(s);
    psi_rad : constant float := 2.0*pi/float(theta_range)*float(psi-1);
    t_mm   : constant float := Radius(t);
    theta_r : constant float := 2.0*pi/float(theta_range)*float(theta-1);
    r_mm   : float;
begin
    if abs(t_mm * sin(theta_r) * (s_mm * cos(psi_rad) -
        t_mm * cos(theta_r)) - t_mm * cos(theta_r) *
        (s_mm * sin(psi_rad) - t_mm * sin(theta_r))) < epsilon and
        abs((s_mm * cos(psi_rad) - t_mm * cos(theta_r)) * sin(phi_rad) -
        (s_mm * sin(psi_rad) - t_mm * sin(theta_r)) * cos(phi_rad)) <
        epsilon
    then — numerator + denominator = 0 — no line length as at centre
        r_mm := 0.0;
    else — valid radius calculation
        r_mm := (t_mm * sin(theta_r) * (s_mm * cos(psi_rad) -
            t_mm * cos(theta_r)) - t_mm * cos(theta_r) *
            (s_mm * sin(psi_rad) - t_mm * sin(theta_r))) /
            ((s_mm * cos(psi_rad) - t_mm * cos(theta_r)) * sin(phi_rad) -
            (s_mm * sin(psi_rad) - t_mm * sin(theta_r)) * cos(phi_rad));
    end if;
    — Convert back to an integer radius: find closest entry
    — in thetas
    return Radius_Index(for_radius => r_mm);
end Calc_r;

function Calc_Line_Length(point1, point2 : polar_coord)
    return positive is
    s      : constant float := Radius(point2.r);
    psi    : constant float := 2.0*pi/
        float(theta_range)*float(point2.theta-1);
    t      : constant float := Radius(point1.r);
    theta  : constant float := 2.0*pi/
        float(theta_range)*float(point1.theta-1);
begin
    return Radius_Index(Sqrt(t**2 + s**2 - 2.0*s*t * Cos(theta-psi)));
end Calc_Line_Length;

function Calc_Line_Angle(point1, point2 : polar_coord; d : positive)
    return float is
    psi    : constant float := 2.0*pi/
        float(theta_range)*float(point2.theta-1);
    t      : constant float := Radius(point1.r);
    theta  : constant float := 2.0*pi/
        float(theta_range)*float(point1.theta-1);
    d_mm   : constant float := Radius(d);
begin
    if (t * Sin(theta - psi) / d_mm) > 1.0 then
        return pi/2.0;
    elsif (t * Sin(theta - psi) / d_mm) < -1.0 then
        return -pi/2.0;
    else
        return ArcSin(t * Sin(theta - psi) / d_mm) - psi;
    end if;
end Calc_Line_Angle;

result : polar_coord;
results: pol_coord_array(1..3);
maxs   : array(1..3) of float;
max_1,
max_2  : max_point := ((1,1),0.0);
might_be_1_mode: boolean := true;
unit_circle : constant integer := max_points;
min_line_length: constant integer := unit_circle / 45; — 2.8%
radius_offset : constant integer := unit_circle/25;
begin — Find_Centre

```

```

— Split the intensity data array (of 2 sets of 180 deg worth)
— and find the two peaks, but start out 90 degrees off
Find_Peaks(for_intensity, offset => (0.0,0.0),
           test_angle => zero,
           max_1 => max_1, max_2 => max_2);
if (max_2.max = max_1.max and max_1.pt.r = max_1.pt.r) or
  Calc_Line_Length(max_1.pt,max_2.pt) < min_line_length
then — it was the same point so check by rotating 90 degrees
  Ada.Text_IO.Put_Line("Might be Single moded");
  Find_Peaks(for_intensity, offset => (0.0,0.0),
            test_angle => ninety,
            max_1 => max_1, max_2 => max_2);
else
  might_be_1_mode := false;
end if;
result := max_1.pt;
results(2) := max_1.pt;
results(3) := max_2.pt;
maxs(1) := max_1.max;
maxs(2) := max_1.max;
maxs(3) := max_2.max;
if (max_2.max = max_1.max and max_2.pt.r = max_1.pt.r) or
  Calc_Line_Length(max_1.pt, max_2.pt) < min_line_length
then — still looks like one mode — check for an offset
  for angle in 0 .. 3 loop
    Ada.Text_IO.Put("Checking at offset ");
    scan_io.Put(angle, Width=>1);
    Ada.Text_IO.Put_Line("*pi/2");
    Find_Peaks(for_intensity,
              offset => (Radius(radius_offset), float(angle)*pi/2.0),
              test_angle => zero,
              max_1 => max_1, max_2 => max_2);
    might_be_1_mode :=
      ((max_2.max = max_1.max and max_2.pt.r = max_1.pt.r) or
       (Calc_Line_Length(max_1.pt, max_2.pt) <
        radius_offset+min_line_length/10) or
       (Calc_Line_Length(max_1.pt, max_2.pt) >=
        radius_offset+(min_line_length/10) and
        (abs(max_2.max - max_1.max) > max_1.max/2.0 and
         abs(max_2.max - max_1.max) > max_2.max/2.0)));
    exit when not might_be_1_mode;
  end loop;
else
  might_be_1_mode := false;
end if;
if might_be_1_mode
then — one mode
  Ada.Text_IO.Put("Single moded: Intensity=");
  if max_1.max > maxs(2) and max_1.max > maxs(3) then
    result := max_1.pt; maxs(1) := max_1.max;
    angle_io.Put(maxs(1), Exp => 0);
  elsif max_2.max > maxs(2) and max_2.max > maxs(3) then
    result := max_2.pt; maxs(1) := max_2.max;
    angle_io.Put(maxs(1), Exp => 0);
  elsif maxs(3) > maxs(2) then
    result := results(2);
    angle_io.Put(maxs(3), Exp => 0);
  else
    angle_io.Put(maxs(2), Exp => 0);
  end if;
  Ada.Text_IO.New_Line;
  alpha := 0.0;
  meas_arg := 1;
else
  results(2) := max_1.pt;
  results(3) := max_2.pt;
  maxs(2) := max_1.max;
  maxs(3) := max_2.max;
  Ada.Text_IO.Put("Few moded: Intensity at point 1=");
  angle_io.Put(max_1.max, Exp => 0);
  Ada.Text_IO.Put(", at point 2=");
  angle_io.Put(max_2.max, Exp => 0); Ada.Text_IO.Put(" A=");
  scan_io.Put(max_1.pt.r, Width=>1); Ada.Text_IO.Put(', ');
  scan_io.Put(max_1.pt.theta, Width=>1); Ada.Text_IO.Put(" B=");
  scan_io.Put(max_2.pt.r, Width=>1); Ada.Text_IO.Put(', ');
  scan_io.Put(max_2.pt.theta, Width=>1); Ada.Text_IO.Put(" d=");

```

```

scan_io.Put( Calc_Line_Length(max_1.pt,max_2.pt), Width=>2);
Ada.Text_IO.Put(' ');
angle_io.Put( Radius( Calc_Line_Length(max_1.pt,max_2.pt) ), Exp => 0);
alpha := Calc_Line_Angle( max_1.pt,max_2.pt,
                          Calc_Line_Length(max_1.pt,max_2.pt) );
Ada.Text_IO.Put(", angle="); angle_io.Put(alpha, Exp => 0);
Ada.Text_IO.New_Line;
— Find the minimum point between the two points
— Start with smallest phi and work around to largest phi.
declare
  theta_s, theta_f : positive;
  r : positive;
  intensity : float;
  backwards : boolean;
begin
  if max_1.pt.theta < max_2.pt.theta then
    theta_s := max_1.pt.theta;
    theta_f := max_2.pt.theta;
    result := max_1.pt;
  else
    theta_s := max_2.pt.theta;
    theta_f := max_1.pt.theta;
    result := max_2.pt;
  end if;
  intensity := for_intensity(result.r,result.theta);
  backwards := (theta_f - theta_s) > half_theta; — > 180 deg
  if backwards then
    Ada.Text_IO.Put_Line("Checking for min with theta reverse.");
    for theta in reverse 1 .. theta_s loop
      r := Calc_r(max_1.pt, max_2.pt, theta);
      if for_intensity(r,theta) < intensity then — more min
        intensity := for_intensity(r,theta);
        result := (r, theta);
      end if;
    end loop;
    for theta in reverse theta_f .. theta_range loop
      r := Calc_r(max_1.pt, max_2.pt, theta);
      if for_intensity(r,theta) < intensity then — more min
        intensity := for_intensity(r,theta);
        result := (r, theta);
      end if;
    end loop;
  else
    for theta in theta_s .. theta_f loop
      r := Calc_r(max_1.pt, max_2.pt, theta);
      if for_intensity(r,theta) < intensity then — more min
        intensity := for_intensity(r,theta);
        result := (r, theta);
      end if;
    end loop;
  end if;
end;
end if;
results(1) := result;
return results; — minima (or maxima) point, i.e. centre
end Find_Centre;

num_scans : natural;
num_points : natural;
bytes : byte_array := (0,0,0,0);
begin — Translate
— Read in the number of scans (2 bytes)
Read_Integer(input, num_scans);
scans_count := num_scans;
Ada.Text_IO.Put("Number of scans: ");
scan_io.Put(num_scans);
Ada.Text_IO.New_Line;
scan_io.Put(parameters, num_scans, Width=> 2);
Ada.Text_IO.New_Line(parameters);
— Read in the number of points (2 bytes)
Read_Integer(input, num_points);
Ada.Text_IO.Put("Number of points: ");
scan_io.Put(num_points);
Ada.Text_IO.New_Line;
scan_io.Put(parameters, num_points, Width=> 2);
Ada.Text_IO.New_Line(parameters);

```

```

— Read in the theta angles (number of points)
— stored in radians as a float (4 bytes)
for point_number in 1 .. num_points loop
  Read_Float(input , thetas(point_number));
end loop;
declare
  intens      : data_array(1..num_points,1..num_scans);
  max_points : constant positive := num_points / 2 + 1;
  max_scans  : constant positive := num_scans * 2;
  intens_pol : data_array(1..max_points, 1..max_scans);
  —centre    : polar_coord;
  centres    : pol_coord_array(1..3);
  r,
  phi        : float;
  r_offset ,
  phi_offset : float;
  r_n,
  phi_n      : float;
begin
  — Read in the counts
  for scan_number in 1 .. num_scans loop
    for point_number in 1 .. num_points loop
      — Read in the data (2 bytes for each short type
      — entry) for each scan and theta angle
      Read_Float(input , intens(point_number,scan_number));
    end loop;
  end loop;
  intens_pol := Convert_To_Polar(from_scan_array => intens);
  centres := Find_Centre(for_intensity => intens_pol);
  r_offset := scale * Sin(thetas(centres(1).r));
  phi_offset := 2.0 * pi / float(max_scans) * float(centres(1).theta -1);
  — Write out key parameters to console for debugging
  Ada.Text_IO.Put("r offset: ");
  angle_io.Put(r_offset , Exp => 0);
  Ada.Text_IO.Put(", phi offset: ");
  angle_io.Put(phi_offset * 180.0 / pi , Exp => 0);
  Ada.Text_IO.New_Line;
  — Write out key parameters to the parameter file
  angle_io.Put(parameters , r_offset , Exp => 0);
  Ada.Text_IO.New_Line(parameters);
  angle_io.Put(parameters , phi_offset , Exp => 0);
  Ada.Text_IO.New_Line(parameters);
  angle_io.Put(parameters , r_offset * cos(phi_offset) , Exp => 0); — x
  Ada.Text_IO.New_Line(parameters);
  angle_io.Put(parameters , r_offset * sin(phi_offset) , Exp => 0); — y
  Ada.Text_IO.New_Line(parameters);
  for c in centres'Range loop
    scan_io.Put(parameters , centres(c).r , Width=> 2);
    Ada.Text_IO.New_Line(parameters);
    scan_io.Put(parameters , centres(c).theta , Width=> 2);
    Ada.Text_IO.New_Line(parameters);
    if intens_pol(centres(c).r,centres(c).theta) < 0.0
    then — nonsense! absorber!
      angle_io.Put(parameters , 0.0 , Exp => 0); — zero intensity
      Ada.Text_IO.Put_Line("Absorber!");
    else — intensity for the polar coordinates (r,theta)
      angle_io.Put(parameters ,
        intens_pol(centres(c).r,centres(c).theta) , Exp=>0);
    end if;
    Ada.Text_IO.New_Line(parameters);
  end loop;
  angle_io.Put(parameters , alpha , Exp => 0);
  Ada.Text_IO.New_Line(parameters);
  — Write out the data
  Ada.Text_IO.Put_Line(output , "phi,r,z"); — Column titles
  for r_index in 1 .. max_points loop
    r := Radius(r_index);
    for angle in 1 .. max_scans loop
      — output the data collected — positive angles
      phi := 2.0 * pi / float(max_scans) * float(angle-1);
      r_n := r;
      phi_n:= phi;
      angle_io.Put(output , phi_n , Exp => 0);
      Ada.Text_IO.Put(output , ',');
      angle_io.Put(output , r_n , Exp => 0);
      Ada.Text_IO.Put(output , ',');
    end loop;
  end loop;
end;

```

```

        angle_io.Put(File => output ,
                    Item => intens_pol(r_index , angle),
                    Exp => 0);
        Ada.Text_IO.New_Line(output);
    end loop;
end loop;
end;
end Translate;

input_file  : prw_IO_sp.File_Type;
param_file  : Ada.Text_IO.File_Type;
output_file : Ada.Text_IO.File_Type;
begin  — prw2csv
— Get the file name
null;
— open the input file
prw_IO_sp.Open(input_file , name => File_Name & ".prw",
               mode => prw_IO_sp.in_file);
— create the output file
Ada.Text_IO.Create(output_file , name => File_Name & ".csv");
— create the parameter file
Ada.Text_IO.Create(param_file , name => File_Name & ".par");
— translate the input to the output
Translate(input_file , output_file , param_file);
— close the files
prw_IO_sp.Close(input_file);
Ada.Text_IO.Close(output_file);
Ada.Text_IO.Close(param_file);
exception
when Name_Error =>
Ada.Text_IO.Put_Line("Could not find file '" & File_Name & ".prw" & "'.");
end prw2csv;

```

## E.2 Modal Intensity to Amplification Power Conversion

**Listing E.2:** *Listing in R for the processing of measured intensity data to convert it to measured power in each mode*

```

#####
## Intensity Profile Matching for a Step Profile Circular Fibre ##
#####
#
# By Ross Summerfield , 22/07/2012
#
# Match the intensity profile for one or two modes in a single or
# two moded step profile circular fibre.
#
# For the data processing, this application assumes that the data
# has been stripped out of the Goniometric Radiometer data file
# (that is, the .prw file produced by the Goniometric Radiometer
# software from the .grs file) and converted into an ASCII/UTF8
# CSV file.
#
## Operating mode ##
## _____ ##
interactively <- FALSE
repeat {
  res <- readline("Interactive? (y/n):")
  if (res == "y") {interactively <- TRUE ; break }
  else { if (res == "n") { break }
        else { if (res == "c") { CalibratePower() } } }
}
# Before running this script, change directory into the location to
# run it from. E.g. with RKWard, choose Workspace|Set Working Directory
# from the menu. In that directory, there should be a file called
# "process_data.lst", which has the first line after the title line as

```

```

# the prefix to any file name (for instance, to point to a sub-directory
# or to be the common part of a file name), then the following is a list
# of file names to process and their number of modes (comma separated),
# thus:
#   FileName, NumModes, Orientation, Radius, Loops, Gain, ModesIn,
#   MinAC0, MaxAC0, MinAC90, MaxAC90, PumpPwr.
# Here, NumModes is the number of modes out (by observation),
#   ModesIn is the modes injected into the fibre,
#   Gain is the sensitivity gain level set in the goniometric
#   radiometer,
#   MinAC0 is the minimum Angular Centroid at 0 degrees,
#   MaxAC0 is the maximum Angular Centroid at 0 degrees,
#   MinAC90 is the minimum Angular Centroid at 90 degrees,
#   MaxAC90 is the maximum Angular Centroid at 90 degrees,
#   Orientation is the second mode injection angle (either 0
#   for none or in the first plane or 1 for at 90 degrees to
#   the first plane),
#   Radius is the bend radius,
#   Loops is the number of turns of the fibre for that bend, and
#   PumpPwr is the pump power applied in Watts.
# The first line after is typically of the form:
#   LMA-GSF-15-123_,0,0,0,0.0,0,0,0.00,0.00,0.00,0.00,0.0
# Subsequent lines might look like:
#   01,1,0,280,0.75,90,1,-0.20,0.10,-0.60,0.21,0.0
BatchName <- "process_data.lst"
batch <- as.matrix(read.table(BatchName, header=TRUE, sep=","))
## Set up the result file
ResultName <- "results.csv"
ResultTitles <- paste("File","ModesIn","NumModes","Orientation","BendRadius",
                      "Loops","A1","A2","Angle","PowerIn","PumpPwr",
                      "PowerMeasured","Gain","P1","P2",sep=",")
if (interactively==FALSE) {
  write.table(x=ResultTitles, file=ResultName, append=FALSE, quote=FALSE, sep="," ,
             row.names=FALSE, col.names=FALSE) }
## Library ##
## ----- ##
if (interactively==TRUE) {
  library(rgl)
} else {
  library(scatterplot3d)
}
library(pracma)
#
# Calculation of refractive index of silica
nSilica <- function (l) {
  b1 = 0.6961663; b2 = 0.4079426; b3 = 0.8974794
  w1 = 0.0684043^2; w2 = 0.1162414^2; w3 = 9.896161^2
  n = 1^2 * b1/(1^2 - w1) + 1^2 * b2/(1^2 - w2) + 1^2 * b3/(1^2 - w3)
  sqrt(n+1) }
nCore <- function (na, ncl) sqrt(na^2 + ncl^2)

## Constants ##
## ----- ##
# Key constants:
lambda <- 1060 # nm
NAp <- 0.08
rho <- 15e-6 / 2
ncl <- nSilica(lambda/1000) # Assume pure silica
nco <- nCore(NAp, ncl)
epsilon0 <- 1e-9/(33 * pi) # approximately
mu0 <- 4e-7 * pi
c <- 1 / sqrt(mu0 * epsilon0) # ~3x10^8 m/s
errdiff <- 1e-2 # Allowed error difference
maxmodes <- 5 # The maximum number of modes this system can support
# Constants for building a 3-dimensional profile of the data
clad_plot <- 1.8 # multiple of rho to plot cladding out to.
num_radials <- 173 ; radial_inc <- (rho * clad_plot) / num_radials
gr_scand <- 1 #0.0827 # Goniometric Radiometer nominal scan distance
# Constants located in external files
PMeasName <- "power_meas.csv"
PScaleName <- "power_scale.csv"
# Power constant defaults:
Pin <- -6.65 # dBm measured as the power output from the single mode
# fibre used to excite the test fibre.
Pscale <- 1.00 # W Scale factor (to be calculated from measured power)
# Calibrate from: Pscale <- Pmeas / Power(ampl,alpha)

```

```

# Power constants measured
Pin      <- subset(read.table(PMeasName, header=TRUE, sep=","),
                  BendRadius==0, select=c(Power))[1,1]
Pscale   <- read.table(PScaleName, header=TRUE, sep=","[1,1]
#
## Library for calculating power ##
## _____ ##
# Liu (2009, p122) uses the parameter h in the calculation of intensity
h <- function(kco, beta) sqrt(kco^2 - beta^2)
kco <- function(omega, nco) sqrt(omega^2 * nco^2 / c^2)
# Liu (2009, p122) also uses the parameter gamma in the calculation of
# intensity
gamma <- function(kcl, beta) sqrt(beta^2 - kcl^2)
kcl <- function(omega, ncl) sqrt(omega^2 * ncl^2 / c^2)
#
# The theoretical intensity distribution of a mode is mapped from
# the following formula (Liu 2009, p133):
#
Intens_Dist <- function (amp, r, phi, m) {
  beta <- 2 * pi / (lambda * 1e-9) * (nco + ncl)/2 # approximately, inferred
  omega <- 2 * pi * c / (lambda * 1e-9)           # from S+L p283
  if (r < rho) {
    inten <- 1 / ((besselJ(x=(h(kco(omega, nco), beta) * rho), nu=m))^2 *
                  (besselJ(h(kco(omega, nco), beta) * r, nu=m))^2 * (cos(m * phi))^2
  ) else {
    inten <- 1 / ((besselK(x=(gamma(kcl(omega, ncl), beta)*rho), nu=m))^2 *
                  (besselK(gamma(kcl(omega, ncl), beta)*r, nu=m))^2 * (cos(m*phi))^2
  )
  }
  inten * abs(amp) ^2
}
# In the above, the amplitude incorporates the constants. This disentangles it.
# |a'|^2=0.5*nco*sqrt(epsilon0/mu0) * |a|^2
# so |a|^2 = 2/(sqrt(epsilon0/mu0)*nco) * |a'|^2
Amp_m <- function(amp) {
  sqrt((amp ^ 2) * 2 / (sqrt(epsilon0 / mu0) * nco))
}
Amp_p <- function(amp) {
  sqrt((amp ^ 2) * nco * sqrt(epsilon0 / mu0)) / 2
}
# To translate the radius and angle for a translated mode, the
# cosine rule and the tangent relationship is applied
Offset <- function(r, theta, alpha, s) {
  radius <- sqrt(r^2 + s^2 - 2*r*s*cos(theta-alpha))
  angle <- atan2((r * sin(theta-alpha)), (r * cos(theta-alpha) - s)) #(y,x)
  c(radius, angle)
}
OffsetInt <- function(r, phi, alpha, poffset) {
  if (alpha < 0) {
    (Offset((r*radial_inc), (phi*angle_inc), -alpha, poffset))
  } else {
    (Offset((r*radial_inc), (phi*angle_inc), ((2*pi)-alpha), poffset))
  }
  # (Offset((r*radial_inc), (phi*angle_inc), alpha+pi/2, poffset))
}
# And the inverse:
InverseOffset <- function(p, phi, alpha, s) {
  radius <- sqrt(s^2 + p^2 - 2*s*p*cos(pi-phi))
  angle <- atan2((p * sin(phi)), (p * cos(phi) + s)) + alpha
  if (angle > (2 * pi)) { angle <- angle - (2*pi) }
  if (angle < -(2 * pi)) { angle <- angle + (2*pi) }
  if (angle < 0) { angle <- angle + 2 * pi }
  c(radius, angle)
}
#
# Phase distribution
Phase_Dist <- function(amp, r, phi, m, deltaB, L) {
  if (m == 2) {
    id <- 1.0
    for (md in 1:m) {
      id <- id * amp[md] * sqrt(Intens_Dist(amp[md], r, phi, md-1))
      id <- id * cos(deltaB * L)
    }
  } else {
    0
  }
}
}

```

```

#
# The total theoretical intensity for the 2 modes involved is in
# accordance with the following formula:
#  $I = |E|^2$ 
#  $= |a_1|^2 |\psi_1|^2 + |a_2|^2 |\psi_2|^2 +$ 
#  $2 \operatorname{Re}\{a_1 \psi_1 a_2^* \psi_2^* e^{j(\Delta\beta z)}\}$ 
# The last term is the phase difference at the end of the fibre due
# to length and stress. It may be feasible to incorporate that into
# the equation for the mode.
# Generate an intensity profile
IntensProfile <- function(startmode, nummodes, ampl, alpha, offset) {
  betaave <- 2 * pi / (lambda * 1e-9) * (nc0 + nc1)/2 # approximately, inferred
  deltaB <- 0.01
  L <- 2.4
  for (r in 0:(num_radials-1)) {
    for (phi in 0:(num_scans-1)) {
      model[r*num_scans+phi+1,1] <- phi * angle_inc # in radians
      model[r*num_scans+phi+1,2] <- r * radial_inc
      model[r*num_scans+phi+1,3] <- 0.0
      for (m in startmode:nummodes) {
        rtheta <- OffsetInt(r, phi, alpha[m], offset[m])
#cat(phi, phi*angle_inc, alpha[m], r, offset[m], rtheta[1], rtheta[2], "\n")
        model[r*num_scans+phi+1,3] <- model[r*num_scans+phi+1,3] +
          Intens_Dist(ampl[m], rtheta[1], rtheta[2], m-1) +
          Phase_Dist(ampl, rtheta[1], rtheta[2], m, deltaB, L) }
      }
    }
  }
}
# Phase profile plots out the phase difference and may not practically be
# used for the plots here, but is included for completeness.
PhaseProfile <- function(startmode, nummodes, ampl, alpha) {
  deltaB <- 0.01
  L <- 2.4
  for (r in 0:(num_radials-1)) {
    for (phi in 0:(num_scans-1)) {
      model[r*num_scans+phi+1,1] <- phi * degree_inc * pi / 180
      model[r*num_scans+phi+1,2] <- r * radial_inc
      model[r*num_scans+phi+1,3] <- 0.0
      for (m in startmode:nummodes) {
        model[r*num_scans+phi+1,3] <- model[r*num_scans+phi+1,3] +
          Phase_Dist(ampl, r*radial_inc, (phi*degree_inc+alpha*(m-1))*pi/180,
            m, deltaB, L) }
      }
    }
  }
}
# The power in a specific mode, m
PowerMode <- function(m, ampl, alpha, offset) {
  deltaB <- 0.01
  L <- 2.4
  dA <- gr_scand / (num_scans * num_radials) # increments across pi*r^2
  power <- 0 # in Watts
  for (r in 0:(num_radials-1)) {
    for (phi in 0:(num_scans-1)) {
      rtheta <- OffsetInt(r, phi, alpha[m], offset[m])
      power <- power + (Intens_Dist(ampl[m], rtheta[1], rtheta[2], m-1) +
        Phase_Dist(ampl, rtheta[1], rtheta[2], m, deltaB, L)) * dA
    }
  }
  power * Pscale # In Watts: Pscale is in Watts
}
# The total power in all modes
Power <- function(nummodes, ampl, alpha, offset) {
  power <- 0; # dBm relative
  for (m in 1:nummodes) {
    power <- power + PowerMode(m, ampl, alpha, offset)
  }
  power # In Watts
}
#
# Location of a point in a matrix that is nearest fit. The coordinates
# may not exactly match and the angle may at close to 2*pi, both of which
# need to be taken into account.
FindNearestPoint <- function (thematrix, phi, r, phioffset, roffset) {
  if (abs(roffset) > rho) { # have tried to offset outside core
    inverseOff <- InverseOffset(r, phi, phioffset, rho)
    cat("r offset (" , roffset, ") > core radius. Scaling back to core radius\n")
  } else {

```

```

    inverseOff <- InverseOffset(r, phi, phioffset, roffset)
  }
  nearest <- subset(thematrix,
                    abs(thematrix[,1]-inverseOff[2]) < angle_inc/2 &
                    abs(thematrix[,2]-inverseOff[1]) < radial_inc/2)[3]
  if (length(nearest) > 1) {
    nearest <- max(nearest)
  } else {
    if (is.na(nearest)) { # good bet that the inverse offset angle ~ 2*pi
      if (inverseOff[2]+angle_inc/2 > 2*pi) {
        inverseOff[2] <- inverseOff[2]+angle_inc/2 - 2*pi
        nearest <- subset(thematrix,
                          abs(thematrix[,1]-inverseOff[2]) < angle_inc/2 &
                          abs(thematrix[,2]-inverseOff[1]) < radial_inc/2)[3]
      } else { # we have a problem! don't know the cause
        cat(paste("Unknown problem with offsets ", inverseOff[1], ", ",
                  inverseOff[2], "\nfor r=", r, " and phi=", phi, ". Angle is at ",
                  inverseOff[2]+angle_inc/2, " from ", 2*pi, ".\n", sep=""))
      }
    }
  }
  nearest
}
#
## File to match up - Calculate Amplitudes and Power ##
## ----- ##
for (bfn in 2:length(batch[,1])) {
  FileName <- batch[bfn,1]
  # The format of the CSV parameterfile generated by the 3D Intensity
  # Extraction software, prw2csv, is a vertical file with each line
  # containing the following data:
  #   number of scans by the goniometric radiometer through 180 deg.
  #   number of points in each scan
  #   scaled r offset from centre of scan (i.e. r coordinate of actual centre)
  #   scaled phi offset from centre of scan (i.e. phi coord. of actual centre)
  #   x coordinate of the scaled actual centre offset (map from (r,phi))
  #   y coordinate of the scaled actual centre offset (map from (r,phi))
  #   unscaled (i.e., in goniometric radiometer units) centre of scan r
  #   unscaled (i.e., in goniometric radiometer units) centre of scan phi
  #   Intensity in counts at this centre of scan
  #   scaled (i.e., r coordinate) first peak of scan r
  #   unscaled (i.e., in goniometric radiometer units) first peak of scan phi
  #   Intensity in counts at this first peak of scan (for 2 mode measurement)
  #   scaled (i.e., r coordinate) second peak of scan r
  #   unscaled (i.e., in goniometric radiometer units) second peak of scan phi
  #   Intensity in counts at this second peak of scan (for 2 mode measurement)
  #   alpha - the angle of the line between peaks in a 2 mode measurement
  TestFile <- paste(batch[1,1], FileName, ".csv", sep="")
  nummodes <- as.numeric(batch[bfn,2]) ## Number of modes to match up
  ParamFile <- paste(batch[1], FileName, ".par", sep="")
  params <- read.table(ParamFile, header=FALSE) #, sep=",")
  #
  # File specific constants for building a 3-dimensional profile of the data
  num_scans <- params[1,1] * 2 ; angle_inc <- 2 * pi / num_scans
  num_points <- params[2,1]
  # Counts apparently have the range 0-65535. These are the units of
  # the measured data.
  # Key constants for output of the data.
  outputfile <- paste(batch[1], FileName, ".eps", sep="")
  if (nummodes < 2) {
    graphtitle <- "modal power for the fundamental mode"
  } else {
    graphtitle <- paste("modal power for", nummodes, "modes", sep=" ")
  }
  #
  # Build a 3D model and match
  # Note: this is in polar coordinates
  model <- matrix(NA_real_, nrow=num_scans * num_radials, ncol=3) # phi,r,z
  # Initial guess at controlling variables
  ampl <- 0*1:maxmodes
  ampl[1:nummodes] <- 1+(0:(nummodes-1)) * 7
  alpha <- rep(params[16,1], times=maxmodes) # Match up phase, in radians
  alpha[1] <- 0
  roffset <- 0*1:maxmodes # match point for radial offset between modes
  rho_scale <- 1
  pwr <- 0*1:maxmodes
  peaks <- matrix(0, nrow=nummodes, ncol=3)

```

```

# Match up
model <- IntensProfile(1, nummodes, ampl, 0*1:maxmodes, roffset)
# model <- IntensProfile(1, nummodes, ampl, alpha, roffset)
peaks <- subset(model, (model[,3]==max(model[,3]))) # at no positional xlation
## Load the data base from file
tstdata <- as.matrix(subset(read.table(TestFile, header=TRUE, sep=","),
                             r<0.13395,select=c(phi,r,z),rownames.force = NA)
# Scale up the intensity in accordance with applied gain
gain <- 10^(as.numeric(batch[bfm,6])/10)
tstdata[,3] <- tstdata[,3] / gain
# Quick approximate alignment of scan distance to core diameter
tstdata[,2] <- (tstdata[,2] / gr_scand) * (clad_plot * rho * 7.8)
# Could determine and match the model's core radius of the target signal
# to improve aesthetics, and that would need to be done here.
outerloop <- 0
repeat {
  outerloop <- outerloop + 1
  # Try to zoom in on the optimal amplitude, phase offset
  # Initially determine and match the amplitude of each mode
  for (m in 1:nummodes) {
    if (m==1) {
      if (nummodes==1) {target <- max(tstdata[,3])
      } else { target <- (params[9,1] / gain) }
      loopcntr <- 0
      repeat {
        loopcntr <- loopcntr + 1
        # error is around a central point
        err <- target - FindNearestPoint(model, 0,0, -alpha[m+1],roffset[m+1])
        if ((abs(err)/target <= errdiff) |
            ((loopcntr > 12) & ((abs(err) <= 2*errdiff))) |
            (loopcntr > 20)) break
        if (loopcntr > 10) { # not converging, cut the difference in half
          ampl[m] <- ampl[m] / sqrt(1 - 0.5*err/target)
        } else {
          ampl[m] <- ampl[m] / sqrt(1 - err/target)
        }
        model <- IntensProfile(1, nummodes, ampl, alpha, roffset)
      }
    } else { if (m==2) {
      target <- ifelse((abs((params[12,1]/gain)-
                          FindNearestPoint(model, peaks[1,1], peaks[1,2],
                                              alpha[m], roffset[m]))/
                          (params[12,1]/gain)>0.2 & outerloop == 1),
                      ((params[12,1]/gain)+(params[15,1]/gain))/2,
                      max((params[12,1]/gain),(params[15,1]/gain)))
      loopcntr <- 0
      repeat {
        loopcntr <- loopcntr + 1
        err <- max(FindNearestPoint(model, peaks[1,1], peaks[1,2],
                                    -alpha[m], roffset[m]),
                  FindNearestPoint(model, peaks[2,1], peaks[2,2],
                                    -alpha[m], roffset[m]),
                  subset(model, (model[,3]==max(model[,3])))[,3])
        cat(" l=",loopcntr, " e=",err, " target=",target, "(t-e)/t=", (target-err)/target,
            " ampl[1]=", ampl[1], " ampl[2]=", ampl[2], "\n") # targeting ampl[2]=8.7013367
        if ((abs(target-err)/target <= errdiff) |
            ((loopcntr > 12) & ((abs(target-err) <= 2*errdiff))) |
            (loopcntr > 20)) break
        if (loopcntr > 6) { # not converging, cut the difference in half
          ampl[m] <- ampl[m] / sqrt(1 - 0.5*(target-err)/target)
        } else {
          ampl[m] <- ampl[m] / sqrt(1 - (target-err)/target)
        }
        model <- IntensProfile(1, nummodes, ampl, alpha, roffset)
      }
      if ((outerloop == 1) &
          (length(subset(model, (model[,3]==max(model[,3])))[,3])>1))
          peaks <- subset(model, (model[,3]==max(model[,3])))
    } else { err <- 0 }
  }
}
# Match up any offset between the two modes if two moded
if ((nummodes==2) &
    (abs(1-((params[12,1]/gain)/(params[15,1]/gain)))>errdiff)) {
  # First, shift the fundamental mode to get peak adjustment
  loopcntr <- 0
  # work out which one is to which side

```

```

a <- 12 ; b <- 15
lasterr <- 100
repeat {
  loopcntr <- loopcntr + 1
  err1 <- (params[a,1]/gain) -
    FindNearestPoint(model, peaks[1,1], peaks[1,2], 0, roffset[m])
  err2 <- (params[b,1]/gain) -
    FindNearestPoint(model, peaks[2,1], peaks[2,2], 0, roffset[m])
  err <- abs(max((params[a,1]/gain), (params[b,1]/gain)) -
    max(subset(model, (model[,3]==max(model[,3]))[,3])) /
    max((params[a,1]/gain), (params[b,1]/gain)))
cat(" l=", loopcntr, " e=", err, " e1=", err1/(params[a,1]/gain), " e2=", err2/(params[b,1]/gain),
" ro=", roffset[2], " ao=", alpha[2], "\n")
  if ((err <= errdiff) |
    (abs((err1/(params[a,1]/gain)) - (err2/(params[b,1]/gain))) < errdiff) |
    ((loopcntr > 12) & (abs(err) <= 2*errdiff))) |
    (loopcntr > 20)) break
  if (((err <= errdiff * 4) | (lasterr <= errdiff * 4)) &
    (err > lasterr)) { outerloop <- 21; break }
  else { lasterr <- err }
  if ((err1 < 0) & (err2 > 0)){
    roffset[m] <- roffset[m] - radial_inc / sqrt(1 - sqrt(err)*2)
  } else {
    if ((err1 > 0) & (err2 < 0)){ # move the other way
      roffset[m] <- roffset[m] + radial_inc / sqrt(1 - sqrt(err)*2)
    } else { # both same sign - balance until differences are equal
      if ((roffset[m] == 0) | (loopcntr < 10)) {
        roffset[m] <- roffset[m] +
          ifelse((err1 < 0) & (err2 < 0), 1, -1) * radial_inc / sqrt(1 - sqrt(err))
      } else { if (loopcntr > 12) {
        roffset[m] <- roffset[m] / sqrt(1 - err) } else {
        roffset[m] <- roffset[m] / sqrt(1 - sqrt(err)*2) } }
    } }
  model <- IntensProfile(1, nummodes, ampl, alpha, roffset)
}
# Second, adjust the fundamental mode amplitude to get correct centre
err <- (params[9,1]/gain) - FindNearestPoint(model, 0, 0, -alpha[m], roffset[m])
loopcntr <- 0
}
# Stop when within tolerance
if ((params[9,1]==0) | (abs(err)/(params[9,1]/gain) <= errdiff) |
  (outerloop > 10)) break
}
#
# Match up the x and y axis of the target signal
tstdataPol <- pol2cart(tstdata)
tstdataPol[,1] <- tstdataPol[,1] - (params[5,1]/gr_scand)*(clad_plot*rho/20)
tstdataPol[,2] <- tstdataPol[,2] + (params[6,1]/gr_scand)*(clad_plot*rho/20)
#
# Calculate the power levels
for (m in 1:nummodes) {
  pwr[m] <- PowerMode(m, ampl, alpha, roffset) }
#
# Set up the sub-title
subtitle <- ""
for (m in 1:nummodes) {
  if (m>1) {
    subtitle <- paste(subtitle, ", ", sep="")
  }
  if (abs(Amp_m(ampl[m])) > 0.001) {
    subtitle <- paste(subtitle, "A", m, "=", round(Amp_m(ampl[m]), 3), sep="")
  } else {
    subtitle <- paste(subtitle, "A", m, "=", Amp_m(ampl[m]), sep="") }
}
# Plot the 3D model (for debugging purposes)
if (interactively==TRUE) {
  # Interactive Plot of the 3D model (for debugging purposes)
  plot3d(x=pol2cart(model), type="l", col="blue", main=subtitle, pch=20)
  lines3d(x=tstdataPol, col="red1") # col=rainbow(1000)
  lines3d(x=c(0,0), y=c(0,0),
    z=c(0, max((params[9,1]/gain)*1.01, max(model[,3]))),
    col="magenta")
  grid3d("z")
  if(readline(prompt="Press 'Enter' to continue (s to save)")=="s") { # Pause
    # save out to files
    write.csv(tstdata, file=paste(batch[1,1], FileName, ".dat", sep=""),

```

```

        row.names=FALSE)
    write.csv(model, file=paste(batch[1,1], FileName, ".mdl", sep=""),
             row.names=FALSE)
  }
  # rgl.postscript(outputfile,fmt="eps",drawText=TRUE)
} else {
  postscript(outputfile, horizontal=FALSE,
             onefile=FALSE,height=6, width=8,pointsize=10)
  s3d <- scatterplot3d(x=pol2cart(model), type="l", highlight.3d=FALSE,
                    col.axis="brown3", col.grid="lightblue", color="blue",
                    xlab="x (m)",ylab="y (m)",zlab="Intensity (counts)",
                    main=graphtitle, sub=subtitle, pch=20)
  s3d$points3d(x=tstdataPol, type="l", col="red1", pch=20)
  dev.off()
  # Output to the data file all the details about this particular entry
  write.table(x=paste(paste(batch[1,1],FileName,sep=""),
                    as.numeric(batch[bfm,7]),nummodes,
                    as.numeric(batch[bfm,3]),as.numeric(batch[bfm,4]),
                    as.numeric(batch[bfm,5]),Amp_m(ampl[1]),Amp_m(ampl[2]),
                    params[16,1],Pin,as.numeric(batch[bfm,12]),0,
                    as.numeric(batch[bfm,6]),pwr[1],pwr[2],sep=","),
             file=ResultName,append=TRUE,quote=FALSE,sep=","),
            row.names=FALSE,col.names=FALSE)
}
} # For each file to process
#
## Power Calibration – Run if Pscale needs resetting ##
## ----- ##
# The measurement table for calibration is of the form:
# BendRadius,Power,ModesIn,PumpPwr
# where
# BendRadius is the bend radius for the measurement
# (0 must be included as the point for the power measurement
# at launch into the fibre)
# Power is the measured power
# ModesIn is the number of modes for which this power level
# was measured, and
# PumpPwr is the amount of pump power applied for the
# situation where the fibre contains an amplifier
# Provide the power in Watts for the bend radius to f
# Note: when the following is run without discriminating on the
# modes in, error is double
f <- function(BendRadius, PumpPwr, ModesIn, measdata) {
  pwr <- 0*1:length(BendRadius)
  for (j in 1:length(BendRadius)) {
    for (i in 1:length(measdata$BendRadius)) {
      if ((abs(BendRadius[j]-measdata$BendRadius[i])<6) &
          (PumpPwr[j]==measdata$PumpPwr[i]) &
          (ModesIn[j]==measdata$ModesIn[i]))
        pwr[j] <- (1/1000) * 10 ^ (measdata$Power[i]/10) # W
    }
  }
  pwr # In Watts
}
CalibratePower <- function() {
  pmeas <- read.table(PMeasName, header=TRUE, sep=",") # in dBm
  # Note: if data measured in Watts, convert to dBm via
  # x(dBm) = 10 * log(1000 * P(W)) and store in the PMeasName file, e.g. viz:
  # TodBm <- function(watts) (10 * log10(1000 * watts))
  results <- read.table(ResultName, header=TRUE, sep=",")
  results$PowerMeasured <-
    f(results$BendRadius,results$PumpPwr,results$ModesIn,pmeas)
  # Determine the normalised power
  results$PowerScaled <- 0*1:length(results$File)
  Pscale <- 1.00
  num_scans <- 20 * 2 ; angle_inc <- 2 * pi / num_scans
  for (bfm in 1:length(results[,1])) {
    nummodes <- as.numeric(results$NumModes[bfm])
    ampl <- 0*1:maxmodes
    alpha <- (results$Angle[bfm]*180/pi)*1:maxmodes # Match up phase (degrees)
    alpha[1] <- 0
    roffset <- 0*1:maxmodes
    ampl[1] <- Amp_p(results$A1[bfm])
    ampl[2] <- Amp_p(results$A2[bfm])
    results$PowerScaled[bfm] <- results$PowerMeasured[bfm]/
      Power(nummodes, ampl, alpha, roffset)
  }
}

```

```

}
# Calculate the average scale factor
Pscale <- mean(subset(results , (results$PowerMeasured!=0),c(PowerScaled)))
# Save out the answer
write.table(x="Power", file=PScaleName , append=FALSE, quote=FALSE, sep="," ,
            row.names=FALSE, col.names=FALSE)
write.table(x=Pscale , file=PScaleName , append=TRUE, quote=FALSE, sep="," ,
            row.names=FALSE, col.names=FALSE)
}

## Clean up ##
## _____ ##
rm (num_scans , num_points , angle_inc , num_radials , radial_inc , clad_plot)
#rm (P1turn , P6turn , PW1turn , PW6turn)
rm (nummodes , maxmodes , ampl , alpha , roffset , rho_scale , gr_scand , gain)
rm (model , rho , pwr , Pin , Pscale)
rm (err , err1 , err2 , lasterr , errdiff , a , b , peaks , loopcntr , target , m , bfn)
rm (outerloop)
rm (lambda , NAp , ncl , nco , epsilon0 , mu0 , c)
rm (FileName , TestFile , tstdata , tstdataPol , ParamFile , params)
rm (outputfile , graphtitle , subtitle , s3d)
rm (res , interactively , BatchName , ResultName , ResultTitles , batch)
# Functions:
rm(gamma , kcl , kco , h , nCore , nSilica)
rm(Intens_Dist , IntensProfile , Phase_Dist , PhaseProfile)
rm(InverseOffset , Offset , OffsetInt , FindNearestPoint)
rm(Power , PowerMode)
rm(PMeasName , PScaleName)
rm(Amp_m , Amp_p)
rm(f , CalibratePower)
# Exit
q()

```

A typical output for Program Listing E.2 is shown in Figure E.1.

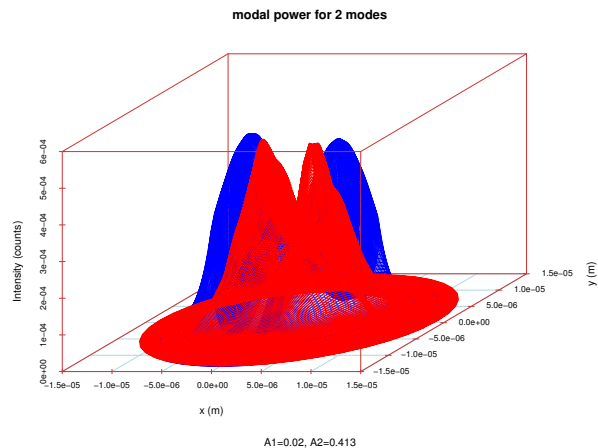


**Figure E.1:** Example 3-dimensional plot of the mapping of theoretical to measured power. Gain=80dB, with axis swap of second mode excitation direction on the Ericsson FSU 995 PM that was used to hold the fibres.

### Listing E.3: Bend radius summary result plots for unamplified fibre

```

#####
## Bend Radius Loss for a Step Profile Circular Fibre ##
#####
#
# By Ross Summerfield , 09/08/2012
#
# Plot the variation of power and phase against bend radius for the
# normal and pi/2 offset input excitation of the second mode.
#

```

```

# Before running this script, change directory into the location to
# run it from. E.g. with Rkward, choose Workspace|Set Working Directory
# from the menu. In that directory, there should be a file called
# "results.csv", which has the summarised results produced by the
# process_data script (in comma separated value form).

## Constants ##
## ----- ##
# Set up the source file name
ResultsName <- "results.csv"
# Set up the global fill colours and border colours
bordercolours <-c("darkblue")
fillcolours <-c("darkblue","red","coral","cyan","lightsalmon","darkgoldenrod")
bordersymbols <-c(21,22,23,24,25,7)
fillsymbols <-c(21)
# Set up the graph details
graphtitle <- "Bend radius against power and phase"
subtitle <- "second mode excitation at 2 different input angles"
outputfile <- "bend_attenuation.eps"
subgraphttl <- "Bend radius against power for differing modes and orientation"
suboutfile <- "bend_slope.eps"
modeoutfile <- "mode_power.eps"

## Bend Loss Profile ##
## ----- ##
# Set up calculation constants for the bend profile
lambda <- 1060 # nm
NAp <- 0.08
rho <- 15e-6 / 2
# Key functions and calculated constants
# Calculation of refractive index of silica
nSilica <- function (l) {
  b1 = 0.6961663; b2 = 0.4079426; b3 = 0.8974794
  w1 = 0.0684043^2; w2 = 0.1162414^2; w3 = 9.896161^2
  n = l^2 * b1/(l^2 - w1) + l^2 * b2/(l^2 - w2) + l^2 * b3/(l^2 - w3)
  sqrt(n+1) }
nCore <- function (na, ncl) sqrt(na^2 + ncl^2)
ncl <- nSilica(lambda/1000) # Assume pure silica
nco <- nCore(NAp, ncl)
delta <- ((nco^2)-(ncl^2))/(2*(nco^2))
k <- 2 * pi / (lambda * 1e-9)
beta <- 2 * pi / (lambda * 1e-9) * (nco + ncl)/2 # approximately
V <- (2 * pi * rho * NAp) / (lambda * 10^(-9))
U <- rho * sqrt(k^2 * nco^2 - beta^2)
W <- sqrt(V^2 - U^2)
gamma <- function (Rb, rho, U, V, W, delta)
  (sqrt(pi * rho/Rb) * V^2 * sqrt(W)/(2 * rho * U^2) *
   exp(-4/3 * delta * Rb * W^3 / (rho * V^2)))
lossdB <- function (Rb, rho, U, V, W, delta, z)
  (20 * log10(exp(1)) * gamma(Rb, rho, U, V, W, delta) * z)
z <- function (Rb, turns) (pi * (Rb * 2) * turns) # pi * bend dia=pi*2(Rb)
bendLoss <- function (Rb, turns) (-lossdB (Rb, rho, U, V, W, delta, z(Rb, turns)))

## Data processing ##
## ----- ##
results <- read.table(ResultsName, header=TRUE, sep=",")
results$File <- factor(results$File)
results <- results[order(results$BendRadius, decreasing=FALSE),]
results$P <- 10 * log10(1000 * (results$P1 + results$P2)) # In dBm
results$P1dBm <- 10 * log10(1000 * (results$P1)) # In dBm
results$P2dBm <- 10 * log10(1000 * (results$P2)) # In dBm
# Spin the angle around on orientation out of phase, but single moded due to
# tight bend radius
results$Angle[(results$Orientation==1) & (results$Angle==0)] <- -pi
# Spin the angle around on orientation out of phase, but single moded due to
# excitation
results$Angle[(results$Orientation==0) & (results$Angle==0)] <- -pi/2
# Normalise the angle: ensure results$Angle is between +/-45 degrees
# (i.e. 0 and +/- pi/4) or at around 90 degrees (i.e. at pi/2)
results$Angle[results$Angle <(-pi)] <-
  results$Angle[results$Angle <(-pi)] + 2 * pi
results$Angle[results$Angle <(-pi/2)] <-
  results$Angle[results$Angle <(-pi/2)] + pi
results$Angle[results$Angle >(pi/2)] <-
  results$Angle[results$Angle >(pi/2)] - pi
results$Angd <- abs(results$Angle * 180 / pi) # Angle in degrees

```

```

# Plot data
plotdata0 <- subset(results , (results$Orientation == 0), select =
                c(BendRadius , P, Angd, Loops))
plotdata1 <- subset(results , (results$Orientation == 1), select =
                c(BendRadius , P, Angd, Loops))
xlimit <- max(as.vector(results$BendRadius))
ylimax <- max(as.vector(results$P))
ylimin <- min(as.vector(results$P))
alimit <- max(as.vector(results$Angd))
alimin <- min(as.vector(results$Angd))
fm0P <- lm(P ~ bendLoss(BendRadius/1000,Loops), data=plotdata0)
fm0 <- lm(Angd ~ BendRadius, data=plotdata0)
if (length(unique(results$Orientation)) > 1) {
  fm1P <- lm(P ~ bendLoss(BendRadius/1000,Loops), data=plotdata1)
  fm1 <- lm(Angd ~ BendRadius, data=plotdata1)
} else {
  subtitle <- "second mode excitation at 1 input angle"
}
# Plot the result:
postscript(outputfile , horizontal=FALSE,
           onefile=FALSE,height=6, width=7,pointsize=10)
par(oma=c(0,0,0,1.2))
plot(as.vector(plotdata0$BendRadius),as.vector(plotdata0$P),
     type="p", pch=bordersymbols[1],
     xlab="Bend Radius (mm)", ylab="Power (dBm)", cex.lab=1.2,
     xlim=c(0,xlimit), ylim=c(ylimin,ylimax),
     col.axis=bordercolours, col=fillcolours[1], cex.axis=1.3,
     main=graphtitle, sub=subtitle)
lines(13:xlimit, bendLoss((13:xlimit)/1000,1)+as.vector(fm0P$coefficients[1]),
      type="l", col=fillcolours[1])
if (length(unique(results$Orientation)) > 1) {
  points(as.vector(plotdata1$BendRadius),as.vector(plotdata1$P),
        type="p", pch=bordersymbols[2], col=fillcolours[2])
  lines(18:xlimit, bendLoss((18:xlimit)/1000,1)+as.vector(fm1P$coefficients[1]),
      type="l", col=fillcolours[2])
}
par(new=TRUE)
plot(as.vector(plotdata0$BendRadius),as.vector(plotdata0$Angd),
     type="p", pch=bordersymbols[3], col=fillcolours[3],
     xlab="", ylab="", xaxt="n", yaxt="n", axes=FALSE,
     xlim=c(0,xlimit), ylim=c(alimin,alimit))
lines(x=c(min(results$BendRadius), max(results$BendRadius)),
      y=c(as.vector(fm0$coefficients[2]) * min(results$BendRadius)+
          as.vector(fm0$coefficients[1]),
          as.vector(fm0$coefficients[2]) * max(results$BendRadius) +
          as.vector(fm0$coefficients[1])), type="l", col=fillcolours[3])
text(xy.coords(xlimit - 88, alimit - 0.05), pos=4, col=fillcolours[3],
     eval(substitute(expression(y == mval*x+bval),
                      list(mval = round(fm0$coefficients[2],3),
                          bval = round(fm0$coefficients[1],2))))), cex=1.1)
text(xy.coords(xlimit - 88, alimit - 5), pos=4, col=fillcolours[3],
     paste("P-value =",round(summary(fm0)$coefficients[2,4],4),sep=""), cex=1.1)
if (length(unique(results$Orientation)) > 1) {
  points(as.vector(plotdata1$BendRadius),as.vector(plotdata1$Angd),
        type="p", pch=bordersymbols[4], col=fillcolours[4])
  lines(x=c(min(results$BendRadius), max(results$BendRadius)),
      y=c(as.vector(fm1$coefficients[2]) * min(results$BendRadius)+
          as.vector(fm1$coefficients[1]),
          as.vector(fm1$coefficients[2]) * max(results$BendRadius) +
          as.vector(fm1$coefficients[1])), type="l", col=fillcolours[4])
  text(xy.coords(xlimit - 88, alimin+8), pos=4, col=fillcolours[4],
      eval(substitute(expression(y == mval*x+bval),
                        list(mval = round(fm1$coefficients[2],3),
                            bval = round(fm1$coefficients[1],2))))), cex=1.1)
  text(xy.coords(xlimit - 88, alimin+3), pos=4, col=fillcolours[4], cex=1.1,
      paste("P-value =", round(summary(fm1)$coefficients[2,4],4), sep=""))
}
mtext("Angle (deg)", side=4, outer=TRUE, cex=1.2)
axis(side=4,col.axis=bordercolours, cex.axis=1.3)
legendx <- xlimit - 108 #88
legendy <- alimin + (alimit - alimin) * 40/100
#legendy <- alimit - 8
legendcoords <- xy.coords(legendx,legendy)
if (length(unique(results$Orientation)) > 1) {
  legend(legendcoords,
        legend=c("Power at 0","Power at 90","angle at 0","angle at 90"),
        col=fillcolours,
        pch=bordersymbols, title="Gonio Orientation (degrees)")
}

```

```

} else {
  legend(legendcoords ,
        legend=c("Power at 0","angle at 0"),
        col=c(fillcolours [1], fillcolours [3]),
        pch=bordersymbols , title="Gonio Orientation (degrees)")
}
dev.off()

## Sub-set plot of results ##
## ----- ##
plotsub <- subset(results , ((results$BendRadius > 56) &
                             !((results$ModesIn==1) &
                               ((results$BendRadius ==229)!(results$BendRadius==225)))) ,
                 select=c(BendRadius , P , Orientation , ModesIn , Loops))
xlimit <- max(as.vector(plotsub$BendRadius))
alimin <- min(as.vector(plotsub$BendRadius))
ylimit <- min(as.vector(plotsub$P))
alimit <- max(as.vector(plotsub$P))
plotsub1 <- subset(plotsub , (plotsub$Orientation==0 & plotsub$ModesIn==1),
                  select=c(BendRadius , P))
plotsub2 <- subset(plotsub , (plotsub$Orientation==0 & plotsub$ModesIn==2),
                  select=c(BendRadius , P))
plotsub3 <- subset(plotsub , (plotsub$Orientation==1 & plotsub$ModesIn==2),
                  select=c(BendRadius , P))
postscript(suboutfile , horizontal=FALSE,
          onefile=FALSE,height=6, width=7,pointsize=10)
plot(as.vector(plotsub1$BendRadius),as.vector(plotsub1$P),
     type="p" , pch=bordersymbols [1],
     xlab="Bend Radius (mm)" , ylab="Power (dBm)" ,
     xlim=c(alimin , xlimit) , ylim=c(ylimit , alimit) ,
     col.axis=bordercolours , col=fillcolours [1],
     main=subgraphttl)
lines(unique(plotsub1$BendRadius),
      tapply(plotsub1$P , plotsub1$BendRadius , mean),
      type="l" , col=fillcolours [1])
points(as.vector(plotsub2$BendRadius),as.vector(plotsub2$P),
       type="p" , pch=bordersymbols [2], col=fillcolours [2])
lines(unique(plotsub2$BendRadius),
      tapply(plotsub2$P , plotsub2$BendRadius , mean),
      type="l" , col=fillcolours [2])
points(as.vector(plotsub3$BendRadius),as.vector(plotsub3$P),
       type="p" , pch=bordersymbols [3], col=fillcolours [3])
lines(unique(plotsub3$BendRadius),
      tapply(plotsub3$P , plotsub3$BendRadius , mean),
      type="l" , col=fillcolours [3])
legendx <- xlimit - 80
legendy <- ylimit + 0.75
legendcoords <- xy.coords(legendx , legendy)
legend(legendcoords ,
      legend=c("0 deg , 1 mode" ,"0 deg , 2 modes" ,"90 deg , 2 modes" ) ,
      col=fillcolours ,
      pch=bordersymbols , title="Gonio Orientation (degrees)")
dev.off()

## Average Power for each mode plot of results ##
## ----- ##
# Graph plotting limits:
xlimit <- max(as.vector(results$BendRadius))
alimin <- min(as.vector(results$BendRadius))
ylimax <- max(max(as.vector(results$P1dBm) ,
                 max(as.vector(subset(results , P2!=0 , select=c(P2dBm))))))
ylimit <- min(min(as.vector(results$P1dBm) ,
                 min(as.vector(subset(results , P2!=0 , select=c(P2dBm))))))
alimit <- max(as.vector(results$P1dBm),as.vector(results$P2dBm))
# Outlier or bend radiusexclusion:
dBmclip<- ylimit * 3 / 4 # exclude outliers: knock the bottom off
resclip<- 35 # the bend cut-off point: > min(results$BendRadius)
fm11 <- lm(P1dBm ~ BendRadius , subset=BendRadius>resclip ,
          data=subset(results , P2==0 , select=c(BendRadius ,P1dBm)))
fm21 <- lm(P1dBm ~ BendRadius , subset=P1dBm>dBmclip ,
          data=subset(results , P2!=0 , select=c(BendRadius ,P1dBm,P2dBm)))
fm22 <- lm(P2dBm ~ BendRadius , subset=P2dBm>dBmclip ,
          data=subset(results , P2!=0 , select=c(BendRadius ,P1dBm,P2dBm)))
# Plot the result:
graphtitle <- "Bend radius against power for each mode"
postscript(modeoutfile , horizontal=FALSE,

```

```

        onefile=FALSE,height=6, width=7,pointsize=10)
plot(as.vector(subset(results , P2==0, select=c(BendRadius ,P1dBm))),
     type="p", pch=bordersymbols [1],
     xlab="Bend Radius (mm)", ylab="Power (dBm)",
     xlim=c(0,xlimit), ylim=c(ylimin,ylimax),
     col.axis=bordercolours , col=fillcolours [1],
     main=graphtitle)
points(as.vector(subset(results , P2!=0, select=c(BendRadius ,P1dBm))),
       type="p", pch=bordersymbols [2], col=fillcolours [2])
points(as.vector(subset(results , P2!=0, select=c(BendRadius ,P2dBm))),
       type="p", pch=bordersymbols [3], col=fillcolours [3])
lines(x=c(resclip , max(results$BendRadius)),
      y=c(as.vector(fm11$coefficients [2]) * resclip + # min(results$BendRadius)+
          as.vector(fm11$coefficients [1]),
          as.vector(fm11$coefficients [2]) * max(results$BendRadius) +
          as.vector(fm11$coefficients [1])), type="l", col=fillcolours [1])
lines(x=c(resclip , max(results$BendRadius)),
      y=c(as.vector(fm21$coefficients [2]) * resclip +
          as.vector(fm21$coefficients [1]),
          as.vector(fm21$coefficients [2]) * max(results$BendRadius) +
          as.vector(fm21$coefficients [1])), type="l", col=fillcolours [2])
lines(x=c(resclip , max(results$BendRadius)),
      y=c(as.vector(fm22$coefficients [2]) * resclip +
          as.vector(fm22$coefficients [1]),
          as.vector(fm22$coefficients [2]) * max(results$BendRadius) +
          as.vector(fm22$coefficients [1])), type="l", col=fillcolours [3])

legendx <- xlimit - 80
legendy <- ylimin + (ylimax - ylimin) * 40/100
legendcoords <- xy.coords(legendx,legendy)
legend(legendcoords ,
       legend=c("Single: Mode 1","2 modes: Mode 1","2 modes: Mode 2"),
       text.col=fillcolours , col=fillcolours ,
       pch=bordersymbols , title="Mode")
legendy <- ylimin + (ylimax - ylimin) * 16/100
legendcoords <- xy.coords(legendx,legendy)
text(legendcoords , pos=4, col=fillcolours [1],
     eval(substitute(expression(R^2 == rsqd),
                     list(rsqd = round(summary(fm11)$adj.r.squared,4)))) )
legendy <- ylimin + (ylimax - ylimin) * 12/100
legendcoords <- xy.coords(legendx,legendy)
text(legendcoords , pos=4, col=fillcolours [2],
     eval(substitute(expression(R^2 == rsqd),
                     list(rsqd = round(summary(fm21)$adj.r.squared,4)))) )
legendy <- ylimin + (ylimax - ylimin) * 8/100
legendcoords <- xy.coords(legendx,legendy)
text(legendcoords , pos=4, col=fillcolours [3],
     eval(substitute(expression(R^2 == rsqd),
                     list(rsqd = round(summary(fm22)$adj.r.squared,4)))) )
dev.off()

## Clean up ##
## ----- ##
rm(lambda, NAp, rho, ncl, nco, delta, k, beta, U, V, W)
rm(bendLoss, z, gamma, lossdB, nSilica, nCore)
rm(ResultsName, results, plotdata0, plotdata1)
rm(fm0, fm1, fm0P, fm1P)
rm(bordercolours, fillcolours, bordersymbols, fillsymbols)
rm(legendx, legendy, legendcoords, xlimit, ylimax, ylimin, alimit, alimin)
rm(graphtitle, subtitle, outputfile)
rm(plotsub, plotsub1, plotsub2, plotsub3, suboutfile, subgraphttl)
rm(fm11, fm21, fm22, dBmclip, resclip, modeoutfile)
# Exit
q()

```

## APPENDIX F: TEST REPORTS

### F.1 2 Mode Fibre Bending Loss

#### F.1.1 Aims

1. To investigate the bend radius in 2 mode fibre where the second mode is stripped out.
2. To determine if power in the fundamental mode is also lost up to this point.
3. To analyse the degree of stability in mode orientation of the second mode.
4. To provide data for use in analysing the power within each mode.

#### F.1.2 Background

This work is done to prepare for the fibre amplification experiments. It is premised on the intensity formula of Liu (2005, pp 133), supported by formulae from Liu (2005, pp 122) and inferences from Snyder and Love (1983, pp 283). Then, applying the generally agreed formula for power and its relationship to intensity (see Liu (2005, pp 126) and Snyder and Love (1983, pp 313)), the theoretical profile for the fibre may be produced. Section 3.3 provides the full details.

A full account of the testing is contained in the author's log book.

#### F.1.3 Method

1. Test is to be conducted on on Nufern part number FUD-3913 LMA-GSF-15/123, lot number 11-C0232-10-4B-02-05, unused 25m roll, with specifications as per Table F.1. To inject the second mode, this fibre needs to be single clad. This fibre should approximately match the LMA-GDF-15/130.

**Table F.1:** *Specifications for Nufern LMA-GSF-15/123 fibre*

Item	Value
Part number	FUD-3913
Operating wavelength (nm)	800 – 1600
Core Numerical Aperture	$0.08 \pm 0.005$
Core diameter ( $\mu\text{m}$ )	$15 \pm 2$
Cladding diameter ( $\mu\text{m}$ )	$123 \pm 1$
V at 1060nm	3.56

2. Refer to Figure F.1 for the test set-up. Apply the custom built face plate for direct measurement to the Goniometric Radiometer.
3. Load the test fibre, switch on the 1060nm source laser and align to the Goniometric Radiometer, with the Aperture Source Distance set as close to 0 as possible, ensuring that the Angular Centroid at  $0.0^\circ$  and at  $90^\circ$  are at as close to  $0.0$  degrees as possible.

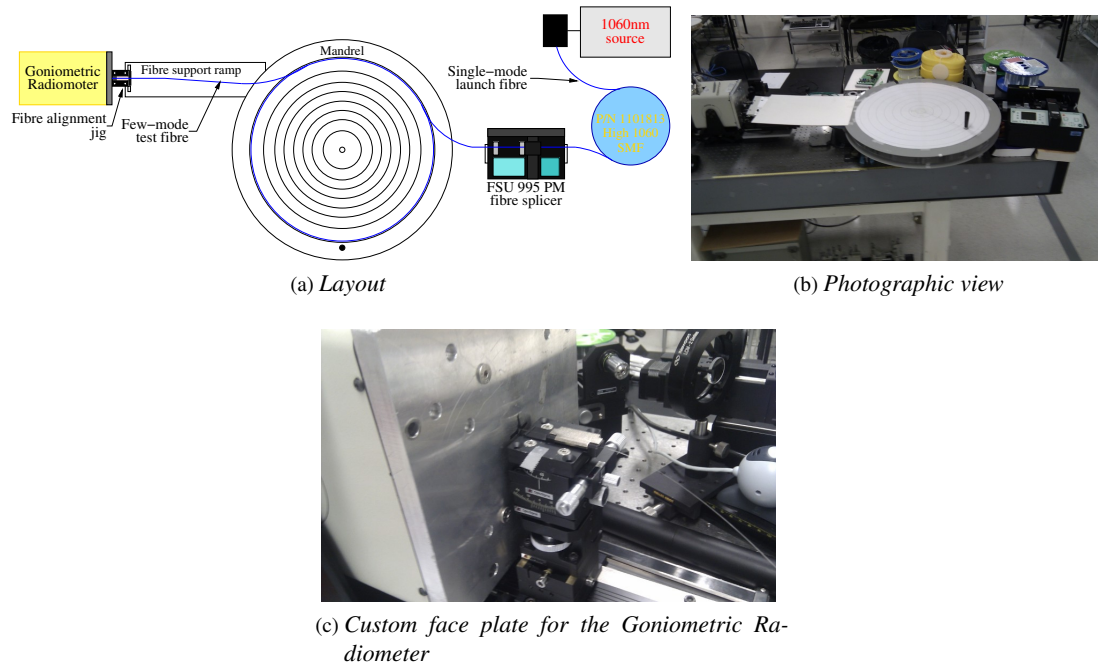


**Figure F.1:** Test set-up for measuring power under differing bending radii using the Photon Inc. Goniometric Radiometer

4. Set up the FSU 995 PM to align the light source single-moded launch and few-moded test fibres, with the fibres as close to each other as possible, then turn off the vacuum pump. Realign the fibres if necessary. With the fibres aligned, the Goniometric Radiometer should be observing just a single mode at the end of the few mode fibre.
5. Load the fibre on the mandrel in a single turn.
6. Adjust and note down the gain for the Goniometric Radiometer to get a good signal without clipping.
7. Take two sets of scan measurements in both 2-D and 3-D using the Goniometric Radiometer.
8. Repeat from Step 6, reducing the fibre diameter by coiling in a figure-of-8 to have 2, 4, etcetera turns, until the diameter is small enough to have cut off (by stripping power into the cladding) for all but the fundamental mode (if the fibre were excited with two or more modes).
9. Offset the fibres in just one direction in the FSU 995 PM to ensure 2 modes are injected into the fibre, as observed by the Goniometric Radiometer.
10. Repeat from Step 5 to Step 8.
11. Offset the fibres in the orthogonal direction to that in Step 9, then repeat from Step 5 to Step 8.
12. Using a power meter, measure the power in the fibre for the tightly coiled (second mode stripped into the cladding), with a single turn and also measure the power emitted from the light source launch fibre.

## F.1.4 Results

The fibre splicer was set up for a single mode injection, that is, with the launch fibre aligned with the test fibre. Details of the measurements taken are in Table F.2. The tolerances on the bend radius are visually estimated and is influenced by the width of the bunch of fibres in the coil. Included in the table are the

single mode measurements taken at the maximum bend radius tested immediately prior to injecting the second mode in the “normal” and orthogonal directions.

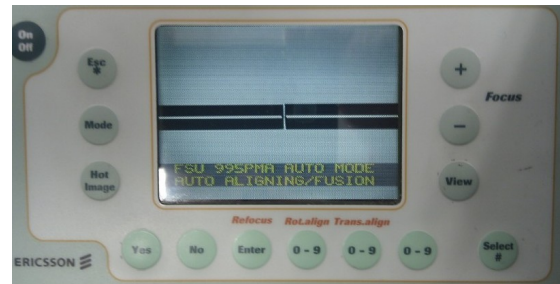
**Table F.2:** Details of the recordings for the injection of 1 mode into the fibre

File name	Bend radius (mm)	Gain (dB)	Angular Centroid		Notes
			at 0°	at 90°	
LMA-GSF-123-15_b05.grs	228 ± 2	64	0.0	0.0	
LMA-GSF-123-15_b06.grs	228 ± 2	64	0.0	0.0	
LMA-GSF-123-15_b07.grs	118 ± 2	64	0.4 - 0.5	-0.2 - 0.4	Appeared to have some second mode component
LMA-GSF-123-15_b08.grs	118 ± 2	64	0.4 - 0.5	-0.2 - 0.4	
LMA-GSF-123-15_b09.grs	58 ± 2	64	0.25 ± 0.1	-1.0 ± 0.2	
LMA-GSF-123-15_b10.grs	58 ± 2	64	0.25 ± 0.1	-0.1 ± 0.2	A substantial second peak off the side of the fundamental mode peak, indicating some 2nd mode behaviour.
LMA-GSF-123-15_b11.grs	47.5 ± 2	64	0.25 - 0.35	-0.47 - 0.52	At 50 samples. No 2nd mode observed
LMA-GSF-123-15_b12.grs	47.5 ± 2	64	0.25 - 0.35	-0.47 - 0.52	At 100 samples
LMA-GSF-123-15_b13.grs	29.5 ± 2	64	0.30 - 0.37	-0.45 - 0.57	At 50 samples
LMA-GSF-123-15_b14.grs	29.5 ± 2	64	0.30 - 0.37	-0.45 - 0.57	At 100 samples
LMA-GSF-123-15_b15.grs	229 ± 2	64	0.07 - 0.30	-0.75 - -0.96	Set up just prior to exciting the second mode
LMA-GSF-123-15_b16.grs	229 ± 2	64	0.05 - 0.30	-0.75 - -0.97	
LMA-GSF-123-15_b27.grs	225 ± 5	65	0.43 - 0.56	-0.80 - -0.88	Set up just prior to exciting the second mode in the orthogonal direction
LMA-GSF-123-15_b28.grs	225 ± 5	65	0.43 - 0.56	-0.80 - -0.90	

The fibre splicer was set up for two modes, with the fibre orientation being as per Figure F.2. The far-field for two modes, as detected by the Goniometric Radiometer, are as per Figure F.3. Details of the measurements taken are in Table F.3.



(a) Vertical view



(b) Horizontal view

**Figure F.2:** Injection of source laser into fibre for two modes

The fibre splicer then had the mode injection applied orthogonally to that originally, with the fibre orientation as per Figure F.4, resulting in the far-field being translated by 90° as shown in Figure F.5. Details of the measurements taken are in Table F.4.

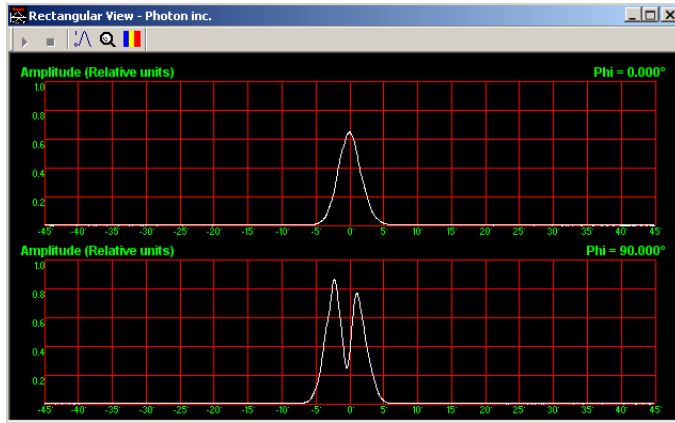


**Figure F.3:** Two mode injection far-field rectangular view of the LMA-GSF-15-123 fibre for  $\phi = 0^\circ$  and  $\phi = 90^\circ$

**Table F.3:** Details of the recordings for the injection of 2 modes into the fibre

File name	Bend radius (mm)	Gain (dB)	Angular Centroid		Notes
			at $0^\circ$	at $90^\circ$	
LMA-GSF-123-15_b17.grs	$229 \pm 2$	89	-0.07 - 0.05	-0.50 - -0.66	
LMA-GSF-123-15_b18.grs	$229 \pm 2$	89	-0.07 - 0.08	-0.50 - -0.70	
LMA-GSF-123-15_b19.grs	$118 \pm 2$	88	-0.07 - 0.14	-0.52 - -0.77	Gain reduced to stop clipping
LMA-GSF-123-15_b20.grs	$118 \pm 2$	88	-0.07 - 0.14	-0.52 - -0.77	
LMA-GSF-123-15_b21.grs	$58.5 \pm 2$	88	0.37 - 0.50	-0.51 - -0.65	Some saturation experienced on $\phi = 90^\circ$
LMA-GSF-123-15_b22.grs	$58.5 \pm 2$	88	0.37 - 0.52	-0.49 - -0.65	
LMA-GSF-123-15_b23.grs	$47.5 \pm 2$	88	0.70 - 0.85	-0.65 - -0.79	
LMA-GSF-123-15_b24.grs	$47.5 \pm 2$	88	0.70 - 0.85	-0.61 - -0.82	
LMA-GSF-123-15_b25.grs	$29 \pm 3$	88	0.32 - 0.44	-0.58 - -0.70	
LMA-GSF-123-15_b26.grs	$29 \pm 3$	88	0.26 - 0.45	-0.58 - -0.70	

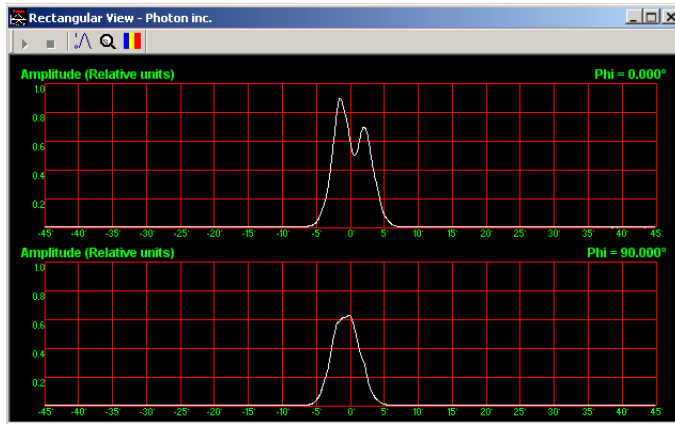


**Figure F.5:** Two mode injection far-field rectangular view of the LMA-GSF-15-123 fibre for  $\phi = 0^\circ$  and  $\phi = 90^\circ$  with the second mode excited orthogonally to that originally

The full results of the response of the fibre to bending is plotted in Figure F.6. The  $R^2$  values indicate lines are only an approximation of the general trend. The angles have been normalised (by adding or subtracting  $180^\circ$  or  $360^\circ$  as necessary) in this plot as the angle detection software operates off the mode detection algorithm, which does not necessarily result in the starting direction being from the same perspective relative to the Goniometric Radiometer axes. The orthogonal output translation of the second mode in response to the rotating the input through  $90^\circ$  is clearly evident. Overall, the orientation of the second mode is about  $10^\circ$  off the axes of the Goniometric Radiometer.

The point at which the second mode is stripped out is measured between 30mm and 50mm bend

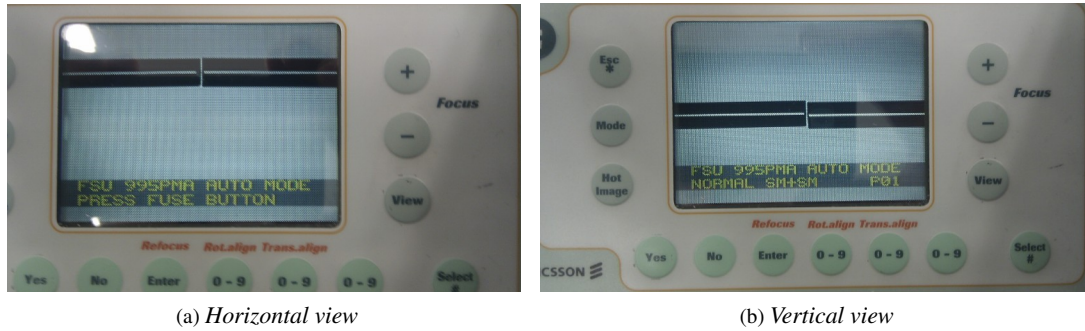


**Figure F.4:** Orthogonal injection of source laser into fibre for two modes

**Table F.4:** Details of the recordings for the injection of 2 modes into the fibre in the orthogonal direction to that in Table F.3.

File name	Bend radius (mm)	Gain (dB)	Angular Centroid		Notes
			at 0°	at 90°	
LMA-GSF-123-15_b29.grs	225 ± 5	80	0.07 - 0.17	-0.52 - -0.67	
LMA-GSF-123-15_b30.grs	225 ± 5	80	0.06 - 0.21	-0.50 - -0.68	
LMA-GSF-123-15_b31.grs	118 ± 5	80	0.14 - 0.36	-0.87 - -1.02	Phase of the 2nd mode appears to be moving a little: amplitude of 2 peaks fluctuating at $\phi = 0^\circ$
LMA-GSF-123-15_b32.grs	118 ± 5	80	0.14 - 0.36	-0.83 - -1.02	
LMA-GSF-123-15_b33.grs	59 ± 3	80	0.02 - 0.20	-0.20 - -0.35	
LMA-GSF-123-15_b34.grs	59 ± 3	80	0.00 - 0.20	-0.13 - -0.35	
LMA-GSF-123-15_b35.grs	29 ± 4	80	0.29 - 0.49	-0.62 - -0.72	Output looks single moded at $\phi = 0^\circ$ and $\phi = 90^\circ$
LMA-GSF-123-15_b36.grs	29 ± 4	80	0.19 - 0.54	-0.57 - -0.89	

radius, with power relatively constant with bend radius for greater bend radii as can be inferred from Figure F.7. The aberration in angle at 49mm radius is with measurement LMA-GSF-123-15\_b10.grs, which appeared to have a measurable second mode. As a consequence, the software estimated the angle of this 'second mode' and injected it into the plot.

When taking the individual measurements using the Goniometric Radiometer, considerable care had to be taken due to a high degree of noise. Precautions, such as ensuring the fibre was laid on a flat surface to minimise the impact of draught from the building air conditioning, and sticking the fibre gently to the surface, were taken, with noticeable positive effect on stability. In addition, the vacuum pump on the FSU 995 PM fusion splicer was switched off to minimise vibration, also with noticeable positive effect.

The power measurements taken by the JDS UniPhase PS3 PDL multimeter were not very stable and tended to vary with the placement of the adapter onto the fibre end. The most stable of measurements are in Table F.5.

**Table F.5:** Power measurements for the bend radius testing of few mode fibre

Fibre	Bend radius	Power (dBm)
LMA-GSF-15/123 test fibre	29 ± 2mm	-8.50 ± 0.07
LMA-GSF-15/123 test fibre	228 ± 4mm	-7.30 ± 0.05
P/N 1101813 single mode source fibre	-	-6.65 ± 0.05

## F.1.5 Discussion

Noise fluctuations and mode fluctuations could be from the following possible sources:

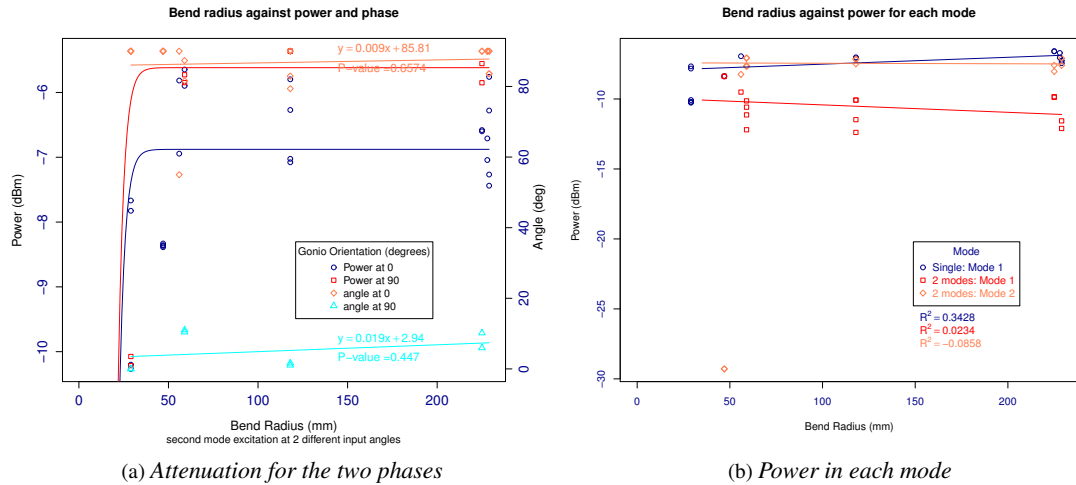


**Figure F.6:** Bending response of the 2 mode fibre

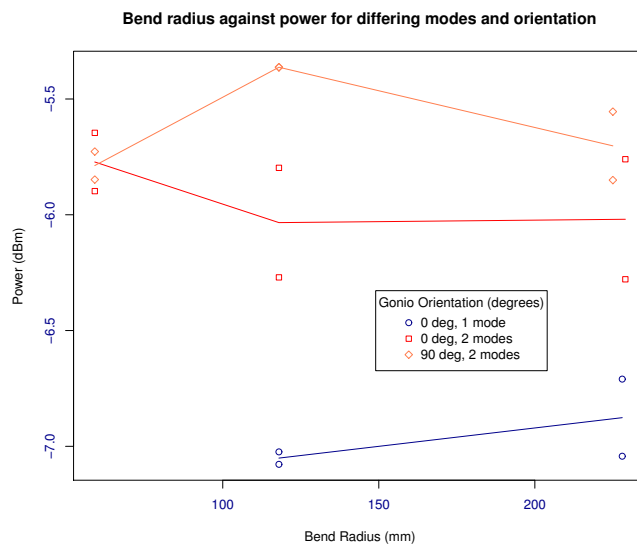


**Figure F.7:** Power for bend radius above the radius where the second mode is stripped out

- fluctuations or other variations at the Ericsson FSU 995 PM splicer. The results are sensitive to fibre alignment in this instrument as evidenced by the variation from the smallest possible movement of one axis when adjusting for single mode. The resolution of its stepper motor is just on the limit of being aligned enough to launch just a single mode into the test fibre.
- fluctuations caused by overlap between the fibres in the coil, and the pressure between the fibres as a consequence of them needing to be stuck down on the circle template attached to the mandrel. There was evidence of this effect when taking samples, particularly between one test run and another, especially as the second mode occasionally appeared for the 2 turn and 4 turn tests at single mode launch. Occasionally, moving the tape around slightly improved results, implying fibre sensitivity to pressure.
- Atmospheric variation from the air conditioners and other air sources. During the early pre-experiment test runs, the system was observed to be very sensitive and the insertion of support platforms seemed to improve result stability.
- vibration in the optic table from vibrations in the building floor from surrounding machinery. The sensitivity there was observed at the end of the tests when the table was repeatedly lightly knocked

for a short time interval.

Marcuse (1993) proposed a formula for the  $LP_{11}$  mode, which required a numerical solution, but noted that it was not very accurate and should only be used for qualitative analysis, a conclusion supported by Poole and Wang (1993).

The orientation analysis of the second mode showed that, for this short 2.9m length of fibre, the orientation was insensitive to the figure-8 bending. The two ends were not rotated in the process, but the fibre in between was subject to bending, including associated stress. This suggests that, for short distances at least, mode orientation through a few-mode fibre can be relied on as stable. Such a result is at odds with the assertion by Randel et al. (2011) that the orientation is not stable. They based their assertion on work by Gordon and Kogelnik (2000) and presumably others, who observed that the two orthogonal modes that make up the fundamental LP mode couple down the fibre and introduce polarisation mode dispersion of that fundamental mode.

Possible reasons are:

- the machine automatically orients the image, but this is not supported by the  $10^\circ$  offset and does not explain the orthogonal change in orientation at the output that was sympathetic to the orthogonal input orientation change;
- the fibre is short, but while this may be a factor to some extent, the fibre was subject to heavy twisting;
- the fibre was actually elliptical, but such an arrangement would prevent the change in output orientation;
- the two ends were fixed, forcing all the figure-8 twisting to cancel itself out, resulting in the output appearing like straight fibre, but this does not take into consideration the stresses introduced into the fibre; or
- the second mode actually maintains its relative polarisation down the fibre and is not noticeably affected by any polarisation introduced by the bending.

Considering these reasons, the following hypothesis is given.

*Theorem 1:* In few-mode fibre, the polarisation tends to just affect the power level, not mode orientation, and the effect on power is immeasurable unless the bend radius is tight (<57mm for LMA-GSF-15/123).

*Corollary 1:* When a fibre is installed, mode orientation remains in place, even if the fibre is disturbed, so the high cost, slow Multiple Input, Multiple Output (MIMO) devices and similar technologies are not required.

*Theorem 2:* The power is stripped into the cladding prior to polarisation effecting mode orientation in few-mode fibre.

*Corollary 2:* The effect of polarisation on mode orientation in few-mode fibre cannot be measured.

The data were collated and analysed using the software of Listing E.1 to provide the intensity profile and the orientation of the two modes with respect to the the Goniometer x-axis, Listing E.2 to determine the amplitude of the modes for a matching theoretical model and Listing E.3 to present the graphs of the results (see Figure F.6 and Figure F.7). The approach taken for the theoretical model matching was to make the amplitudes match by varying the mode parameters, then using the power information from Table F.5, scaled

to give a value in dBm. This draws on the theory analysis in Section 3.3. Although the results were collected in the far field, they do appear to consistently match the theoretical calculations of power using the near-field model, as evidenced by there being no unexplained variances in the graph of Figure F.6.

## F.1.6 Conclusions

This experiment demonstrated the approach of matching the near-field model to the far-field measurements made by the Goniometric Radiometer is a sound approach. It also demonstrated that the approach could be used for power amplification analysis of fibre amplifiers.

The approach identified the bending radius required for the 2-mode LMA-GSF-15/123 fibre. The experiment also showed that, in the case of two modes in short lengths of few-mode fibre, mode orientation is not measurably affected by fibre flexing or other movement. Further mode orientation testing with longer lengths should be conducted at some future point to determine if this result is maintained for data centre internal cabling lengths (hundreds of metres) and for longer lengths for short, medium and long haul.

## F.2 2-Mode Fibre Amplification Measurement

### F.2.1 Aim

1. To investigate the effect on each mode from the application of power amplification of a fibre.

### F.2.2 Background

A prior experiment has been conducted to determine the capability to measure the power in each mode. Specifically, the power is proportional to the intensity amplitude, which is readily measured in three dimensions using a goniometric radiometer. The details of the experiment are contained in Section F.1 above.

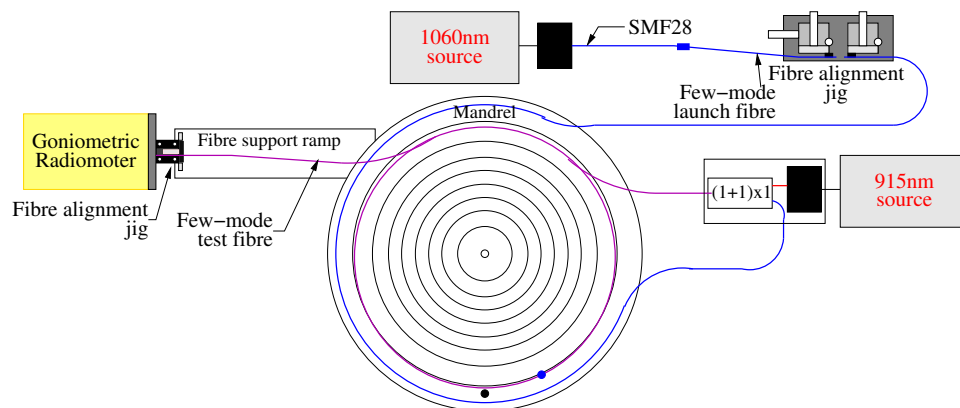
### F.2.3 Method

1. Test is to be conducted using two lengths of Nufern part number FUD-3913 LMA-GSF-15/123, lot number 11-C0232-10-4B-02-05 (see Table F.1 for specifications), about 2m of Nufern LMA-YDF-15/130-VIII, lot number 11-A1576-20-3B-02A-02 as detailed in Table F.6 and an AOFR  $(1 + 1) \times 1$  combiner built using LMA-GDF-15/130.
2. To ensure the LMA-GSF-15/123 is still behaving as expected with the test configuration, rerun a selection of the bend radius tests for single mode excitation and two mode excitation at 1060nm as detailed in Section F.1 using the test set-up of Figure F.1.
3. Splice a  $(1 + 1) \times 1$  combiner (fabricated by the AOFR factory) onto the end of the LMA-GSF-15/123.
4. Re-run the selection of bend radius tests, with the input signal being injected into the LMA-GSF-15/123 and the output being measured at the output of the  $(1 + 1) \times 1$  combiner (with no connection to the pump laser input to the combiner) to confirm two modes can still be generated and the system performs as expected.

**Table F.6:** Specifications for Nufern LMA-YDF-15/130 fibre

Item	Value
Part number	FUD-3539
Operating wavelength (nm)	1060 – 1115
Core Numerical Aperture	$0.08 \pm 0.01$
Cladding Numerical Aperture	0.46
Cladding absorption at 915nm (dB/m)	$1.8 \pm 0.3$
Cladding absorption at 975nm (dB/m)	6.0
Core diameter ( $\mu\text{m}$ )	$15 \pm 2$
Cladding diameter ( $\mu\text{m}$ )	$130 \pm 5$
V at 1060nm	3.56

- Select a laser diode (975nm would give maximum gain in the LMA-YDF-15/130 but 915nm is adequate and provides stability in gain level for any variance in wavelength), mount it to a block and splice it into the pump laser input side of the  $(1 + 1) \times 1$  combiner, then test its output power at the output end of the combiner. Plot the current-to-power curve, determining the relationship between power supply current and laser output power.
- Connect approximately 2m of LMA-YDF-15/130 to the output of the  $(1 + 1) \times 1$  combiner and splice another approximately 2m length of LMA-GSF-15/123, with a combiner at one end to inject 915nm of amplification power.
- Install the fibre, its source waveform laser and the amplifier laser in circuit as per Figure F.8.

**Figure F.8:** Few-mode power amplification test set-up

- Connect up the 915nm amplification pump laser source but do not switch it on at this point.
- Set up the signal injection fibre alignment jig to align the light source single-moded launch and few-moded test fibres, with the fibres as close to each other as possible. With the fibres aligned, the Goniometric Radiometer should be observing just a single mode at the end of the few mode fibre.
- Switch on the 1060nm source laser and align the test fibre to the Goniometric Radiometer, with the Aperture Source Distance set as close to 0mm as possible, ensuring that the Angular Centroid at  $0.0^\circ$  and at  $90^\circ$  are at as close to  $0.0$  degrees as possible.
- Load the fibre on the mandrel in the outer-most turn.
- Adjust and note down the gain for the Goniometric Radiometer to get a good signal without clipping.
- Take two sets of scan measurements in both 2-D and 3-D using the Goniometric Radiometer.
- Use a power meter to measure the output of the fibre with the 915nm pump laser switched off.

15. Using a power meter, measure the response of the system to the 915 pump laser's current supply. Plot the curve to determine the safe values of pump power to inject into the system without damaging the Goniometric Radiometer.
16. Connect the output fibre back into the Goniometric Radiometer and reduce its gain to 0, then apply amplification by switching on the 915nm amplification source, setting its power level to give modest gain, in the order of 20dB when compared to a >2m length of LMA-GSF-15/123 without any gain fibre attached.
17. Take two sets of scan measurements in both 2-D and 3-D using the Goniometric Radiometer.
18. Repeat from Step 12, reducing the fibre diameter of the length of LMA-GSF-15/123 closest to the Goniometric Radiometer by coiling it in a figure-of-8 to have 2, 4, etcetera turns, until the diameter is small enough to have cut off (by stripping power into the cladding) for all but the fundamental mode (if the fibre were excited with two or more modes).
19. Set the output length of LMA-GSF-15/123 to the outer diameter of the mandrel. Offset the fibres in just one direction in the fibre alignment jig to ensure 2 modes are injected into the fibre, as observed by the Goniometric Radiometer.
20. Repeat from Step 17 to Step 18.
21. Offset the fibres in the orthogonal direction to that in Step 19, then repeat from Step 11 to Step 18.
22. Re-align the fibres in the fibre alignment jig, then repeat from Step 11 to Step 19, with a higher pump laser power level.
23. Using a power meter, measure the power in the fibre for the tightly coiled (second mode stripped into the cladding), with turns on the outer-most ring of the mandrel and also measure the power emitted from the light source launch fibre.

## F.2.4 Results

For the re-run of a selection of the bend radius tests as a process validation, the fibre under test was not the same piece originally tested. This test fibre was about 1.7m longer. The 2 mode output did not have even power distribution in the second mode as evidenced from the red measured profile in Figure F.9. The Angular Centroid was adjusted to try to average around 0 degrees for each pair of measurements. Table F.7 outlines the record of results.

The results are not indicative of a good quality fibre due to the lack of consistency with the bend radius experiment. Its unsuitability was confirmed after splicing it into the start of the  $(1 + 1) \times 1$  combiner, where the second mode could not be launched.

The bend radius test was then re-run on the piece of fibre used in the original bend radius test. The record of results are outlined in Table F.8 and the power in each of the modes is plotted in Figure F.10. As with the first round of experiments, the  $R^2$  values indicate the lines are only an approximation of the power trend.

The last four entries relate to a check on the  $(1 + 1) \times 1$  combiner, which was inserted post the LMA-GSF-15/123 fibre and laid out on the test bench with large circles or sweeping arcs to ensure no tight bend radius. As there was noise in the signal, one of the results for the 2 mode signal injection was interpreted by the algorithm as single moded; one of the peaks was much lower than the other and quite close leading

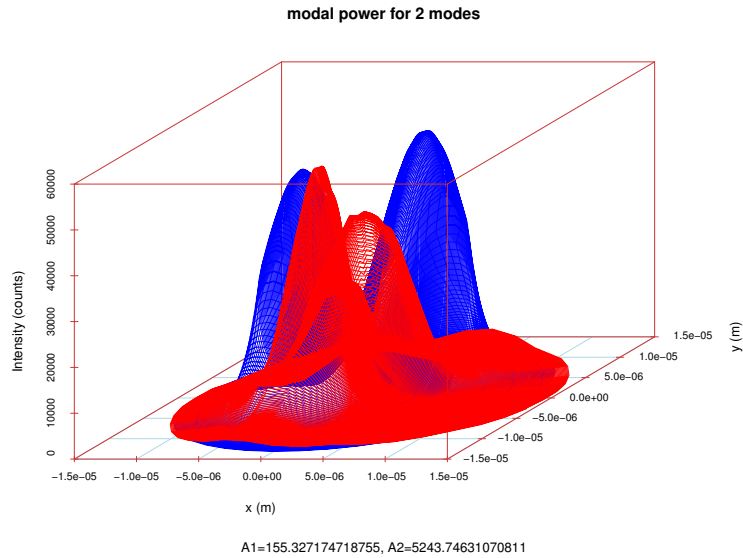


**Figure F.9:** Run 7 two mode power measurement recorded for the test set-up validation on the 3.7m fibre, where the blue profile is the theoretical and the red profile is that measured with the goniometric radiometer.

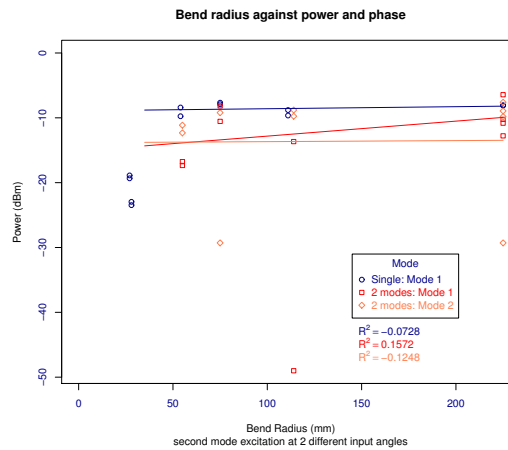


**Figure F.10:** Re-run recording plot of the bend radius against power in each of the modes for the injection of 2 modes into the 2.4m fibre

to the misinterpretation. The graphical result of the other measurement, which was for the two modes, is shown at Figure F.11.

The power laser diode was inserted into circuit with the  $(1 + 1) \times 1$  combiner and the power measured prior to insertion of the LMA-YDF-15/13 and its tail LMA-GSF-15/123 and its response against current was measured, with the results and statistical analysis graphed in Figure F.12. The relationship is  $P = 0.89I - 0.3$  with  $R^2 = 0.999$ .

The power out of the system was measured using a UDT 5370 Optimeter power meter, set to the nearest wavelength of 1050nm for measuring the 1060nm signal, prior to connecting it to the goniometric radiometer. Check point measurement results without amplification are at Table F.9 and a plot of the power output response to pump laser input current is at Figure F.13.

After ensuring the LMA-YDF-15/13 gain fibre provided power, the Bend radius test was repeated with 1060nm source and the 915nm pump laser switched on, and the 1060 source providing either one or two modes. The results indicated potential issues with signal amplification, probably due to Amplified Spontaneous Emission (ASE) swamping the 1060nm input signal. A typical “3D Rectangular” output

**Table F.7:** Details of the bend radius re-run recordings for the injection of 2 modes into the 3.7m fibre

File name	Bend radius (mm)	Gain (dB)	Angular Centroid		Notes
			at 0 °	at 90 °	
LMA-GSF-123-15_01.grs	268 ± 5	58	-0.10 - 0.10	-0.30 - 0.10	Some second mode popped in at beginning; difficult to remove.
LMA-GSF-123-15_02.grs	268 ± 5	58	-0.10 - 0.10	-0.30 - 0.10	
LMA-GSF-123-15_03.grs	67 ± 4	58	-0.10 - 0.10	-0.20 - -0.70	Angular Centroid at $\phi = 90^\circ$ would not adjust to positive.
LMA-GSF-123-15_04.grs	67 ± 4	58	-0.10 - 0.10	-0.20 - -0.70	
LMA-GSF-123-15_05.grs	33 ± 2	58	-0.10 - 0.10	-0.20 - -0.70	Regular ~2sec beat to Angular Centroid $\phi = 0^\circ$ .
LMA-GSF-123-15_06.grs	33 ± 2	58	-0.10 - 0.10	0.00 - -0.20	
LMA-GSF-123-15_07.grs	270 ± 10	82	-1.00 - -1.40	-0.20 - 0.20	Several goes at getting gain for 3D scan correct, even though correct for 2D.
LMA-GSF-123-15_08.grs	270 ± 10	82	-1.00 - -1.40	-0.20 - 0.20	
LMA-GSF-123-15_09.grs	135 ± 5	82	0.10 - -0.30	0.00 - -0.40	Angular Centroid tended to skew toward -0.8, esp. at $\phi = 90^\circ$ .
LMA-GSF-123-15_10.grs	135 ± 5	82	0.10 - -0.30	0.00 - -0.90	
LMA-GSF-123-15_11.grs	65 ± 5	82	0.50 - -1.30	0.10 - -3.20	Small signal
LMA-GSF-123-15_12.grs	65 ± 5	82	0.50 - -1.30	0.10 - -3.20	
LMA-GSF-123-15_13.grs	34 ± 3	82	0.10 - 1.40	-0.20 - 0.70	Very small signal at 82dB gain. Regular ~1.8sec beat to Angular Centroid $\phi = 0^\circ$ .
LMA-GSF-123-15_14.grs	34 ± 3	82	0.10 - 1.40	-0.20 - 0.70	
LMA-GSF-123-15_15.grs	17 ± 2	110	0.30 - -0.50	1.00 - -8.50	High level of noise after saving this scan.
LMA-GSF-123-15_16.grs	17 ± 2	110	-0.10 - 0.10	-0.10 - 0.10	Reset loop and reconfigured laser to have less stress on the output fibre.
LMA-GSF-123-15_17.grs	17 ± 2	110	-0.10 - 0.10	-0.10 - 0.10	

produced by the Photon Goniometric Radiometer software for any of the amplified signal results is shown in Figure F.14, along with a spectral recording from an Optical Spectrum Analyser (OSA) of this signal. Details of the optical spectrum analyser results are in Table F.10. Additional test runs using the OSA were run on a different day, to confirm the results and to expand on them, also measuring the system response to no seed signal.

For the additional run on the different day, the gain required to see the unamplified two modes using the goniometric radiometer was much lower, at 108dB, compared to 120-130dB previously required. This time, a very small amount of the second mode was visible through the ASE when the signal was subject to amplification, both in the OSA plot as a distinct narrow peak and on the 3-D goniometric radiometer plot.

The P/N 1101813 fibre was removed from circuit and the SMF28 fibre coming out of the seed laser was connected to a short length of LMA-GSF-15/123 to provide better matching of the mode shape. This resulted in a reduction of loss somewhere in the order of 16 to 20dB.

The final round of power tests without amplification are contained in Table F.12, with amplification for 1 mode in Table F.13 and with amplification for 2 modes in Table F.14. The amplification data is summarised in the box plots of Figure F.15. Figure F.16 demonstrates the logarithmic relationship between pump power and gain for the one or two injected mode test. Here, for the single injected mode case, the relationship has multiple  $R^2 = 0.999$  (highly proportional relationship), while for the two injected mode case, for total power (that is power for the fundamental and second mode added together), multiple  $R^2 = 0.983$ , for the fundamental mode, multiple  $R^2 = 0.988$  and for the second mode, multiple  $R^2 = 0.974$  (not as strong a relationship as with a single injected mode).

A plot of the gain coefficient, developed using the equations of Section 3.3, is at Figure 5.6 on page 33 in Chapter 5 Section 5.3. The value of  $U$  is calculated from the Eigenvalue Equation 3.7 given that  $V = 3.56$  for this fibre (see Table F.6). Then, given  $U$  and  $V$ ,  $\eta$  is calculated using Equation 3.19 and Equation 3.8. Rearranging Equation 3.20 results in Equation F.1, from which the values of the gain coefficient,  $\gamma$ , are calculated. The unamplified power,  $P(0)$ , is taken from the average power for the relevant mode (that is, either the single excited mode case, the first mode of the two excited modes case or the second mode of the two excited modes case). The gain fibre (see Table F.6) was cut to a measured length of  $z = 2.0\text{m}$ .

**Table F.8:** Details of the bend radius re-run recordings for the injection of 2 modes into the 2.4m fibre

File name	Bend radius (mm)	Gain (dB)	Angular Centroid		Notes
			at 0 °	at 90 °	
LMA-GSF-15-123_01	225 ± 5	45	0.1 - 0.3	-0.4 - -0.1	Aligned Angular Centroid.
LMA-GSF-15-123_02	225 ± 5	45	0.12 - 0.38	-0.46 - -0.12	
LMA-GSF-15-123_03	111 ± 4	45	-0.75 - -0.2	0.1 - 0.5	
LMA-GSF-15-123_04	111 ± 4	45	-0.4 - -0.1	0.1 - 0.2	
LMA-GSF-15-123_05	54 ± 3	45	-0.42 - -0.05	-0.1 - 0.35	Very low signal level.
LMA-GSF-15-123_06	54 ± 3	45	-0.4 - 0.25	-0.7 - 0.3	
LMA-GSF-15-123_07	28 ± 2	45	-0.1 - 0.5	0.2 - 0.35	
LMA-GSF-15-123_08	28 ± 2	45	-0.1 - 0.5	0.08 - 0.4	
LMA-GSF-15-123_09	225 ± 5	65	-0.02 - 0.05	-0.02 - 0.02	Had to restart after bumping the fibre splicer. Re-aligned the Angular Centroid. Took photos after starting measurements.
LMA-GSF-15-123_10	225 ± 5	65	-0.21 - 0.4	-0.15 - 0.32	
LMA-GSF-15-123_11	225 ± 5	75	-0.07 - 0.0	-0.06 - 0.06	
LMA-GSF-15-123_12	225 ± 2	75	-0.07 - 0.42	-0.1 - 0.2	
LMA-GSF-15-123_13	114 ± 2	75	0.0 - 0.25	-0.22 - 0.15	
LMA-GSF-15-123_14	114 ± 2	75	0.0 - 0.25	-0.25 - 0.15	
LMA-GSF-15-123_15	55 ± 1	75	0.0 - 0.15	-0.2 - 0.13	
LMA-GSF-15-123_16	55 ± 1	75	-0.2 - 0.3	-0.7 - 0.25	
LMA-GSF-15-123_17	27 ± 2	75	0.18 - 0.41	0.1 - 0.16	
LMA-GSF-15-123_18	27 ± 2	75	0.15 - 0.41	0.1 - 0.16	
LMA-GSF-15-123-1+1_01	~75	45	-0.04 - 0.02	-0.01 - 0.03	Test against single mode injection.
LMA-GSF-15-123-1+1_02	~75	45	-0.05 - 0.07	-0.01 - 0.07	
LMA-GSF-15-123-1+1_03	~75	85	-0.21 - -0.01	-0.02 - 0.08	Test against 2 mode injection.
LMA-GSF-15-123-1+1_04	~75	85	-0.21 - 0.05	-0.1 - 0.08	

**Table F.9:** Power measurements from the gain fibre with the pump laser switched off

Bend Radius (mm)	Power (nW)	Power (dBm)
25 ± 2	18.36 ↔ 19.00	-47.287 ± 0.074
92 ± 2	57.10 ↔ 57.90	-42.403 ± 0.030
285 ± 10	57.20 ↔ 58.00	-42.396 ± 0.030

$$\gamma = \frac{\log_{10} \frac{P(z)}{P(0)}}{z\eta \log_{10} e} \quad (\text{F.1})$$

## F.2.5 Discussion

In between the initial tests described in Section F.1 and the running of this test, the test bench and associated equipment was moved. This meant revalidation of results was an important precursor to ensure consistency. One of the fibre lengths used and retested was problematic with a high level of signal attenuation, perhaps due to flaws that could have been introduced into the fibre in the move. The original test fibre was eventually re-used and gave results similar to the original tests.

The introduction of the  $(1 + 1) \times 1$  combiner into the circuit resulted in additional attenuation but still appeared to allow the transmission of one or two modes, as injected, down the fibre. The addition of the gain fibre added even more attenuation, but still appeared to allow the transmission of one or two modes, as injected, down the fibre, albeit at weak signal levels, requiring an additional approximately 40dB of sensitivity gain to be applied to the goniometric radiometer. The power meter used for this experiment was different to that used in the test described in Section F.1 and required recalibration, but its output appeared consistent and it suggested a difference caused by loss from the LMA-YDF-15/130 gain fibre and the  $(1 + 1) \times 1$  combiner of close to 40dBm, consistent with the observations from the goniometric radiometer.

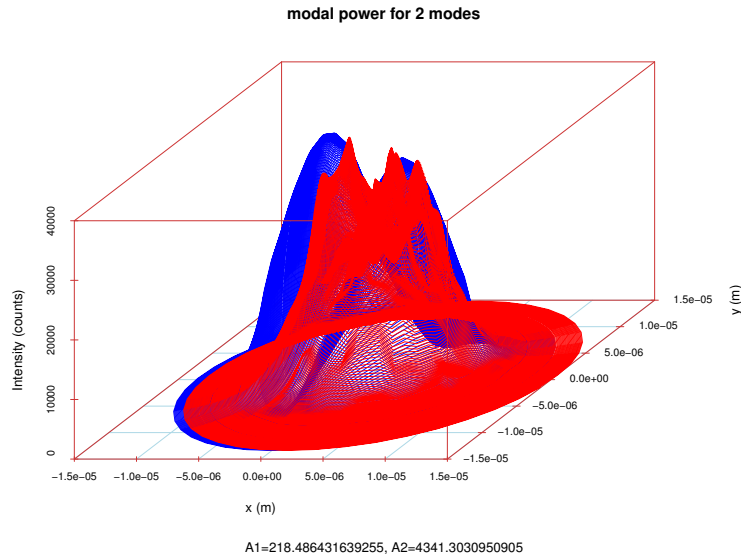


**Figure F.11:** Run 3 two mode power measurement recorded for the 1+1 combiner joined to the 2.4m fibre test set-up validation, where the blue profile is the theoretical and the red profile is that measured with the Radiometric Goniometer.

**Table F.10:** Optical Spectrum Analyser measurements of the power in the system with and without amplification (bend radius=280mm for all runs except for the first entry, which was a direct connection between the 1060nm source and the OSA).

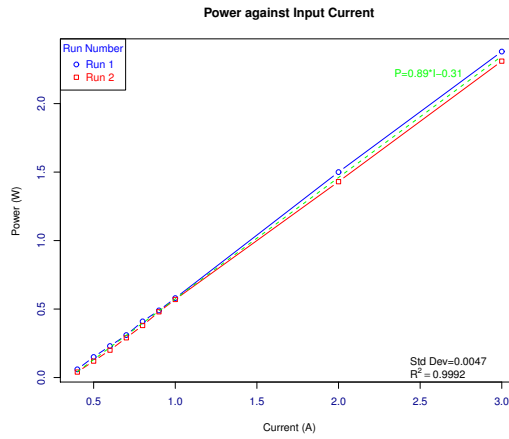
Run	-	11	12	38
File name	G0000	G0001	G0002	G0003
Modes	1	2	2	2
Pump power (W)	0	0.58	0.58	1.025
Peak amplitude (dBm)	-46.7	-55.0	-41.0	-33.5
Width at noise peak (nm)	40	24	160	140
Width at OSA floor (nm)	70	30	220	240

However, the earlier power measurements of Section F.1 were significantly different to the measurements taken by the optical spectrum analyser, which had the output of the 1060nm source laser at around -46.5dBm against -6.5dBm from the JDS UniPhase PS3 PDL multimeter. The difference of 13.5dBm between the measurement of the UDT 5370 Optimeter and the optical spectrum analyser for the no amplification power case is also more than can be attributed to experimental variance. The optical spectrum analyser may also have been out of calibration. For the relative comparison analysis of the fibre for the lack of amplification of individual modes, this difference is unimportant provided the optical spectrum analyser was consistent in its calibration drift.

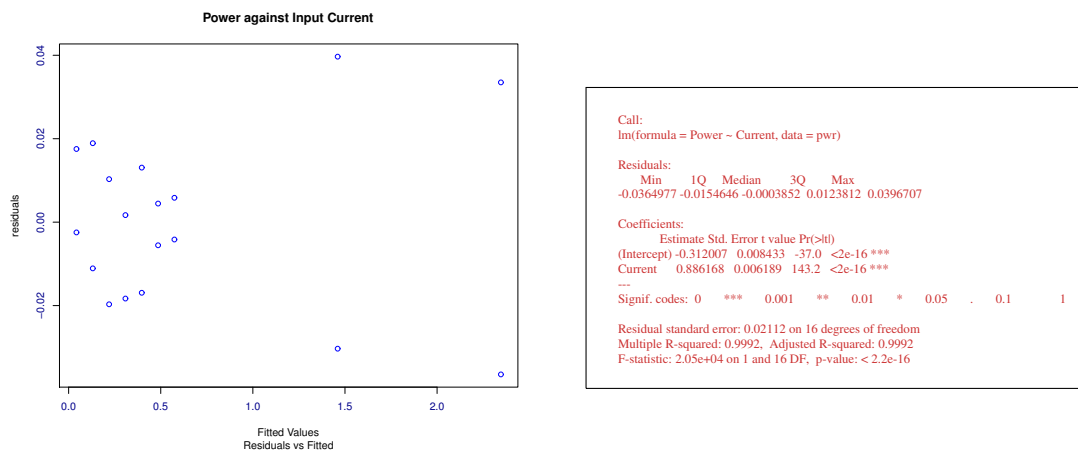
The lack of the presence of modes together with the smoothing of the signal power, in the goniometric radiometer measurements was likely due to Amplified Spontaneous Emission (ASE). The spectrum analysis supports this conclusion. This suggests that having adequate signal level fed into the fibre amplifier is important to the amplifier working correctly. Even using the difference between the UDT 5370 Optimeter, less the 13.5dBm, and the JDS UniPhase PS3 PDL multimeter of being at least 22.5dBm, it is likely that the 1060nm source was delivering less power this time around.

Operation of the test system without any seed power clearly demonstrated a peak at around 1060nm in addition to one at the pump wavelength, giving further weight to the conclusion that the seed power requires adequate strength to overcome the effect of ASE. A second test, with higher seed power also confirmed this.

In addition to any splice losses and the 8% glass-air-glass interface loss in the fibre alignment jig, a major source of loss is from the aligning fibres at the fibre alignment jig, where the incoming 1060nm single



(a) Power against Current



(b) Residuals against fitted, showing a tight congregation around 0

(c) Textual description of variation, constructed using tools from R Development Core Team (2010)

**Figure F.12: Power diode output response against current**

mode Corning part number 1181013 fibre has a core diameter of  $5\mu m$  and the outgoing LMA-GSF-15/123 test fibre has a core diameter of  $15\mu m$ , resulting in misalignment of the fundamental mode and therefore significant power loss through the different field size. Reconfiguration to launch directly from the SMF-28 fibre connected to the seed laser into a short length of LMA-GSF-15/123 and using that as the input side to the fibre alignment jig had a significant positive effect on the amount of power transmitted into the test fibre, with in the order of 16dB less sensitivity gain needing to be applied to the goniometric radiometer to get a viewable signal.

From comparison of the data used to generate Table F.12 through to Table F.14 against observed results in the goniometric radiometer’s three dimensional rectangular view, it was seen that refinement of the 3-dimensional intensity extraction algorithm for better two mode detection resulted in no errors in the correct categorisation of the output as being either one or two modes.

Measurement of total power using a power meter required disconnection from the goniometric radiometer, connection into a bare fibre adaptor connector, power measurement, then cleaving prior to insertion back into the goniometric radiometer. Each time the available test fibre became shorter, which was problematic over the large number of tests. Consequently only a few tests were actually measured. Those measurements suggest the power measurement out of the system was a reasonable approximation for 2 injected modes, but significantly different (out by at least  $10^3$ ) for a single injected mode. There are at least two possible causes. The calibration data set was not large and so the calibration multiplier constants may

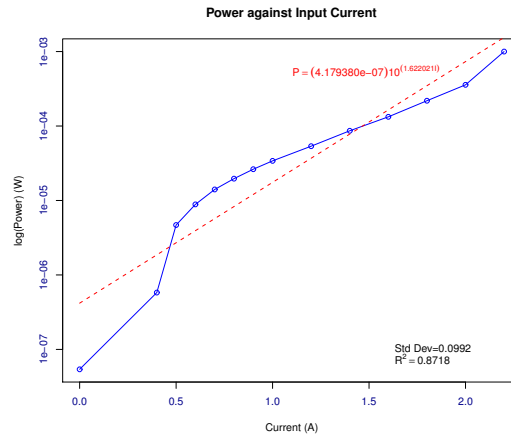


**Figure F.13:** Power measurements from the gain fibre with the pump laser switched on

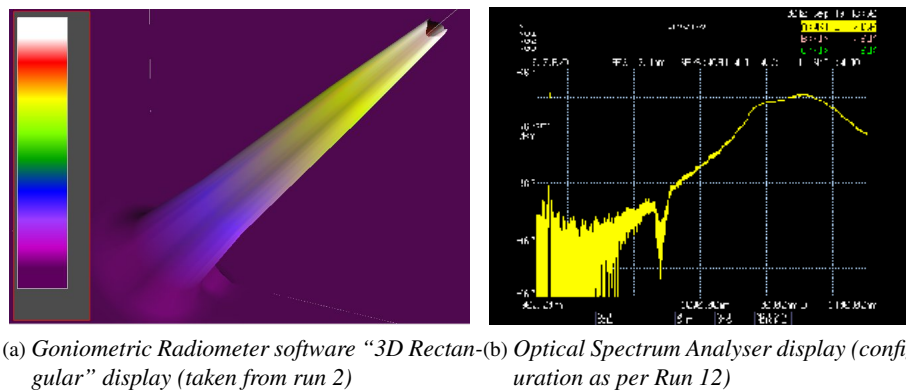


**Figure F.14:** Typical amplified signal output for the first round of amplified signal measurements (in both cases, radius=280mm, pump power=0.58W)

be quite wrong. The system may be better tuned with a different multiplier for the different number of injected modes. The calibration curves of the experiment at Section F.3 suggest the latter to be the case. Further, the implementation of the model effectively guesses  $\beta$  and this should be slightly different for each mode (thereby affecting  $U$  and  $W$ , which ultimately depend on its value). As it could be considered as rolled up into the calibration constant, setting one up for each mode should cater for its currently unaccounted for variation.

The relative evenness of the power that is spread between the two modes in the tests where two modes were injected is quite noticeable in Figure F.15a and Figure F.15b, where it can be seen that both have been subject to a gain of close to 50 per cent. This would ordinarily be at odds with what would be expected, except that Figure F.15c shows that there was approximately 25% more power in the second mode than in the fundamental mode prior to amplification. Therefore, the fundamental mode amplification would, under normal seed power circumstances, get a greater level of amplification than the second mode.

A difference more difficult to explain is the lower degree of gain, in the order of between about 6dB and 10dB, for the tests involving a single injected mode into the test fibre when compared to the two injected mode test. The single injected mode has a higher seed power level than for the two mode tests since all the power is concentrated into the fundamental mode. However, as Figure F.16a shows, gain is not linear with pump power, rather it is logarithmic. This means that the average gain is much lower than might otherwise be expected. But for two modes, as Figure F.16b shows, the gain to pump power relationship is also logarithmic, for the cases of each mode and for the total gain. So it does not explain the discrepancy in the gain between the single injected mode tests and the two injected mode tests, rather just the quartile

**Table F.11:** Second set of Optical Spectrum Analyser measurements of the power in the system (bend radius ~280mm for all runs).

Equivalent Run	OSA File name	GR File name	Seed signal	Pump power (W)	Peak amp. @ 1060nm (dBm)	Width at noise peak (nm)	Width at OSA floor (nm)	G/R rel. amp + sens. (rel) + (dB)
-	0M_1-0A		None	0.58	-65.5	80	105	-
-	0M_1-5A		None	1.025	-59	50	90	-
11	SM_0-0A	LMA-GSF-15-123_01	1 mode	0	-46	5	40	0.8 + 80
12,13	SM_1-0A		1 mode	0.58	-41	5	150	
38,39	SM_1-5A		1 mode	1.025	-37	5	>150	
1,21	2M_0-0A	LMA-GSF-15-123_02	2 modes	0	-69	all noise	all noise	0.4-0.8 + 108
2,22	2M_1-0A	LMA-GSF-15-123_04	2 modes	0.58	-64	~2	~4	0.4 + 80
36,37	2M_1-5A		2 modes	1.025	-59.5	~2	30	

**Table F.12:** Second run for the unamplified signal - baseline test

File name	Injected modes	Bend radius (mm)	Gain (dB)	Pump Pwr (W)	Measured Power ( $\mu W$ )	Calc Power ( $\mu W$ )	Notes
LMA-GSF-15-123_01	1	265	71	0	$90 \pm 3$	$151.8009 \times 10^3$	
LMA-GSF-15-123_02	1	265	71	0	$90 \pm 3$	$149.1239 \times 10^3$	
LMA-GSF-15-123_03	1	88	71	0	0	$122.7998 \times 10^3$	
LMA-GSF-15-123_04	1	88	71	0	0	$121.5253 \times 10^3$	Break for lunch
LMA-GSF-15-123_05	1	47	71	0	0	$127.5145 \times 10^3$	High intensity fluctuations
LMA-GSF-15-123_06	1	47	71	0	0	$125.6705 \times 10^3$	
LMA-GSF-15-123_07	1	25	71	0	$70 \pm 4$	$114.4747 \times 10^3$	
LMA-GSF-15-123_08	1	25	71	0	$70 \pm 4$	$115.5993 \times 10^3$	
LMA-GSF-15-123_09	1	12	120	0	0	1.1297	
LMA-GSF-15-123_10	1	12	120	0	0	1.0851	

offset differences in the box plots. But with two modes, the fields extend further into the cladding than for the single mode. Therefore, at least in these short test fibres, more amplification takes place with two (or more) modes than with single mode.

The lower level of gain for a single injected mode when compared to two injected modes is clearly visible when comparing the two graphs of Figure F.16. Figure F.16b also demonstrates that, for two injected modes, the gain of each mode is almost the same and both are almost the same as the total gain.

Analysis of the gain coefficient, developed using Equation F.1 above and plotted in the box plots of Figure 5.6 on page 33, shows that the gain coefficient was much higher for a single injected mode than for each mode of the two injected mode case (and even for the sum of the gain coefficients for the two injected mode case), even though there was a lower degree of total gain. The average gain coefficient value for each mode for the two injected mode case is roughly the same for each value of pump power, which accords with the observation in F.16b. Figure 5.6 shows that, as expected,  $n_i \propto P_{pump}$ .

## F.2.6 Conclusions

This experiment reconfirmed the importance of checking the fibre quality upon installation and the importance of adequate signal level at amplification.

**Table F.13:** *Second run for the amplified signal for one mode*

File name	Injected modes	Bend radius (mm)	Gain (dB)	Pump Power (W)	Measured Power ( $\mu W$ )	Calculated Power( $\mu W$ )		Notes
						Mode 1	Mode 2	
LMA-GSF-15-123_63	1	255	74	0	0	$83.1021 \times 10^3$	0	Re-cleaved prior to test
LMA-GSF-15-123_64	1	255	70	0.224	0	$204.8064 \times 10^3$	0	
LMA-GSF-15-123_65	1	255	66	0.402	0	$513.5695 \times 10^3$	0	
LMA-GSF-15-123_66	1	255	62	0.580	0	$1246.8598 \times 10^3$	0	
LMA-GSF-15-123_67	1	255	53	1.025	0	$9111.3723 \times 10^3$	0	
LMA-GSF-15-123_68	1	75	74	0	0	$79.7979 \times 10^3$	0	
LMA-GSF-15-123_69	1	75	70	0.224	0	$203.3751 \times 10^3$	0	
LMA-GSF-15-123_70	1	75	66	0.402	0	$520.0139 \times 10^3$	0	
LMA-GSF-15-123_71	1	75	62	0.580	0	$1170.3754 \times 10^3$	0	
LMA-GSF-15-123_72	1	75	53	1.025	0	$9161.0448 \times 10^3$	0	
LMA-GSF-15-123_73	1	38	74	0	0	$76.4298 \times 10^3$	0	
LMA-GSF-15-123_74	1	38	70	0.224	0	$186.8887 \times 10^3$	0	
LMA-GSF-15-123_75	1	38	66	0.402	0	$463.8294 \times 10^3$	0	
LMA-GSF-15-123_76	1	38	62	0.580	0	$1106.8506 \times 10^3$	0	
LMA-GSF-15-123_77	1	38	53	1.025	0	$8046.4259 \times 10^3$	0	
LMA-GSF-15-123_78	1	24	74	0	57.5	$70.912 \times 10^3$	0	
LMA-GSF-15-123_79	1	24	70	0.224	98	$187.4173 \times 10^3$	0	
LMA-GSF-15-123_80	1	24	66	0.402	151.5	$473.3477 \times 10^3$	0	
LMA-GSF-15-123_81	1	24	62	0.580	232	$1080.3046 \times 10^3$	0	
LMA-GSF-15-123_82	1	24	53	1.025	637.5	$9036.5601 \times 10^3$	0	

The experiment showed that two modes get amplified, with the fundamental mode getting significantly more amplification than the second mode if the fundamental mode has equal or more power than the second mode, in line with the theory. However, if the second mode has more power than the fundamental mode, then the gain in each of the modes is adjusted accordingly. Further, the experiment demonstrated the logarithmic relationship between gain and pump power, irrespective of whether there was a single injected mode or two injected modes and irrespective of the mode in the two injected mode case.

The experiment also highlighted the need for a relatively large calibration data set and also the likely need for different calibration multiplier constants for the different number of modes.

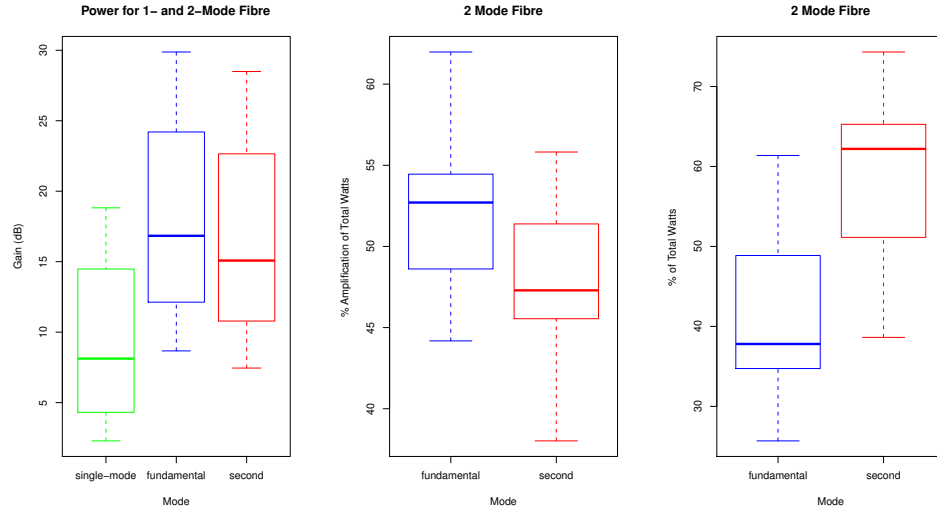
## F.3 Fibre Power Calibration Measurement

### F.3.1 Aim

1. To investigate the linearity of the model for each mode in a fibre.
2. To provide data to calibrate the power scaling constant for the model for future use with AOFR's Photon Inc. Goniometric Radiometer.

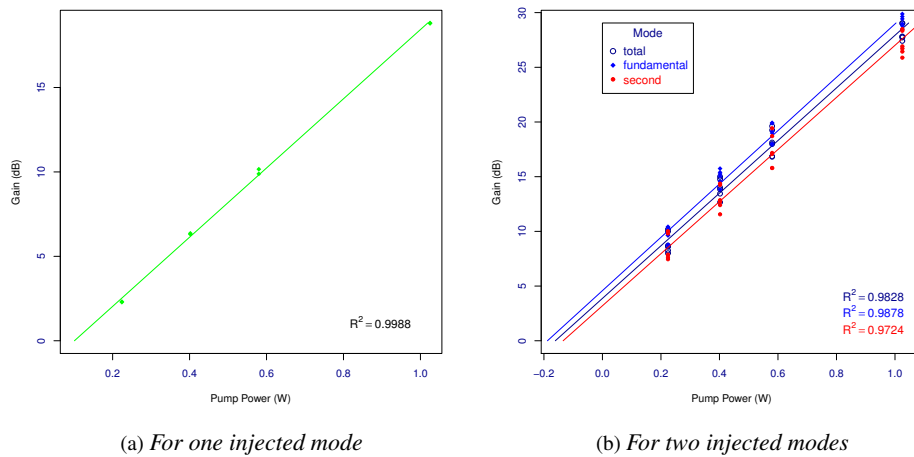
### F.3.2 Background

Prior experiments have been conducted to determine the capability to measure the power in each mode. In particular, the experiment contained in Section F.1 above gave initial validation of the concept, with further testing required to confirm the linearity, stability and consistency of the concept.



(a) Gain comparison for a single injected mode and for two injected modes  
 (b) Relative degree of amplification of each mode (calculated from  $\% = \frac{P_{mode}}{P_{total}}$ )  
 (c) Amount of power in each mode injected prior to amplification for two injected modes

**Figure F.15: Ytterbium-doped fibre amplifier amplification comparisons**



(a) For one injected mode

(b) For two injected modes

**Figure F.16: Pump power to Ytterbium-doped amplifier gain relationship**

### F.3.3 Method

1. Test can be conducted using two lengths of Nufern part number FUD-3913 LMA-GSF-15/123, lot number 11-C0232-10-4B-02-05 (see Table F.1 for specifications), about 2m of Nufern LMA-YDF-15/130-VIII, lot number 11-A1576-20-3B-02A-02 as detailed in Table F.6 and a  $(1 + 1) \times 1$  combiner built using LMA-GDF-15/130, but the fibre amplifier need not be powered on.
2. Refer to Figure F.8 for the test set-up. Leave the pump signal power source switched off.
3. Switch on the 1060nm source laser and align to the Goniometric Radiometer, with the Aperture Source Distance set as close to 0 as possible, ensuring that the Angular Centroid at  $0.0^\circ$  and at  $90^\circ$  are at as close to  $0.0$  degrees as possible.
4. Set up the fibre alignment jig to align the light source single-moded launch and few-moded test fibres, with the fibres as close to each other as possible. With the fibres aligned, the Goniometric Radiometer should be observing just a single mode at the end of the few mode fibre.

5. Set up the UDT 5370 Optimeter power meter for the nearest wavelength to 1060nm, namely 1050nm (it has 15nm increments).
6. Load the fibre on the mandrel in a single turn.
7. Adjust and note down the gain for the Goniometric Radiometer to get a good signal without clipping.
8. Take two sets of scan measurements in both 2-D and 3-D using the Goniometric Radiometer.
9. Remove the fibre from the end of the Goniometric Radiometer, insert it into an ST male adaptor, connect it to the UDT 5370 Optimeter power meter and take a power level measurement.
10. Repeat from Step 7, reducing the fibre diameter by coiling in a figure-of-8 to have 2, 4, etcetera turns, until the diameter is small enough to have cut off (by stripping power into the cladding) for all but the fundamental mode (if the fibre were excited with two or more modes).
11. Offset the fibres in just one direction in the FSU 995 PM to ensure 2 modes are injected into the fibre, as observed by the Goniometric Radiometer.
12. Repeat from Step 6 to Step 10.

### F.3.4 Results

Table F.15 details the manual recording component of the test results. The result from processing the data, which used the tests marked with “\*” as the calibration samples to calibrate the 3D Model Generation software and the whole data suite as validation data, is plotted in Figure F.17.

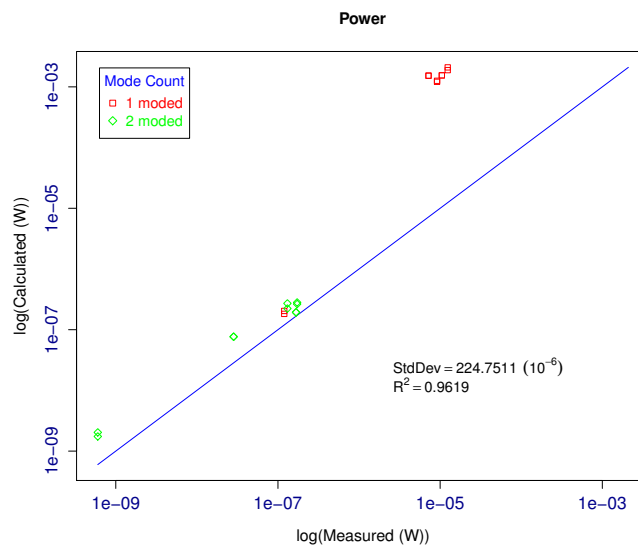


**Figure F.17:** Power level accuracy test

The fit, shown on a log-log scale has  $R^2 = 0.96$ . Although not shown on the graph, error in the measured results were seen to vary by between  $\pm 1\%$  and  $\pm 10\%$ .

### F.3.5 Discussion

With  $R^2 > 0.9$ , the fit is adequate for purposes of demonstrating the validity of the model. Higher accuracy for the power calibration constant could be achieved with a larger sample set. Also, the plot suggests that different calibration constants based on the number of modes would provide a higher degree of accuracy.

Variation in error of the measured results was probably mostly due to continuous fluctuation in the mode peaks observed using the goniometric radiometer.

Having calibrated the scaling constant in the model from just three samples so that the model can be validated, the whole sample set is now available for reuse as calibration data for the other experiments.

### **F.3.6 Conclusions**

This test, in addition to providing calibration data for the scaling constant to use in all other experiments, demonstrated the validity of the mode power measurement model. with a larger sample set, the model could be refined to use per-mode scaling constants.

**Table F.14:** Second run for the amplified signal for 2 modes

File name	Injected modes	Bend radius (mm)	Gain (dB)	Pump Power (W)	Measured Power (nW)	Calculated Power( $\mu W$ )		Notes
						Mode 1	Mode 2	
LMA-GSF-15-123_11	2	265	100	0	0	71.6265	114.7291	
LMA-GSF-15-123_12	2	265	100	0	0	68.1457	116.1545	
LMA-GSF-15-123_13	2	265	93	0.224	0	688.7447	597.6893	
LMA-GSF-15-123_14	2	265	93	0.224	0	685.5395	633.7887	
LMA-GSF-15-123_15	2	265	88	0.402	0	2382.7332	1932.5938	
LMA-GSF-15-123_16	2	265	88	0.402	0	2494.1292	1995.1909	
LMA-GSF-15-123_17	2	265	84	0.580	0	6157.829	5392.8343	
LMA-GSF-15-123_18	2	265	84	0.580	0	5903.5905	5283.2605	
LMA-GSF-15-123_19	2	265	74	1.025	0	$59.0079 \times 10^3$	$48.5208 \times 10^3$	
LMA-GSF-15-123_20	2	265	74	1.025	0	$56.4689 \times 10^3$	$50.8115 \times 10^3$	
LMA-GSF-15-123_21	2	82	98	0	0	161.2619	113.3116	
LMA-GSF-15-123_22	2	82	98	0	0	97.4464	202.5278	
LMA-GSF-15-123_23	2	82	91	0.224	0	784.3102	990.4064	
LMA-GSF-15-123_24	2	82	91	0.224	0	821.8734	1038.3166	
LMA-GSF-15-123_25	2	82	86	0.402	0	2581.6229	2754.4322	
LMA-GSF-15-123_26	2	82	86	0.402	0	2796.7147	2828.9937	
LMA-GSF-15-123_27	2	82	82	0.580	0	7258.1206	9058.1506	
LMA-GSF-15-123_28	2	82	82	0.580	0	7326.3349	7679.8489	
LMA-GSF-15-123_29	2	82	72	1.025	0	$72.4704 \times 10^3$	$70.5777 \times 10^3$	
LMA-GSF-15-123_30	2	82	72	1.025	0	$68.5708 \times 10^3$	$73.0939 \times 10^3$	
LMA-GSF-15-123_31	2	82	100	0	0	32.8641	55.563	Re-cleave
LMA-GSF-15-123_32	2	82	100	0	0	78.4807	49.3909	required.
LMA-GSF-15-123_33	2	48	100	0	0	30.3245	87.7577	
LMA-GSF-15-123_34	2	48	100	0	0	56.2334	87.9485	
LMA-GSF-15-123_35	2	48	93	0.224	0	548.8253	575.2328	
LMA-GSF-15-123_36	2	48	93	0.224	0	564.2883	627.1705	
LMA-GSF-15-123_37	2	48	88	0.402	0	2140.0003	1798.3921	
LMA-GSF-15-123_38	2	48	88	0.402	0	1800.7246	1481.2802	
LMA-GSF-15-123_39	2	48	84	0.580	0	4711.0752	3922.1426	
LMA-GSF-15-123_40	2	48	84	0.580	0	4628.7237	3931.1682	
LMA-GSF-15-123_41	2	48	74	1.025	0	$65.3014 \times 10^3$	$40.0562 \times 10^3$	
LMA-GSF-15-123_42	2	48	74	1.025	0	$52.5426 \times 10^3$	$45.5441 \times 10^3$	
LMA-GSF-15-123_43	2	25	108	0	0	24.7079	0	
LMA-GSF-15-123_44	2	25	108	0	0	25.4502	0	
LMA-GSF-15-123_45	2	25	97	0.224	0	384.0859	0	
LMA-GSF-15-123_46	2	25	97	0.224	0	391.9187	0	
LMA-GSF-15-123_47	2	25	91	0.402	0	1473.0046	0	
LMA-GSF-15-123_48	2	25	91	0.402	0	1462.586	0	
LMA-GSF-15-123_49	2	25	87	0.580	0	4078.8567	0	
LMA-GSF-15-123_50	2	25	87	0.580	0	3997.2416	0	
LMA-GSF-15-123_51	2	25	77	1.025	0	$38.6273 \times 10^3$	0	
LMA-GSF-15-123_52	2	25	77	1.025	0	$39.6671 \times 10^3$	0	
LMA-GSF-15-123_53	2	12	139	0	$15 \pm 2$	0.0057	0	
LMA-GSF-15-123_54	2	12	139	0	$15 \pm 2$	0.0055	0	
LMA-GSF-15-123_55	2	12	136	0.224	$665 \pm 1.6$	0.0477	0	
LMA-GSF-15-123_56	2	12	136	0.224	$665 \pm 1.6$	0.0543	0	
LMA-GSF-15-123_57	2	12	129	0.402	$123 \pm 2$	0.2704	0	
LMA-GSF-15-123_58	2	12	129	0.402	$123 \pm 2$	0.2677	0	
LMA-GSF-15-123_59	2	12	124	0.580	$187 \pm 2$	0.7549	0	
LMA-GSF-15-123_60	2	12	124	0.580	$187 \pm 2$	0.7297	0	
LMA-GSF-15-123_61	2	12	114	1.025	$540 \pm 2$	7.8266	0	
LMA-GSF-15-123_62	2	12	114	1.025	$540 \pm 2$	7.9429	0	

**Table F.15:** Details of the bend radius recordings for the power calibration test

File name	Injected modes	Bend radius (mm)	Gain (dB)	Angular Centroid		Measured Power (nW)	Notes
				at 0 °	at 90 °		
LMA-GSF-15-123_01	1	280	90	-0.2 - 0.1	-0.6 - 0.21	10390 - 10600	
LMA-GSF-15-123_02	1	280	90	-0.2 - 0.1	-0.8 - 0.21	10390 - 10600	
LMA-GSF-15-123_03	1	84	90	-0.3 - 0.15	0.05 - 0.25	9000 - 9320	
LMA-GSF-15-123_04	1	84	90	-0.3 - 0.2	0.05 - 0.25	9000 - 9320	Break for lunch
LMA-GSF-15-123_05	1	48	90	-0.15 - 0.3	0.18 - 0.66	12280 - 12520	High intensity
LMA-GSF-15-123_06	1	48	90	-0.25 - 0.41	0.18 - 0.82	12280 - 12520	fluctuations
LMA-GSF-15-123_07	1	25	90	-0.04 - 0.04	-0.04 - 0.03	6950 - 7430	
LMA-GSF-15-123_08	1	25	90	-0.04 - 0.05	-0.04 - 0.07	6950 - 7430	
LMA-GSF-15-123_09	1	13	130	-0.08 - 0.11	-0.14 - 0.12	110.1 - 129.0	
LMA-GSF-15-123_10	1	13	130	-0.15 - 0.25	-0.14 - 0.12	110.1 - 129.0	
LMA-GSF-15-123_11	2	275	128	-0.25 - 0.15	-0.3 - 0.2	171.8 - 173.1	Noisy signal: not clean
LMA-GSF-15-123_12	2	275	128	-0.25 - 0.2	-0.4 - 0.36	171.8 - 173.1	2 mode
LMA-GSF-15-123_13	2	91	128	-0.2 - 0.48	-0.1 - 0.48	165.1 - 169.1	2nd mode not so
LMA-GSF-15-123_14	2	91	128	-0.2 - 0.5	-0.1 - 0.48	165.1 - 169.1	obvious
LMA-GSF-15-123_15	2	46	128	-0.25 - 0.15	-0.15 - 0.35	129.6 - 132.0	Fibre stress mark from
LMA-GSF-15-123_16	2	46	128	-0.3 - 0.15	-0.25 - 0.35	129.6 - 132.0	ST adaptor observed
LMA-GSF-15-123_17	2	25	128	-0.25 - 0.5	-0.15 - 0.35	26.00 - 30.80	Single mode output
LMA-GSF-15-123_18	2	25	128	-0.6 - 0.5	-0.15 - 0.55	26.00 - 30.80	
LMA-GSF-15-123_19	2	12	139	-35 - 50	-15 - 10	0.4 - 0.8	No observable signal.
LMA-GSF-15-123_20	2	12	139	-35 - 50	-15 - 30	0.4 - 0.8	B/gnd is 2.0 - 2.3nW